Effects of Shear Viscoelasticity and Free Polymers on Tribological Properties of Phospholipid Polymer Brushes

林　楓昌

2024 年 3 月

Table of Contents

List of Figures

1. Introduction

1.1 Ultralow Friction by Hydration Lubrication

In the pursuit of advancing energy efficiency and achieving carbon neutrality, addressing the fundamental challenge of friction in mechanical systems is critical. Ultralow friction is not just a desirable mechanical feature; it is imperative to conserve energy and reduce carbon emissions associated with industrial and transportation systems. Remarkably, a significant proportion of the world's energy consumption is expended to overcome friction, highlighting the profound impact of friction reduction on global energy savings and environmental sustainability [1]–[3].

Within this context, the concept of hydration lubrication has emerged as an exceptionally promising solution [4]–[7]. This approach to achieving ultralow friction is inherently clean because it utilizes abundant and environmentally benign water molecules as the primary lubricating agent. This is in stark contrast with conventional lubrication methods that often rely on oil-based lubricants, which have a greater environmental impact in terms of resource extraction, production, and disposal.

Hydration lubrication is a phenomenon in which a thin layer of water molecules is trapped between two surfaces in motion relative to one another [8]. These molecules are arranged in structured layers because of the ionic or polar characteristics of the surfaces,

creating a strong repulsive hydration force that keeps the surfaces apart. This mechanism significantly reduces the direct contact between the surfaces, thereby lowering the shear strength and reducing the friction to remarkably low levels. The efficiency of hydration lubrication is a consequence of the unique behavior of water molecules when they are confined and the nature of their interactions with charged surfaces.

An example of hydration lubrication can be found in the human body. The joints of the body, such as the hips and knees, operate under principles similar to hydration lubrication [9], [10]. Synovial fluid, which is primarily composed of water and hyaluronic acid, serves as a natural lubricant in these joints [11], [12]. This fluid creates an environment that allows bones to move against each other with minimal friction, thus exemplifying the effectiveness and natural occurrence of hydration lubrication.

Therefore, the exploration and development of hydration lubrication technology are of considerable interest in the quest to create more sustainable mechanical systems. By emulating natural processes, such as those found in the human body, and applying them to engineering challenges, we can work towards machines that operate with greater energy efficiency and minimal environmental impact, aligning with global sustainability objectives.

1.2 Hydration Lubrication by Polymer

1.2.1 Previous Studies of Hydration Lubrication by Polymer Brush

The phenomenon of hydration lubrication by polymers has garnered extensive research interest owing to its significant potential for reducing the coefficient of friction (COF) [13]–[16]. Polymers, especially those with hydrophilic characteristics, are known to exhibit enhanced lubricity when hydrated because they can retain water molecules within their matrix, forming a lubricious layer that facilitates smooth sliding with minimal resistance [17], [18]. This property has led to the exploration of various polymers for their ability to provide effective hydration lubrication under various environmental conditions.

Among these polymers, 2-Methacryloyloxyethyl phosphorylcholine (MPC) has emerged as a promising material. MPC is a phospholipid zwitterionic polymer that mimics cell membrane structure (molecular structure shown in Fig. 1.1). MPC polymers show promise as coating materials for preventing biofouling [19]. Furthermore, they exhibit a high lubricity [20]. Owing to their biocompatibility and lubricity, MPC polymers have been used as coatings for sliding surfaces in artificial joints. Moro et al. reported that MPC polymer coatings reduced the coefficient of friction (COF) between the metal and polyethylene used in artificial joints to 0.1 and increased the service life of the joint (shown in Fig. 1.2) [21]. On atomically flat substrates, the hydrated MPC polymer coating exhibited a COF of less than 0.01, which agrees with the general definition of superlubricity [22], [23]. Tairy et al. used a surface force apparatus (SFA) and found that

the COF could be as low as 10^{-5} under precisely controlled sliding gaps (shown in Fig. 1.3) [24]. The high lubricity of MPC polymer coatings is attributed to their ability to absorb the surrounding water (in the case of artificial joints, water from the body) to form a gel-like thin film.

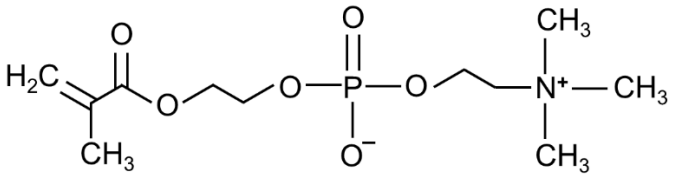

Fig. 1.1 Molecular structure of MPC monomer.

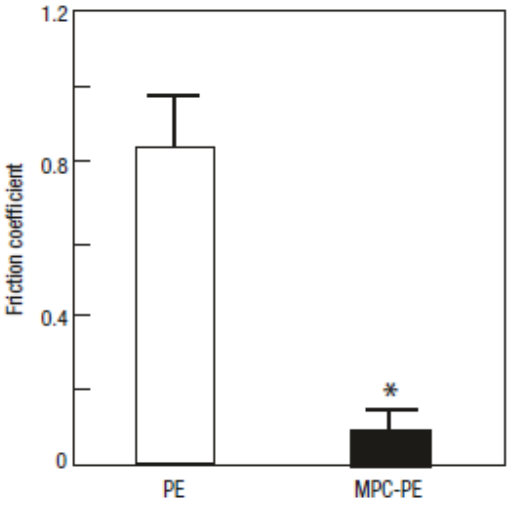

Fig. 1.2 Comparison of COF of polyethylene with and without MPC polymer coating [21].

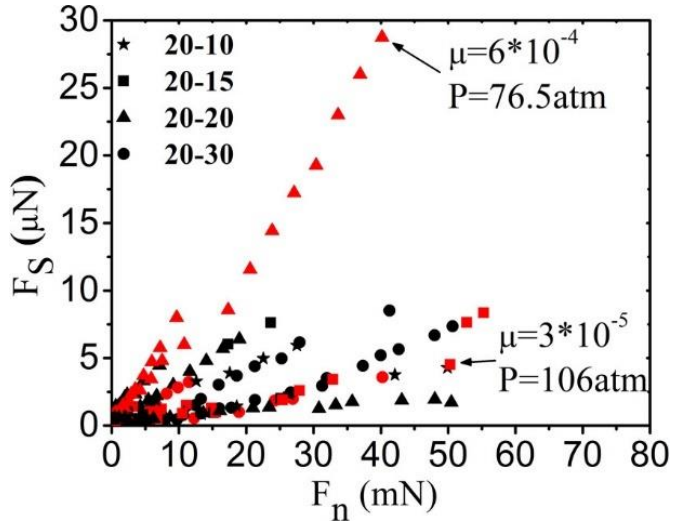

Fig. 1.3 Friction force and normal load of MPC polymer brushes (black symbols) [24].

Klein et al. explained that hydration lubrication originates from the high mobility (i.e., low viscosity) of water in nanoscale sliding gaps, where other liquids tend to be highly viscous [8], [25]. Therefore, the chemical composition of the polymer coating that confers hydrophilicity to the surface plays an important role in this phenomenon. Kobayashi et al. reported that the COF of MPC polymer film decreased with increasing humidity (shown in Fig. 1.4) [26]. This finding proves that increasing the water adsorption leads to higher lubricity.

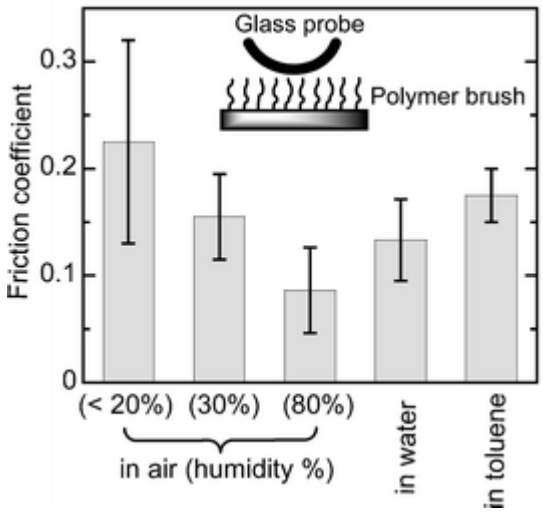

Fig. 1.4 COF of MPC polymer brush in air, water and toluene [26].

Ishihara et al. found that the friction properties of hydrated MPC polymer coatings differ depending on whether the molecular adsorption state is physical adsorption, chemical adsorption, or brush-like chemical grafting (brush-like). Specifically, hydrated brush-like MPC polymers exhibit the lowest COF (Fig. 1.5) [17]. The friction properties also exhibit a unique dependence on sliding speed (shown in Fig. 1.6) [27]–[29]. These properties differ from those of hard thin-film coatings that obey Coulomb's friction law, thus suggesting that the viscoelasticity of the polymer brush is a dominant factor in lubricity. To the best of our knowledge, whether hydration lubricity is due to the intervention of a molecularly thin water film at the sliding interface or whether the inclusion of water increases the flexibility (i.e., changes the viscoelasticity) of polymer chains and contributes to lubricity remains unclear.

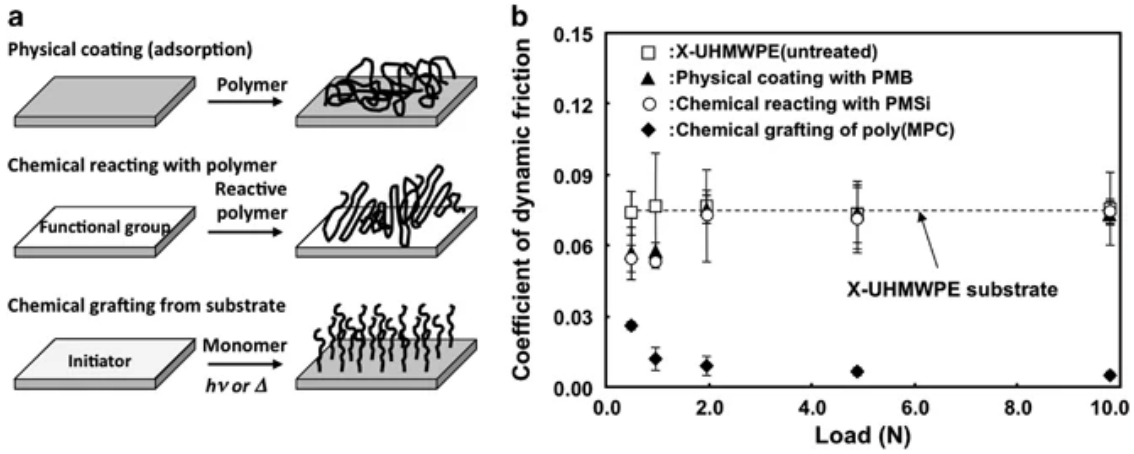

Fig. 1.5 (a) Various modification modes of polymers and (b) their COF comparison [17].

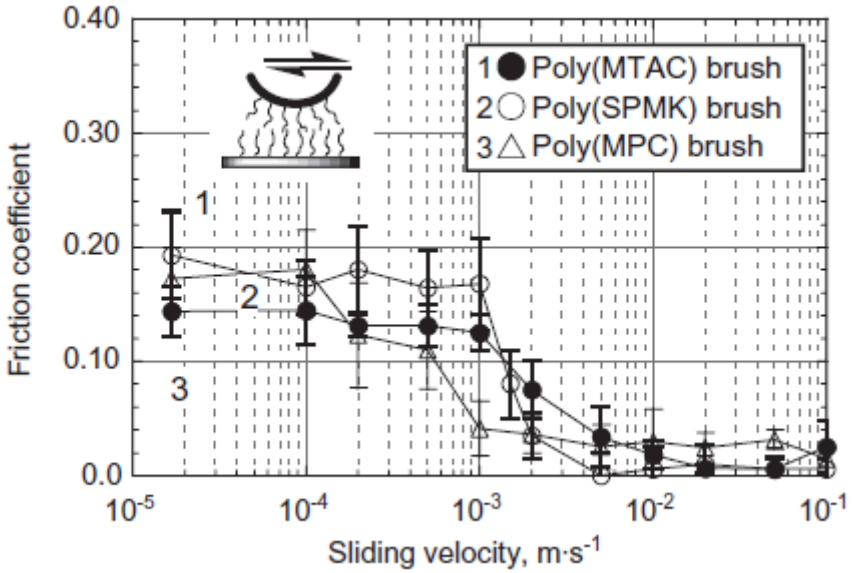

Fig. 1.6 COF's velocity dependence of MPC polymer brushes (triangle) in water [27].

The results from both theoretical calculations and molecular dynamics simulations indicate that the density of polymer brushes in a good solvent varies depending on their distance from the surface [30]–[35]. Similar experimental results were obtained using

neutron reflectometry [36]–[39]. This density distribution becomes more complex when the polymer is confined in the gap between the sliding surfaces.

For example, as the gap narrows, the density of the grafted polymer film increases and the water retained in the film by osmotic pressure is expelled from the polymer chains [40]. The viscoelasticity of the film depends on the changes in the density and water content. However, no previous studies have successfully quantified viscoelasticity with respect to changes in the sliding gap. At the sliding interface, changes in the gap imply changes in load. In joint prostheses, the load changes in a complex manner in response to human movements. Furthermore, in mechanical systems, the load changes depending on operating and environmental conditions. Practical lubricants require the ability to maintain lubricity despite changes in load (i.e., changes in the gap). Therefore, the gap dependence of viscoelasticity must be clarified to understand the lubricity of hydrated MPC polymer brush films. However, hydrated MPC polymer brush films typically have a thickness of less than 1 μm, and no method has yet been established to measure the viscoelasticity of such films with precisely controlled nanogaps.

Although SFA affords high accuracy in measuring gaps, it applies a load to narrow the gap and the repulsive force of the film must balance the load to set the desired shear gap [41]. Therefore, measurements are limited to a gap range in which the repulsive force of the film is sufficiently large owing to the nanoconfinement. As the hydrated polymer chains are distributed over several hundred nanometers from the substrate, the gap

dependence of the shear viscoelasticity of such films has not yet been successfully measured using SFA.

Recently, nanoindentation tests have been developed to measure the viscoelasticity of soft and thin films [42]. However, because the nanoindentation test detects the mechanical response by vibrating a probe perpendicular to the substrate, the influence of the mechanical properties of the substrate cannot be ignored when measuring the properties of a thin film. The excitation amplitude of the probe should be sufficiently small to avoid the influence of the substrate. However, if the thin film is soft, measurement sensitivity may be insufficient. Consequently, no study has successfully quantified the gap dependence of the viscoelasticity of hydrated thin films using nanoindentation.

1.2.2 Free Polymer's Effect on Improving Lubricity

Although significant efforts have been made to analyze the role of polymer brushes in hydration lubrication, the factors that influence hydration lubrication in practical lubrication environments are diverse and complex. Notably, the effect of free polymers, which are unbound and freely moving polymer chains, on the lubrication performance of lubrication fluids has been extensively studied [43]. The high lubricity in natural joint lubrication is attributed to the high hydration induced by the phospholipid layer of the

joint cartilage, as well as to the complex synovial fluid, which contains phospholipids, hyaluronic acid, and proteins, and reduces friction [44]–[46]. Xiong et al. observed intriguing behavior of the coefficient of friction (COF) in hydrated MPC polymer brush films [47]. They found that the COF increased over time owing to wear; however, the rate of increase gradually decreased. They attributed this phenomenon to the transformation of brush polymers into free polymers owing to the shear-induced cutting. In solution, these free polymers may intervene at the sliding interface and contribute to the friction reduction.

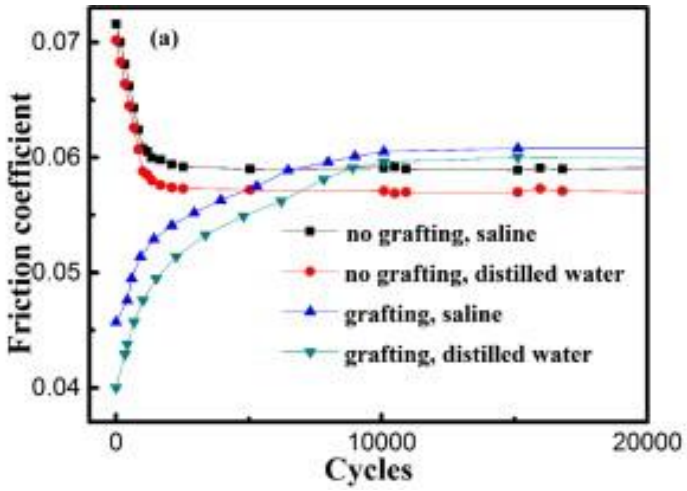

Fig. 1.7 COF of untreated and MPC polymer brush modified UHMWPE [47].

These free polymers, which exist in the surrounding solution, are expected to contribute to the lubrication effect either by simply adsorbing onto the brush layer (thus reducing friction by limiting solid–surface contact) or by coupling with the polymer brush (thus altering the physical properties of the brush, such as its density). For sliding

interfaces with polymer brushes on both surfaces, the interpenetration of the polymer brushes affects the brush density and shear viscoelasticity, leading to deteriorated lubrication performance [48], [49]. Therefore, we speculate that a mechanism different from brush film-to-brush film interpenetration is responsible for the observed effects because free polymers are expected to enhance lubricity. Although numerous studies have been conducted on the behavior of polymer brushes in single-component solvents, the influence of free polymers in these solvents has rarely been explored. Eiser et al. performed surface force apparatus (SFA) measurements to observe the effect of free polymers on the swelling and normal forces of a polymer brush and reported the possibility of coupling between the free polymer chains and polymer brushes [50]. Goujon et al. performed molecular dynamics simulations and reported that a small number of shearing-induced detached polymer chains could significantly improve lubrication properties. They explained that this improvement in the lubrication properties corresponded to the formation of a free-chain region, which exhibited bulk-like behavior in the central area of the shear gap by the detached polymer chains. This phenomenon resulted in an increase in viscosity and minimized the interpenetration of molecular brushes into the upper and lower surfaces [51]. Goicochea et al. conducted extensive simulations, which revealed that adding free polymers to a polymer brush stabilized the film, thereby reducing the friction [52]. Despite extensive simulation-based investigations and interpretations, systematic and experimental studies on the effects of free polymers

on MPC brushes are limited.

1.3 Research Objective

To understand the hydration lubrication mechanism of MPC polymer brush and further enhance its lubrication performance, this study was designed with two primary objectives. The lubrication principles proposed in prior research vary, mainly due to the lack of a unified understanding of the hydration state of the film under different load conditions. Therefore, the first objective was centered on the utilization of an improved fiber wobbling method (FWM) [53] to measure the shear viscoelasticity of a hydrated MPC polymer brush film, specifically investigating how this property is affected by the width of the gap between surfaces, and to elucidate the relationship between the viscoelastic behavior of the film and its frictional properties. FWM is a measurement method developed by Itoh et al.. Unlike nanoindentation, FWM measures the shear viscoelasticity by vibrating the probe in the shear direction. FWM can measure soft and thin-film samples without the influence of the substrate. In our previous study, we successfully measured the shear viscoelasticity of a 2-nm-thick liquid thin film. Therefore, FWM is the most suitable measurement method for this study. This research outcome is expected to elucidate the lubrication mechanisms of MPC polymer brush films under varying degrees of hydration, providing a unified explanation for the lubrication principles proposed in previous studies.

As mentioned in Section 1.2.2, the addition of free polymers is anticipated to enhance the lubrication properties of polymer brush films, reducing wear and extending the lifespan of the lubricant, which is crucial for the maintenance of artificial joints and similar applications. The second objective was to explore the influence of free polymers on the hydration lubrication mechanism of the MPC polymer brushes. We employed various characterization techniques including pin-on-disk (POD) tribometry, neutron reflectivity (NR) measurements, and the fiber wobbling method (FWM) to determine the underlying mechanism of the process. In the POD measurements, the concentration of the free MPC polymer was systematically varied to determine its effect on the COF of the brush film surface. NR measurements were performed to evaluate the changes in the structure of the hydrated brush film caused by the free polymer. FWM was employed to conduct indentation experiments to examine the effects of the free polymer on the shear viscoelasticity of the brush. This approach was adopted because theoretically, the performance of a lubricant film is significantly influenced by its viscoelastic properties [54]–[56]. These findings enhance our understanding of the fundamental mechanisms involved in hydration lubrication and provide insights for designing highly lubricious surfaces using a combination of polymer brush films and free polymers in lubricating fluids.

1.4 Structure of This Paper

This paper methodically explores the concepts, methodologies, and findings surrounding hydration lubrication, with a particular focus on polymer-based systems. The structure is shown in Fig. 1.8, and demonstrated as follows:

Chapter 1 introduces the concept of ultralow friction using hydration lubrication and its significance in the context of energy conservation and carbon neutrality. It delves into the specifics of hydration lubrication using polymers, including a review of previous studies on polymer brushes and the impact of free polymers on improving the lubrication properties. Following this, the research objectives are clearly stated, outlining the scope and direction of this study.

Chapter 2 introduces an innovative shear viscoelastic measurement technique that uses the fiber wobbling method. This chapter is divided into several sub-sections that describe the principle of the fiber wobbling method, experimental setup, and sensitivity of the shear force measurement. Additionally, it addresses the principle of shear gap measurement, calibration of gap versus interference fringe radii, and accuracy of gap measurement.

Chapter 3 provides a detailed analysis of the dependence of shear viscoelasticity on the gap size by utilizing FWM. Initially, the preparation process of the MPC polymer brush was explained, detailing the methods, including photo-induced polymerization,

patterning, and subsequent characterization of the brush film. It then delves into the experimental procedures and results, encompassing the measurements of amplitude, phase shift, and gap size. This is followed by a thorough discussion of how shear viscoelasticity correlates with frictional properties.

Chapter 4 explores lubrication improvements through the synergistic effects of free polymers and polymer brushes. It entails friction tests, neutron reflectivity measurements, and indentation experiments by FWM, offering a comprehensive analysis of the experimental results and discussions on various aspects, such as hydration states, adsorption/desorption of free polymers, and their influence on shear viscoelasticity and lubricity.

Chapter 5 synthesizes the insights and discoveries from the previous chapters, presents a cohesive conclusion to the study, highlights its contributions to the field of lubrication science, and suggests potential avenues for future research.

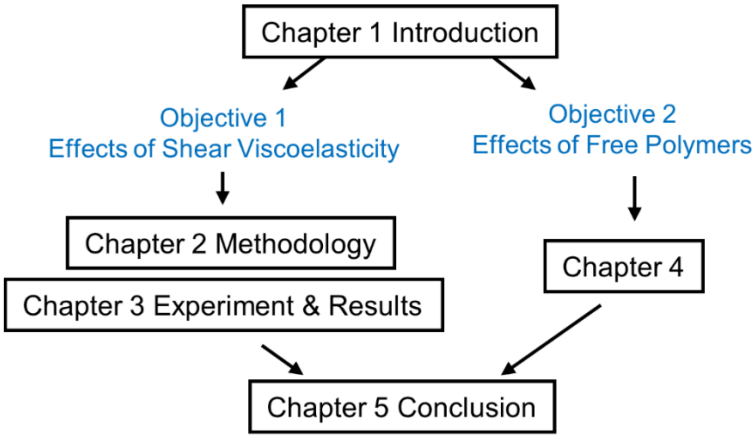

Fig. 1.8 Structure of this paper.

2. Shear Viscoelastic Measurement by Fiber Wobbling Method

2.1 Principle of Fiber Wobbling Method

2.1.1 Shear Force Detection and Viscoelasticity Measurement

FWM is a rheology measurement method that is used to determine the in-plane shear viscoelasticity of thin films, focusing on lateral dynamics [53]. FWM offers advantages such as high detection sensitivity for shear force and precise control of the shear gap width. A schematic of the system is shown in Fig. 2.1(a). FWM uses an optical fiber with a spherical tip as a probe for shear force detection. The optical fiber probe was made of glass with a fiber length of approximately 2 mm, diameter of approximately 100 μm, and spherical tip diameter of approximately 200 μm. The surface roughness of the sphere is approximately 0.2 nm, indicating that it is extremely smooth. The upper end of the probe was fixed to a piezo actuator on a rigid steel base. The piezo actuator is oscillated by a sinusoidal input voltage with constant amplitude and frequency and forces the probe's spherical tip to horizontally shear the film on the substrate. The viscoelasticity of the sample confined in the nanogap caused changes in the oscillation amplitude of probe tip X and phase shift δ, whereas the fixed end of the oscillating probe remained constant. We used the cylindrical surface of the probe as a lens to focus the laser beam on a two-segmented photodiode that served as a position-sensitive detector (PSD) [53] to measure

X and δ. Typically, discussions about the viscoelasticity of objects can utilize the Maxwell model or the Voigt model. In the Maxwell model, the object is simplified as a series combination of a Newtonian damper and a Hookean elastic spring, whereas in the Voigt model, it is a parallel combination of these two elements. The Maxwell model effectively represents materials that begin to stretch immediately upon stress application and continue to stretch gradually over time (viscous flow), making it suitable for expressing long-term viscous flow or creep phenomena. On the other hand, the Voigt model accurately depicts materials that stretch immediately by a fixed amount upon stress application and then stretch little or not at all (a combination of elastic solid behavior and viscosity), making it appropriate for representing immediate responses to short-term stress and elastic recovery after stress removal. The FWM shears the sample at a constant amplitude and high frequency, therefore, the Voigt model was applied as a mechanical model of the hydrated polymer brush film. As shown in Fig. 2.1(b), viscous damping coefficient of the Newtonian damper is c, and elastic modulus of the Hookean elastic spring is k. In addition, we assumed the probe to be a single-degree-of-freedom oscillator consisting of an effective mass m, spring with a spring coefficient k_p, and damper with a damping coefficient c_p. The motion of the system is expressed as

$$m\ddot{x} + k_p(x - x_0) + c_p(\dot{x} - \dot{x_0}) + kx + c\dot{x} = 0 \qquad (2.1)$$

$$x_0 = a_0 sin\omega t \qquad (2.2)$$

Here a_0, ω, and t are the amplitude of the forced oscillation, frequency of the forced oscillation, and time, respectively. By solving Eq. (2.1) and (2.2), the damping coefficient c and elastic modulus k of the sample, which are expressed in Eqs. (2.3) and (2.4), respectively:

$$c = \frac{a_0}{X\omega}\left[\left(k_p - m\omega^2\right)tan\delta + c_p\omega\right]\sqrt{\frac{k_p^2+c_p^2\omega^2}{(1+tan^2\delta)\left[\left(k_p-m\omega^2\right)^2+c_p^2\omega^2\right]}} - c_p \quad (2.3)$$

$$k = \frac{a_0}{X}\left(k_p - m\omega^2 - c_p\omega tan\delta\right)\sqrt{\frac{k_p^2+c_p^2\omega^2}{(1+tan^2\delta)\left[\left(k_p-m\omega^2\right)^2+c_p^2\omega^2\right]}} - \left(k_p - m\omega^2\right) \quad (2.4)$$

The mechanical properties of the probe, namely m, k_p, and c_p, were determined experimentally before viscoelastic measurements [53]. By measuring the values of X and δ, we can obtain the viscoelastic response of the sample, as represented by the viscous damping coefficient c and elastic modulus k. These shear viscoelastic responses were averaged over the region where the spherical probe tip was in contact with the polymer film.

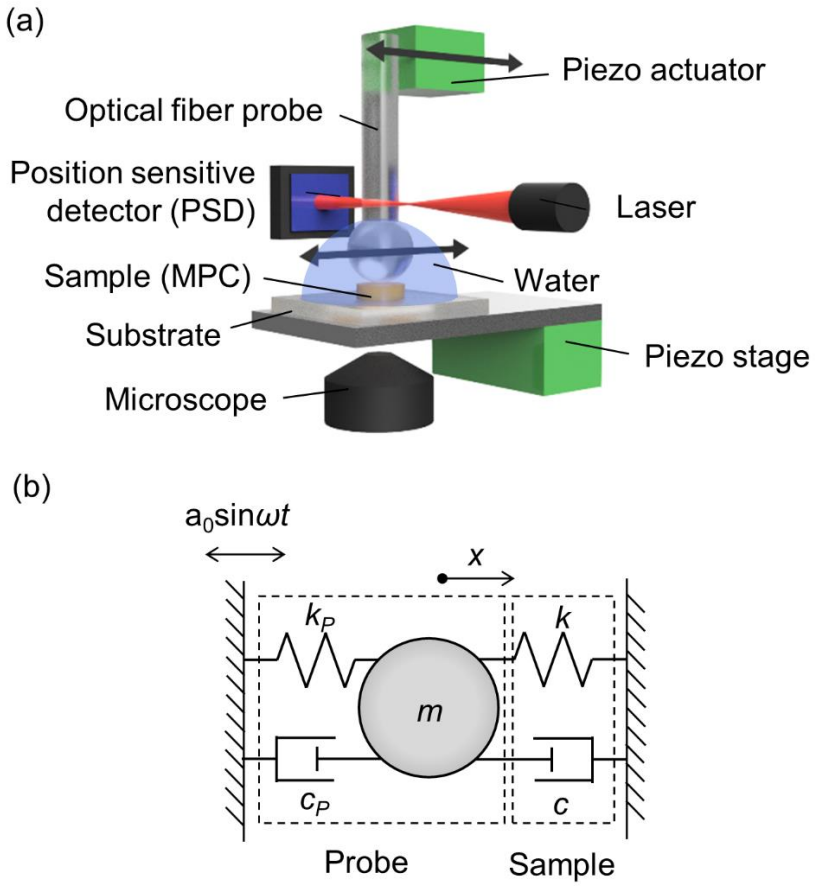

Fig. 2.1 Schematic diagram of FWM. (a) Setup for FWM. (b) Mechanical model of oscillation system for viscoelastic measurements using FWM.

2.1.2 Experimental setup

The experimental setup for viscoelastic measurement using FWM is shown in Fig. 2.2. Figure 2.3 shows photos of the FWM developed in this study. The signal from the function generator was amplified to vibrate the piezo actuator for probe excitation. A laser diode with a wavelength of 633 nm was used to detect probe tip oscillation. The output of the PSD was linear to the displacement of the laser spot focused by the fiber, and was synchronously detected using a lock-in amplifier with the reference signal of the piezo

actuator driving signal. The lock-in amplifier outputs the amplitude X and phase shift δ of the input signal. X and δ are used to calculate damping coefficient c and elastic modulus k of the sample.

The lock-in amplifier also detects the asynchronous component of the probe oscillation to detect the solid contact between the probe tip and substrate surface. When the probe comes in contact with the substrate, the surface asperities act as random forces on the probe and cause an increase in the asynchronous component [53]. All the measurement data from the lock-in amplifier were recorded on a personal computer.

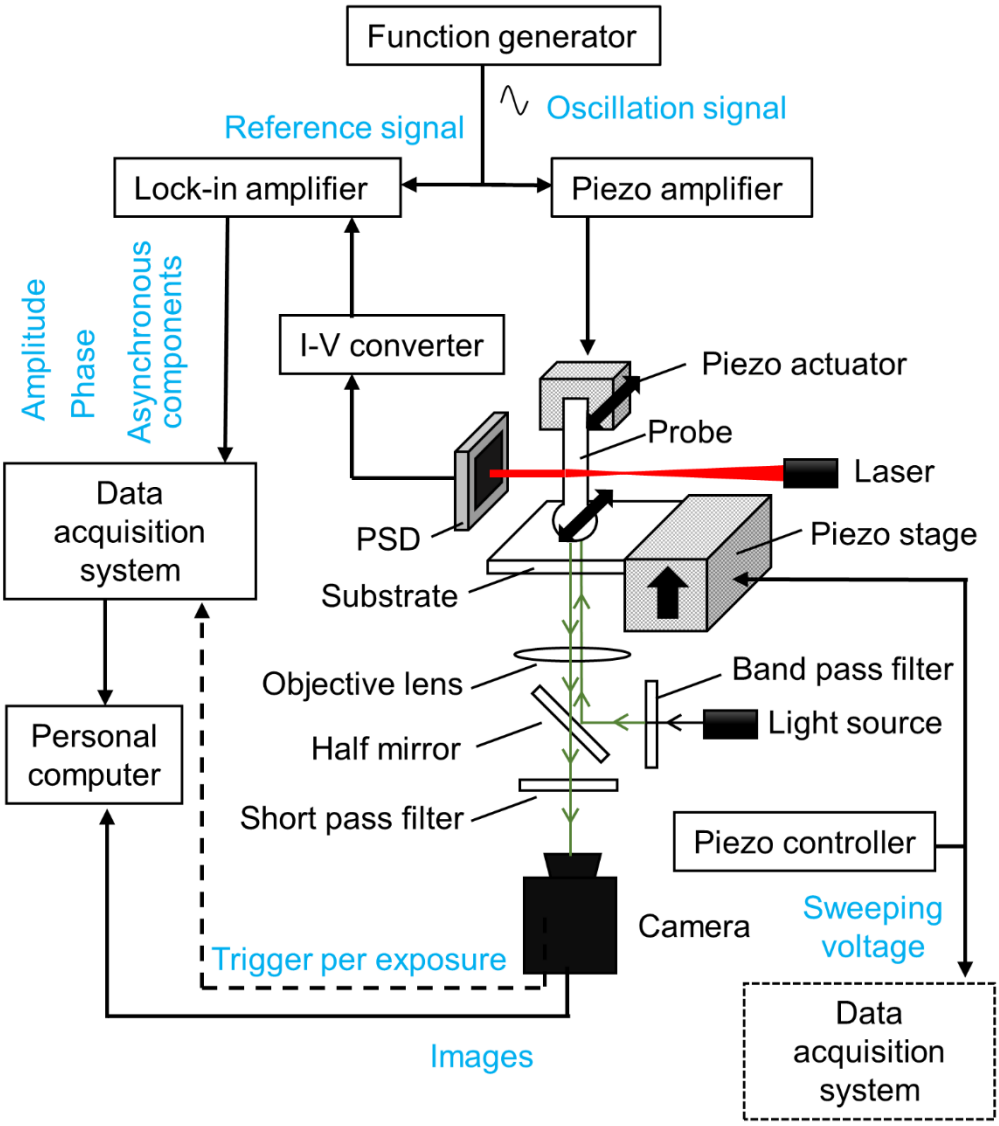

Fig. 2.2 Experimental setup for viscoelasticity and shear gap measurements using FWM.

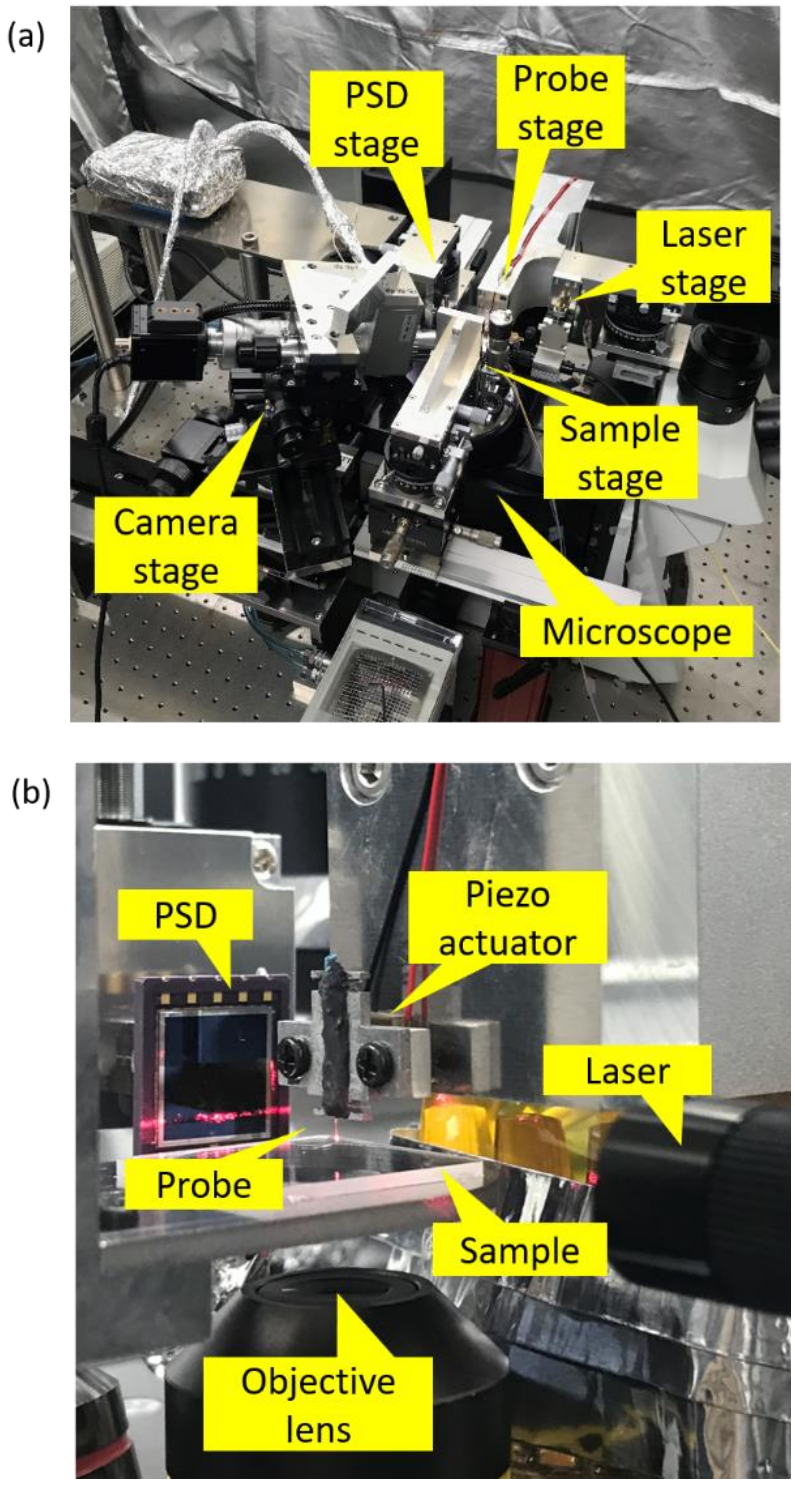

Fig. 2.3 Photos of FWM. (a) System outline. (b) Core part of the system.

The gap between the probe and sample was controlled using a piezo stage. The interference fringes obtained through microscopic observations enabled precise measurements of the shear gaps. We used an IX73 (Olympus) inverted microscope and a TH4-100 (Olympus) halogen lamp as a light source. An FBH520-40 (THORLABS) bandpass filter was used to obtain monochromatic light with a wavelength of 500–540 nm for interference fringe observations. A BSW10R (THORLABS) beam splitter was used as the half-mirror. As laser light with a wavelength of 633 nm was used in the FWM scattered on the probe surface and adversely affected the observation of interference fringes, we used a FESH600 (THORLABS) short-pass filter to cut it. An LMPlanFLN 100X (Olympus) objective lens with an N.A. of 0.80 was used. In the early system, an LCPlanFI 60X (Olympus) objective lens with an N.A. of 0.70 was used. Their performances are compared in Section 2.2.4. Interference fringes were recorded using an ORCA-Flash4.0 V3 Digital CMOS camera C13440 (Hamamatsu Photonics). We used the trigger signal from the camera to synchronize the image capture timing with data acquisition. Images were captured at 100 fps with an exposure time of 10 ms, which was sufficiently high to measure the gap change during the viscoelastic measurements.

2.1.3 Sensitivity of shear force measurement

The sensitivity of shear force measurement was evaluated using the improved system. First, the piezo actuator was calibrated. We vibrated the piezo actuator sinusoidally with

an excitation frequency from 100 Hz to 1 kHz in steps of 100 Hz, and from 1 kHz to 10 kHz in steps of 1000 Hz. For each frequency, the sinusoidal voltage amplitude was changed from 1 to 10 V in step of 1V. The displacement of the piezo actuator surface was measured using a laser Doppler vibrometer. The amplitude was measured using a lock-in amplifier with the excitation signal as a reference. In each test, the piezo actuator was vibrated for 100 s, and the average amplitude was used for calibration. The results are shown in Fig. 2.4.

The amplitude sensitivity of the voltage output was evaluated by measuring the signal-to-noise ratio (SNR). The sensitivity of force measurement was calculated according to Hooke's law. The elastic coefficient of the probe was a known value (approximately 100 N/m). The results of the amplitude measurements are shown in Fig. 2.5. The output signal exhibited good linearity with respect to amplitude. The average noise was 1.43 μV. Signals lower than this value are not detected. Thus, the amplitude detection limit was 0.002 nm, which corresponds to the PSD output signal of 1.43 μV. Therefore, the force detecting limitation was approximately 0.2 nN (varies owing to the difference in the elastic coefficients of the different probes). According to our previous research, the shear force on the probe was approximately 100 nN. Thus, we conclude that the new system can be used for rheological measurements of MPC polymer-brush films.

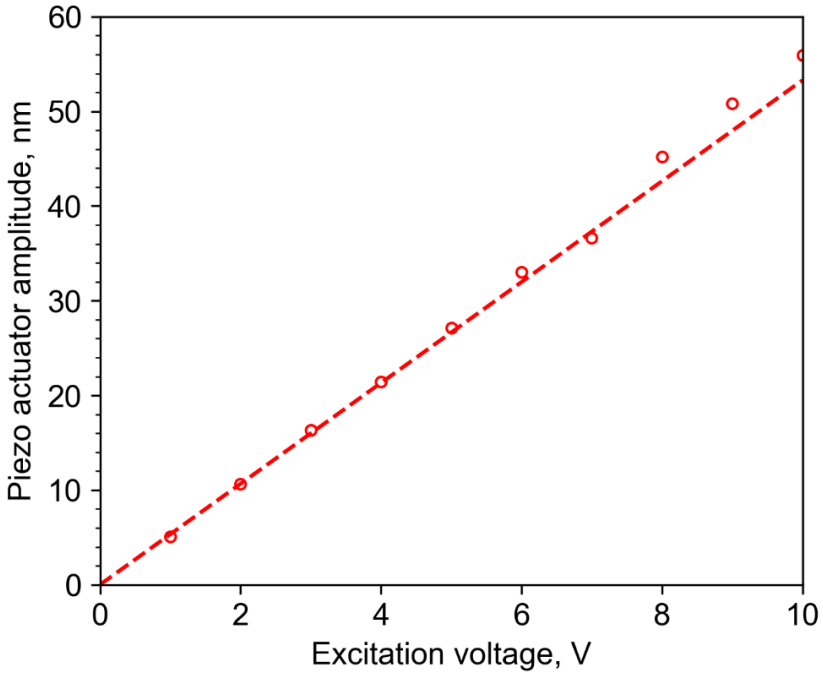

Fig. 2.4 Amplitude of piezo actuator over excitation voltage.

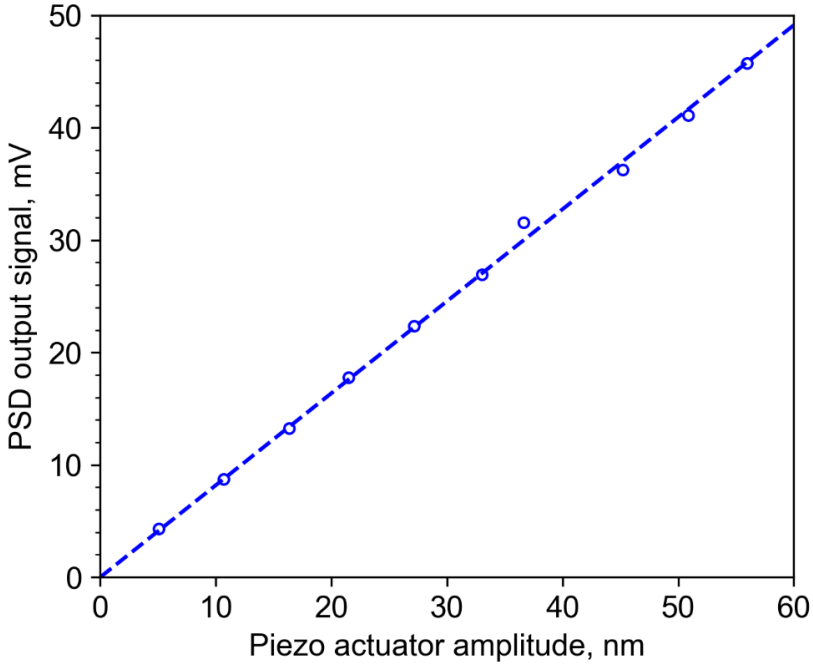

Fig. 2.5 Output signal of PSD over amplitude of piezo actuator.

2.2 Principle of shear gap measurement

2.2.1 Gap measurement by interference fringes

As shown in Fig. 2.6, in our previous study using FWM, we determined the shear gap between the probe tip and substrate by precisely detecting the solid contact by monitoring the increase in asynchronous components. The term 'gap' denotes the minimum distance between the spherical probe tip and the substrate. Figure 2.7 shows the typical asynchronous component of the probe tip measured in pure water in a narrowing gap. If the probe rigidity in the direction perpendicular to the substrate is sufficiently large compared with the sample stiffness (e.g., liquid sample), we can consider the gap change to be the same as the piezo stage displacement. Then, because the piezo displacement is known, the shear gap is known when the origin of the gap, namely the solid contact, is identified. However, the brush film to be measured in this study was chemically bonded to the substrate; therefore, it could not be easily squeezed out from the gap, making it difficult to detect a solid contact. Consequently, we had to measure the shear gaps during the viscoelastic measurement.

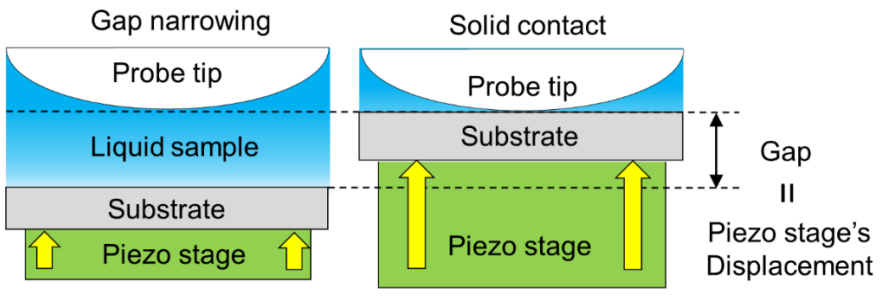

Fig. 2.6 Schematic diagram for determining shear gap with asynchronous detection.

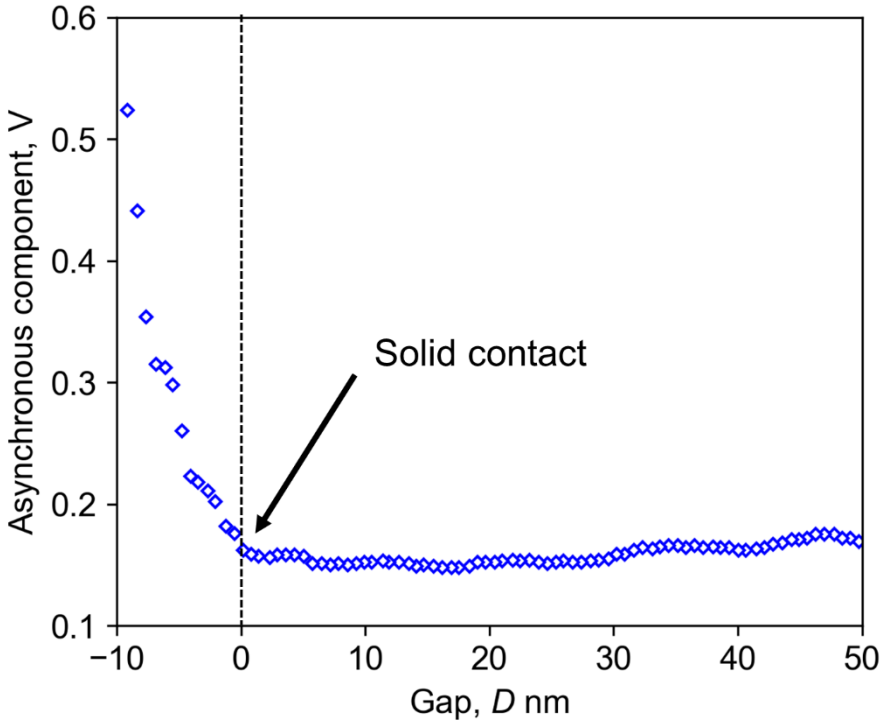

Fig. 2.7 Asynchronous components were measured in pure water with a narrowing gap.

We controlled the shear gap using a piezo stage on which the sample was mounted, and optical interferometry was used to determine the exact shear gap during the viscoelastic measurement. When interferometry is used, the medium in the gap must be homogeneous and have a constant refractive index. However, hydrated polymer brush films have a density distribution in the gap direction, resulting in a distribution of the refractive index. In addition, the refractive index changed with the narrowing of the shear gap during viscoelastic measurements. To avoid the effects of uncertainty in the refractive index, we proposed the method shown in Fig. 2.8(a) and (b). Viscoelastic measurements using FWM require the probe tip to make contact with only a small area of the film

(typically a few micrometers in diameter). Thus, to measure viscoelasticity, it is sufficient to have a patterned film only on the contacting area, instead of a film covering the entire substrate. The shear gap can be measured from the interference fringes (i.e., Newton rings) formed by light passing through the pure water surrounding the MPC film. Figure 2.8(b) shows a schematic of the light interference image observed by the microscope. The fringes of equal chromatic order (FECO) interferometry technique employed in SFA is a well-known method for high-precision gap measurements. However, FECO requires the formation of a precisely designed layered structure on the surface of the probe. The probe used in this study had a spherical shape with a radius of 100 μm, making it difficult to form such a layered structure. Consequently, we employed monochromatic light, specifically within the 500–540 nm wavelength range, to observe the interference fringes. Subsequently, we processed the obtained images through binarization to calculate the radius of the Newton's rings, utilizing the radius to determine the gap. This method can determine the gap with a precision of up to 5 nm (For detailed content, see Section 2.2.4). Although its precision is inferior to that of FECO (at the 0.1 nm level), our proposed method remains valid because the hydrated polymer film thickness measurements in this experiment reach several hundred nanometers. The details of the patterning of the samples are described in Section 3.1.2.

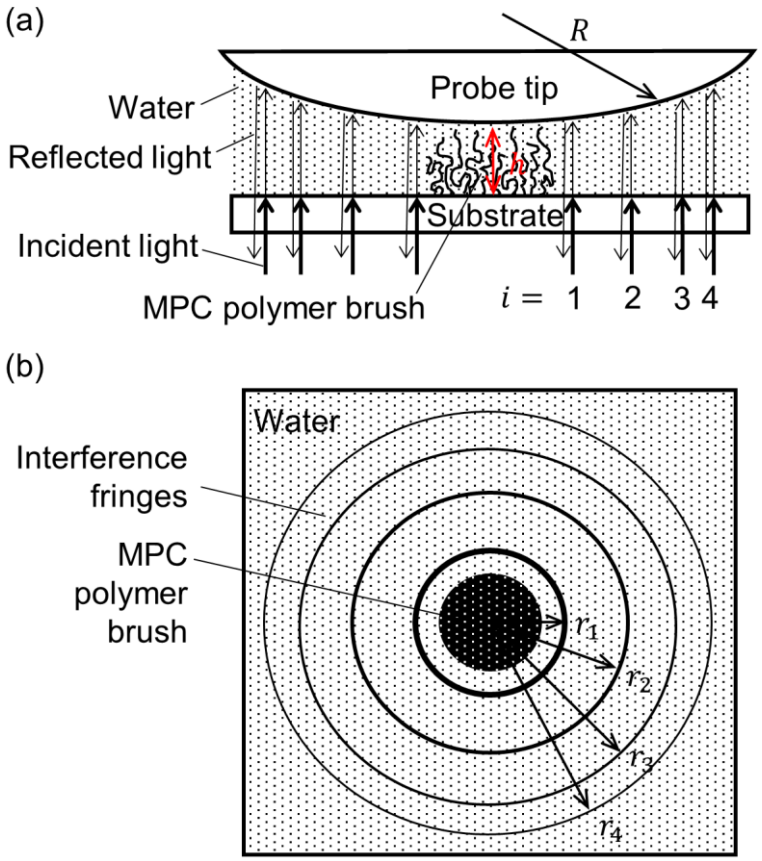

Fig. 2.8 Schematic of (a) light interference due to light reflected from the probe and substrate. (b) Light interference observed under a microscope.

2.2.2 Measurement and analysis of interference fringes

To obtain the radius of the Newton rings, our initial step involved binarization of the images. To mitigate the effect of uneven brightness distribution on the binarization process, we employed the NIblack local binarization algorithm. A representative image of a Newton ring, as shown in Fig. 2.9, was analyzed, where the dark fringes were designated a luminance value of 255 (white) and the remaining areas were set to 0 (black), thereby generating an image of concentric circles.

In image processing, the Hough Circle Transform is a widely recognized method for circle detection. However, given the proximity in the radii of concentric circles, utilizing the Hough Circle Transform poses the risk of misidentifying different order fringes as a single fringe. Additionally, factors such as contamination on the probe tip surface and uneven luminance distribution could result in incomplete fringes or conjoining of fringes of different orders, further complicating circle detection using this method. Consequently, we opted for the dark ring radius methodology reported by Tang et al. [57], which is straightforward and robust for measuring the radii of concentric circles.

Our approach involved a preliminary step to eliminate portions of the binarized image affected by merging or blurring due to contamination of the optical system, which consistently appeared at the same location in the images. This was achieved by applying a mask. In addition, to reduce the computational load, the corners of the image were excluded.

The binarized images were opened in ImageJ, and a rough estimate of the circle center (hypothetical center) was determined using the circle selection tool. Subsequently, we computed the distance (hypothetical radius) from all points with a luminance of 255 to this hypothetical center and sorted these distances in ascending order of their values. The hypothetical radii of points on the same interference fringe are almost equal. Therefore, by sequentially comparing the sorted hypothetical radii, if there is a sudden increase compared to the previous value, we can determine that it belongs to a different

order of interference fringe from the previous one. Following this method, we can group all the hypothetical radii, with each group corresponding to a single interference fringe. Owing to the presence of white dots (noise) between the two fringes, which could be mistakenly identified as part of the interference fringes, we eliminated groups with significantly fewer counts, deeming them noise. The average value for each group provides the estimated radius of each fringe.

This process was initially performed on ten image frames. For each frame, the calculation was repeated in a 5×5 pixel area around the hypothetical center. For each hypothetical center, we calculated the standard error of the hypothetical radii of all groups. The point with the smallest average standard error was designated as the true center for the particular image. The average of the true centers from these ten images were then considered as the accurate centers for all images. Following this methodology, we determined the radii of all the concentric circles across the images. The binarization of the image and mask processing was implemented using a LabVIEW program, while the radius was calculated using a Python script.

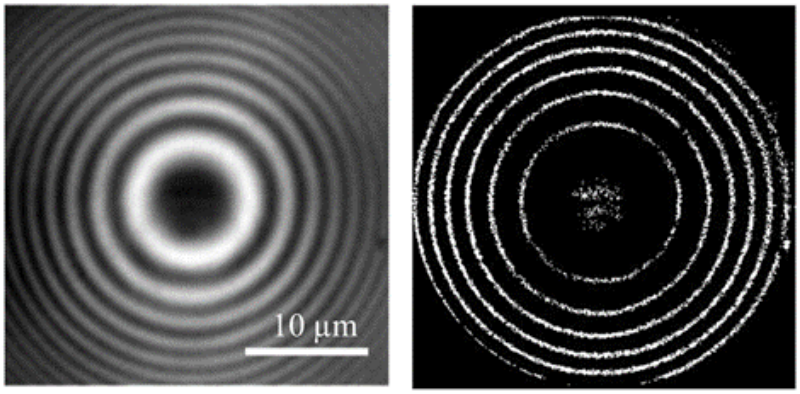

Fig. 2.9 Photo of interference fringes and their binarization result.

2.2.3 Calibration of gap versus interference fringes' radius

To verify the accuracy of the developed gap measurement system, we observed interference fringes on a glass substrate without a brush film, while reducing the gap at a constant rate. The gap between the probe tip and substrate was filled with pure water. As no brush film exists, solid contact between the probe and substrate can be detected by the increase in the asynchronous component, as described in Section 2.2.1. The horizontal axis is the shear gap determined from the displacement of the piezo stage with the point of increase in the asynchronous component as the origin. As we reported previously [58], the asynchronous component can detect solid contacts with high sensitivity for a gap change of 1 nm or less.

As shown in Fig. 2.8(a), the sliding surface is a combination of a spherical surface (probe tip) and a plane surface (substrate), with light incident vertically from the substrate

side. Newton rings are formed by the interference of light reflected from the substrate and probe tip surfaces (Fig. 2.8(b)). According to this geometry, we used the dark rings to measure the minimum shear gap width between the substrate and the probe tip, h, as

$$h = -R + \frac{i\lambda}{2n} + \sqrt{R^2 + r_i^2} \tag{2.5}$$

where R is the curvature radius of the probe tip, i is the order of the dark rings, λ is the wavelength of the incident light, n is the refractive index of the medium (pure water), and r_i is the radius of the i^{th}-order dark Newton ring. As R, n, and λ are constant, h can be obtained by measuring r_i.

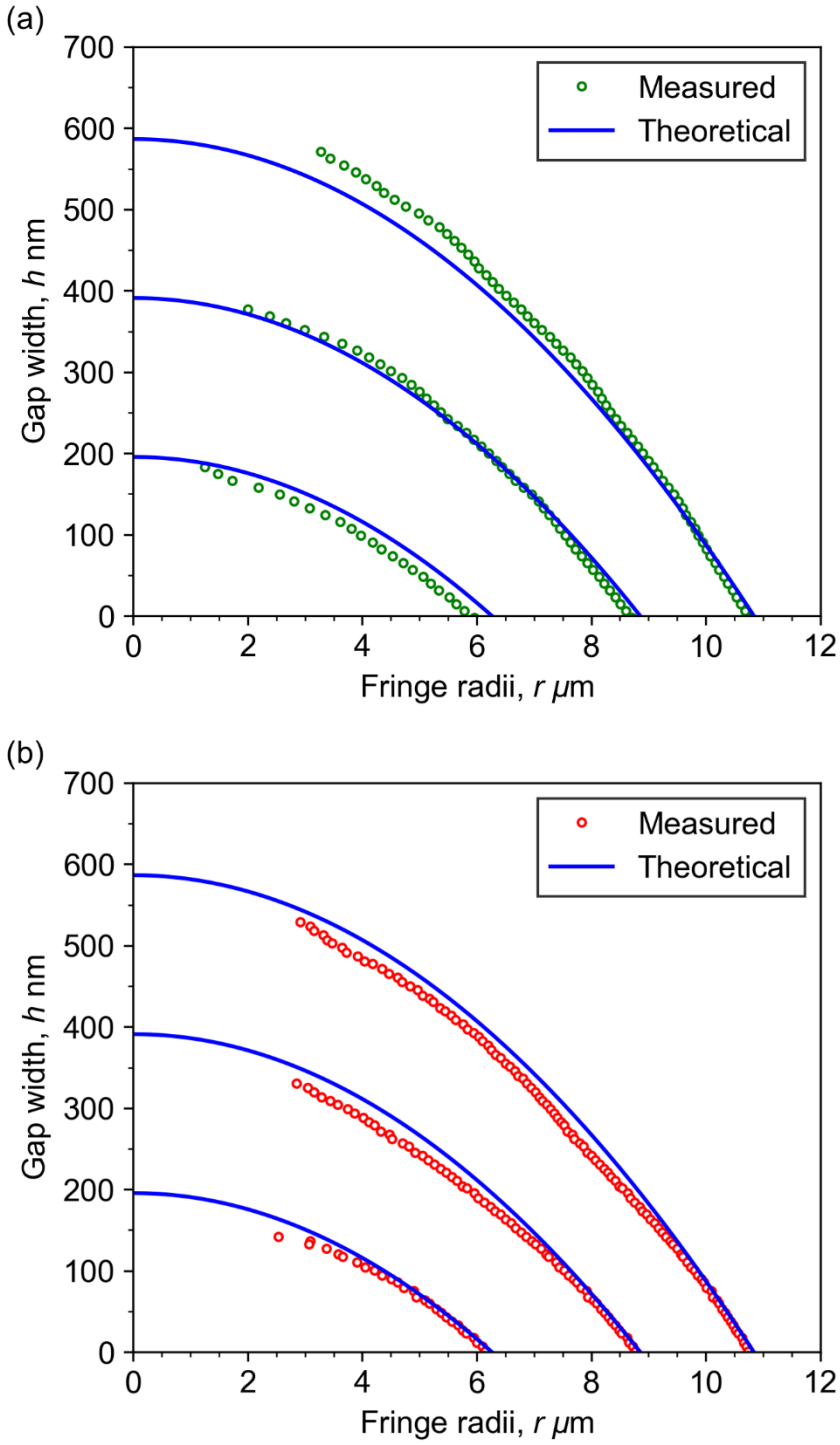

Fig. 2.10 Theoretical and typical experimental results of the relationship between the gap width and radius of the first three fringes measured by (a) LCPlanFl 60X lens, (b) LMPlanFLN 100X.

The relationships between the shear gaps, which were determined by the piezo stage displacement from the solid contact point, and the radii of the 1st, 2nd, and 3rd fringes obtained by microscopic observation are shown in Fig. 2.10. The solid lines in Fig. 2.10 show the theoretical curves of Eq. (2.5) for R = 100.49 μm , n = 1.33, and λ = 0.52 μm. The curvature radius, R, of the probe tip was measured experimentally. The good agreement between the theoretical curve and experimental results indicates the validity of the measurement. However, the larger the gap, the greater is the deviation of the experimental values from the theoretical values. This is attributable to several possibilities, including the incident light not being exactly parallel, and the probe tip not being a perfect sphere. Therefore, we used an experimentally obtained calibration curve to determine the shear gap in viscoelastic measurements. Based on the concept of the shear gap measurement shown in Fig. 2.8, the relationship between the gap and ring radius measured on the glass substrate without a brush film can be applied to the case with patterned brush films. Ten measurements were performed at different positions on the glass substrate to obtain the calibration curve. Based on Eq. (2.5), the experimental data were fitted as follows:

$$h = a + \sqrt{b - r_i^2} \tag{2.6}$$

where a and b are the fitting parameters, as presented in Table. 2.1.

Table. 2.1 (a) Fitting results of parameters in Eq. (2.6) using LCPlanFl 60X.

i	a	b
1	-103.93	10838.37
2	-99.13	9902.86
3	-94.53	9053.36

(b) Fitting results of parameters in Eq. (2.6) using LMPlanFLN 100X.

i	a	b
1	-110.83	12321.01
2	-105.21	11143.98
3	-102.22	10564.92

2.2.4 Gap measurement accuracy

The performances of the two objective lens are compared in Fig. 2.11. The difference between the average of the 10 measurements and the fitting result is shown as the fitting error. This result indicated that the gaps could be identified with an accuracy of approximately 5 nm. We also plotted the random error obtained by calculating the standard deviation of the data from 10 measurements taken at 100 fps. For the LCPlanFl 60X lens, the random error tends to increase with the gap size, being approximately 4–6% of the gap. However, the random error for the LMPlanFLN 100X lens remains stable and comparable to the fitting error. Although the fitting error of the LCPlanFI 60X lens is smaller, the LMPlanFLN 100X lens outperforms it when considering a broader measurement range. The measurement accuracy limit of this system was approximately 5 nm.

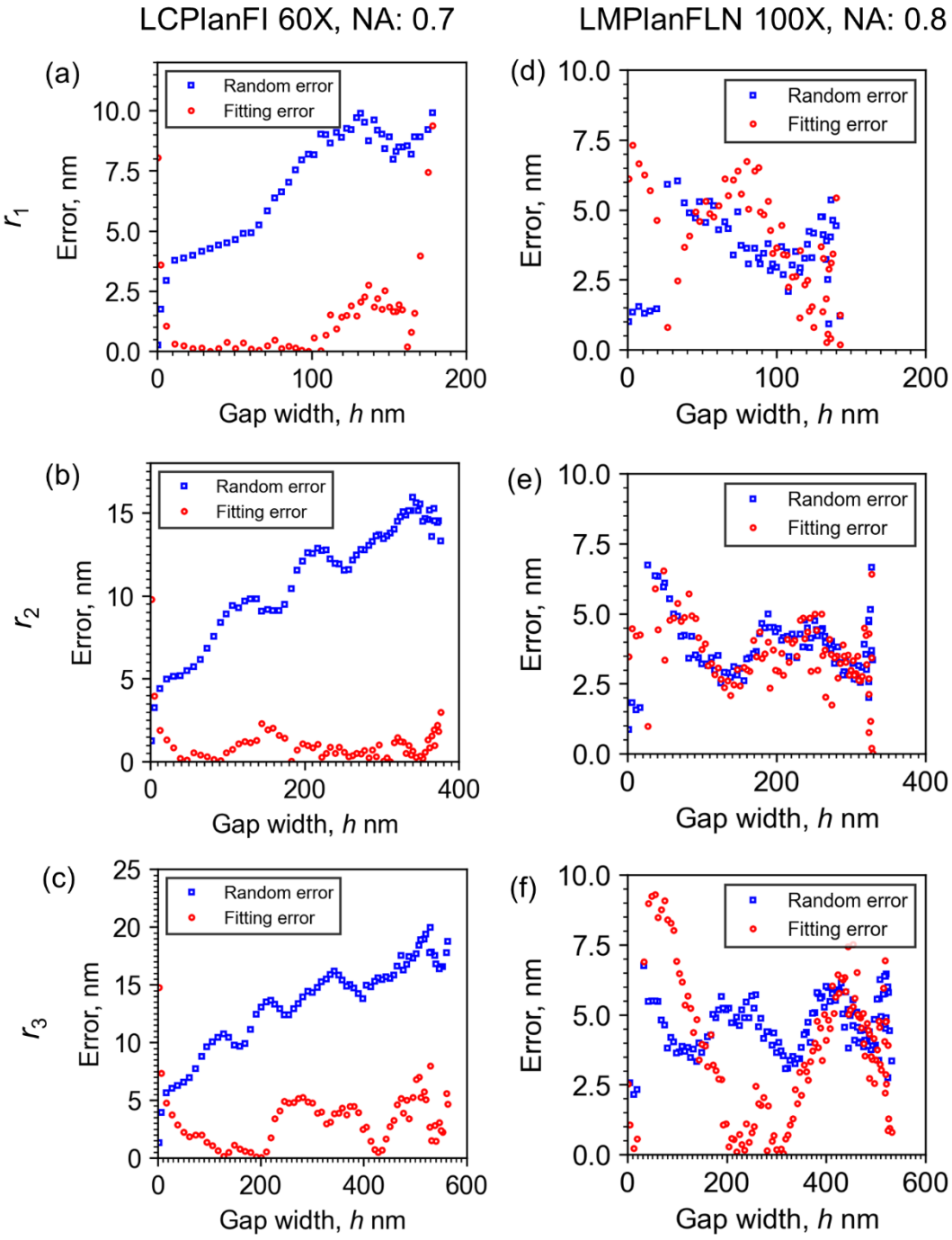

Fig. 2.11 Fitting and random errors of the gap measured with different fringes using LCPlanFl 60X lens ((a) ~ (c) corresponds to fringes r1 ~ r3) and using LMPlanFLN 100X lens ((d) ~ (f) corresponds to fringes r1 ~ r3).

3. Correlation between viscoelastic Response and frictional properties of polymer brush

3.1 Preparation of MPC polymer brush

3.1.1 Photo induced polymerization

The photopolymerization process of MPC polymer brush is show in Fig. 3.1. First, we prepared parylene C coated glass substrate. The quartz glass substrate was treated with oxygen plasma for 15 min to eliminate organic contamination on the surface and to enhance the adherence of parylene C. Parylene C was coated on the substrate by chemical vapor deposition using a parylene coating device (DACS-LAB, KISCO). The initial reactant was di-p-xylylene (dimer). Di-p-xylylene was placed in a vaporizer and heated to 180°C at normal pressure for evaporation. Subsequently, the dimer vapor was passed into a pyrolyzer, where the pressure was reduced to 0.5 atm and the temperature was increased to 650°C; thus, the dimer was pyrolyzed to a monomer. The monomer gas polymerized on any surface in the vapor deposition chamber at room temperature and 0.1 atm to form a thin film of parylene C.

Next, the photopolymerization initiator, benzophenone (Tokyo Chemical Industry Co., Ltd.), was coated on the substrate using a dip-coating device. The parylene C coated substrate was immersed in an acetone solution (1 wt.%) of benzophenone for 1 min so

that benzophenone molecules could adsorb fully to the substrate. Subsequently, the motor pulled the substrate out of the solution at a speed of 0.3 mm/s. A thin film of an acetone solution of benzophenone was forced to form on the surface owing to surface tension. As acetone evaporated quickly, a thin film of benzophenone remained on the surface. The substrate was then dried under 1500 Pa in the dark (benzophenone decomposes in light) to evaporate acetone.

MPC monomer's pure water solution (7.38 wt.%) was used for the polymerization. MPC monomer solution was degassed under 1500 Pa for 30 min to remove oxygen that inhibits the radical reaction. Using a pipette, 10 μL of MPC solution was dropped onto the dried substrate and covered with a cover glass to prevent the solution from evaporating. The center wavelength of the ultraviolet (UV) light was 365 nm and the power was 760 mW/mm^2. The exposure temperature was maintained at 20°C using a cooling-water circulation device. Empirically, with an exposure time of 40 min, an MPC polymer brush film (thickness: 50 nm) was formed. After UV exposure, the substrate was immersed in pure water to wash off residual monomers.

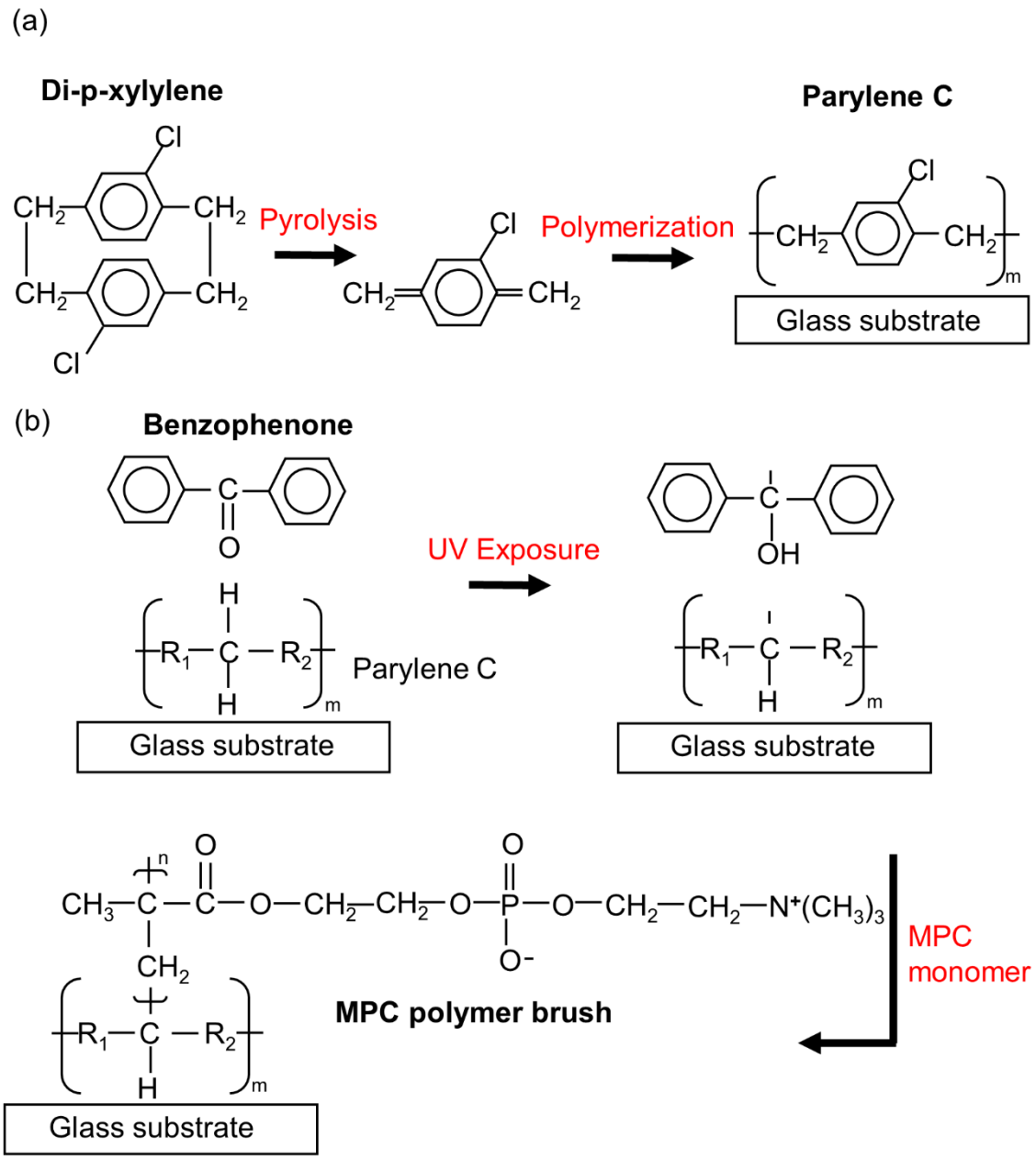

Fig. 3.1 Schematics of (a) chemical vapor deposition of parylene C and (b) photopolymerization of MPC polymer brush on parylene C film.

3.1.2 Patterning of the MPC polymer brush film

The process of patterning the MPC polymer brush films is illustrated in Fig. 3.2. To

form the patterned MPC film, we first patterned the parylene C film using photolithography. Parylene C was coated on a glass substrate by chemical vapor deposition using a parylene coater (DACS-LAB, KISCO) (Fig. 3.2①). The parylene C thin film was then annealed at 300°C for 3 min and naturally cooled to 25°C in vacuum to reduce residual stress and enhance film adhesion. Next, the photoresist (OFPR-800, TOKYO OHKA KOGYO CO.) was coated on the parylene film by spin coating (Fig. 3.2 ②). The substrate was pre-baked at 90°C for 5 min.

We prepared a glass photomask of octagon patterns with a side length of 4 μm. If the octagon is approximated as a circle, its diameter is approximately 10 μm. Each pattern was 200 μm apart; thus, the probe tip (diameter, 200 μm) could make contact with only one patterned film at a time. After exposure through the photomask, the photoresist film was developed using a developer solution (NMD-3, 2.38%) for 60 s (Fig. 3.2③). Next, the substrate was post-baked at 120°C for 5 min. We removed the uncovered parylene C film using an O_2 plasma asher (Fig. 3.2④). The residual photoresist was removed with acetone (Fig. 3.2⑤). We dip-coated the benzophenone film on the parylene C surface using the acetone solution of benzophenone (1 wt%) (Fig. 3.2⑥). The substrate was dried in a light-shielded vacuum desiccator to remove acetone completely. We dropped the degassed MPC monomer's pure water solution (7.38 wt%) on the substrate and covered it with a thin glass plate to prevent water evaporation during photopolymerization (Fig. 3.2⑦). Subsequently, we irradiated the substrate with ultraviolet (UV) light with a center

wavelength of 365 nm and a light power of 760 mW/mm^2 for 40 min (Fig. 3.2⑧). During UV irradiation, the substrate temperature was maintained at 20°C using a chiller. After UV exposure, the substrate was immersed in pure water to remove residual monomers. Finally, the films were naturally dried at room temperature. Figure 3.3 shows typical topographic images of the patterned MPC polymer film measured by atomic force microscopy (AFM). Figure 3.3(c) shows the film profile. The parylene C film had a thickness of 30 nm, and the MPC polymer film had a central film thickness of approximately 70 nm in air. The diameter of the patterned films was about 10 μm.

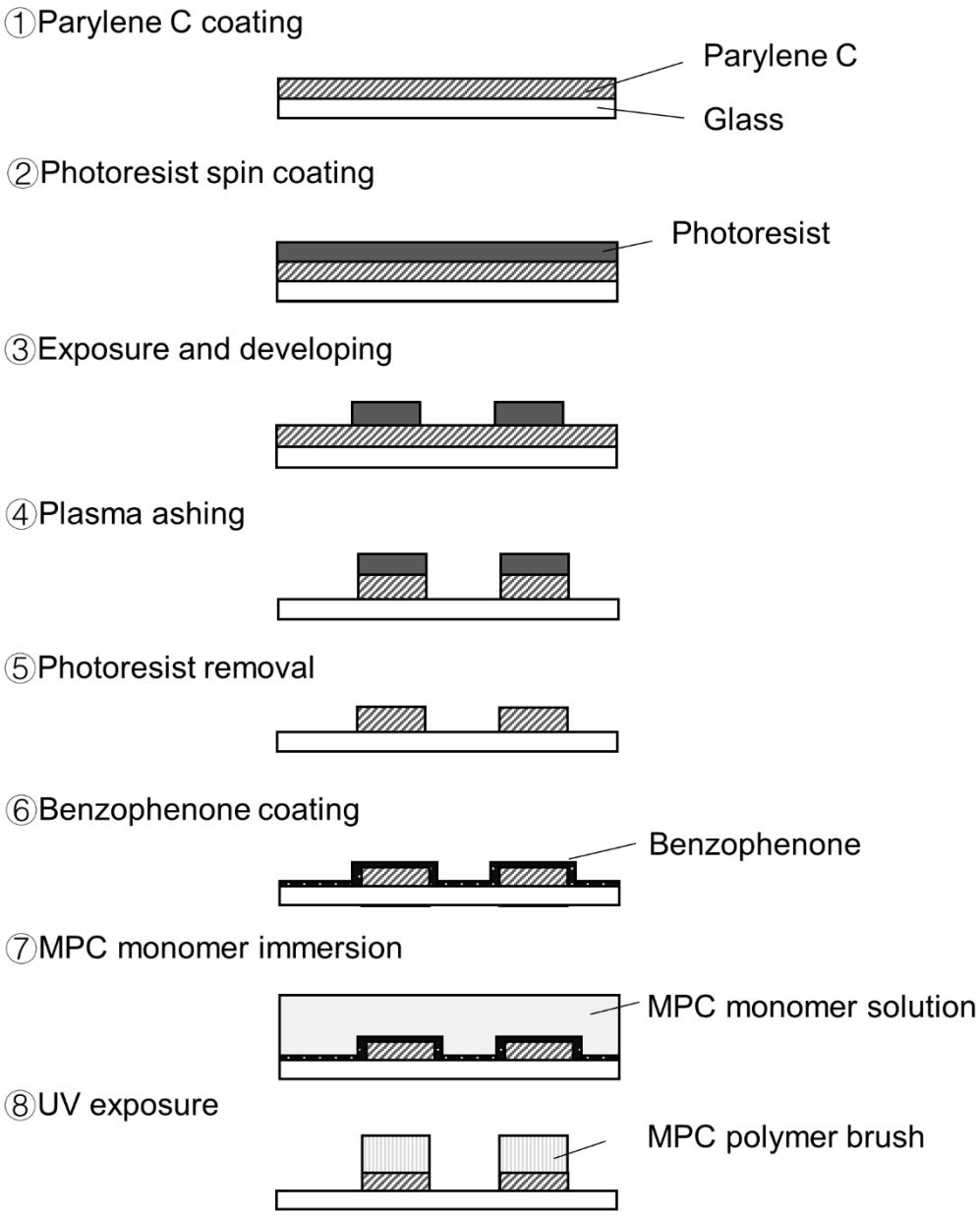

Fig. 3.2 Process of patterning the MPC polymer brush film.

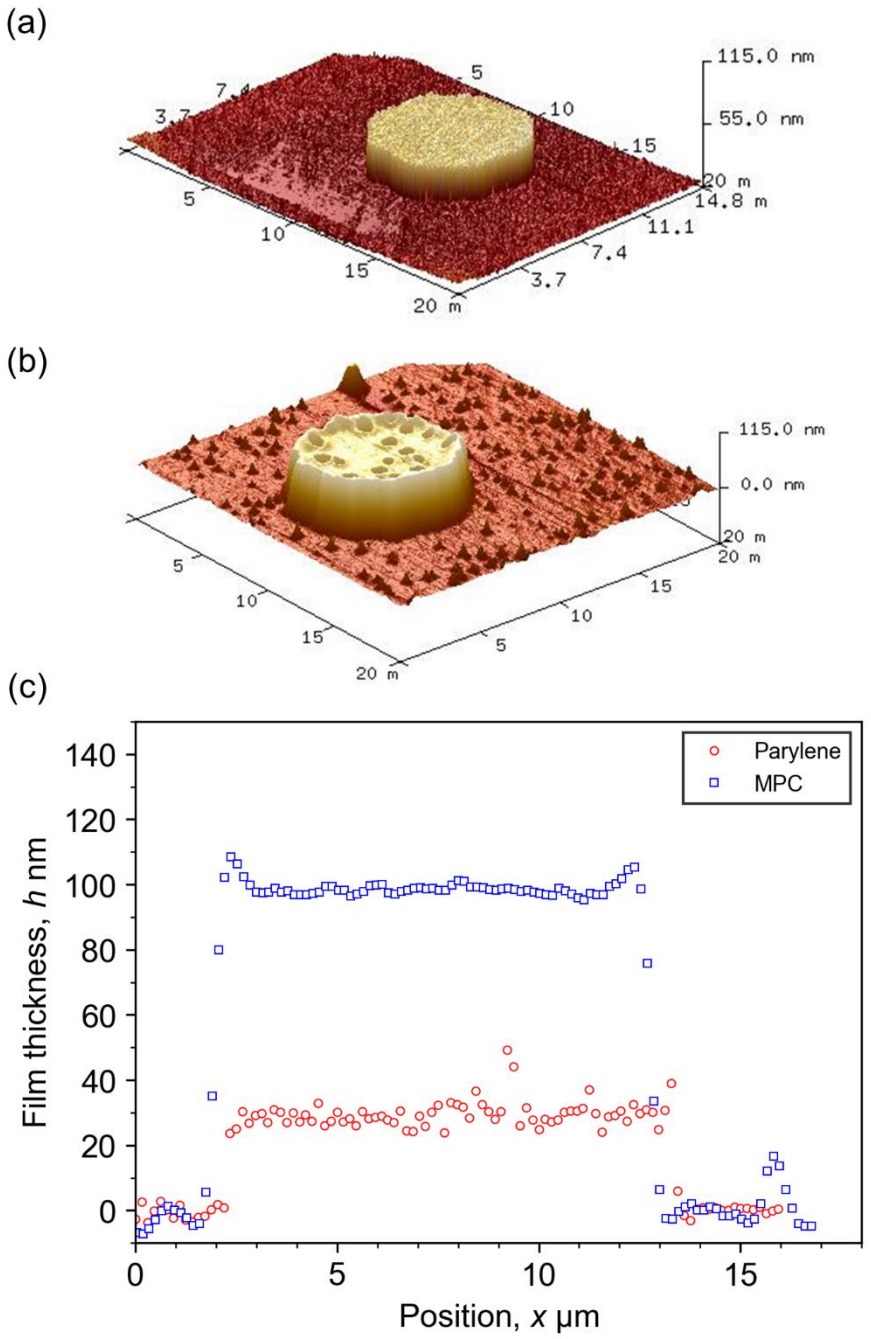

Fig. 3.3 AFM images of (a) parylene film and (b) MPC polymer brush film grafted subsequently. (c) Profile of parylene C and MPC polymer brush films.

3.1.3 Characterization of the MPC polymer brush film

Ellipsometric analysis was employed to characterize the MPC polymer brush films, particularly to obtain the correlation between the film thickness and UV exposure time. The measurement was conducted at room temperature and relative humidity of 30%. As shown in Fig. 3.4, the analysis indicated a linear increase in film thickness in proportion to the exposure time within the span of 8 to 24 min. The linearity of this relationship suggests a negligible effect of reactant concentration variation over time, likely owing to the sufficient supply of reactants and the use of a cover glass to minimize solution evaporation. The error bars, representing the range of the film thickness within the measured data, indicate that the variation in thickness is less than 10 nm. The oxygen dissolved in the solution is known to affect the process of radical polymerization and thus film uniformity [59], [60]. It is posited that the pre-reaction vacuum treatment of the solution effectively removed dissolved oxygen, whereas the cover glass reduced oxygen re-dissolution during the reaction. Thus, the preparation and procedural approach employed here support the efficacy of the method in producing films with consistent thickness and uniformity.

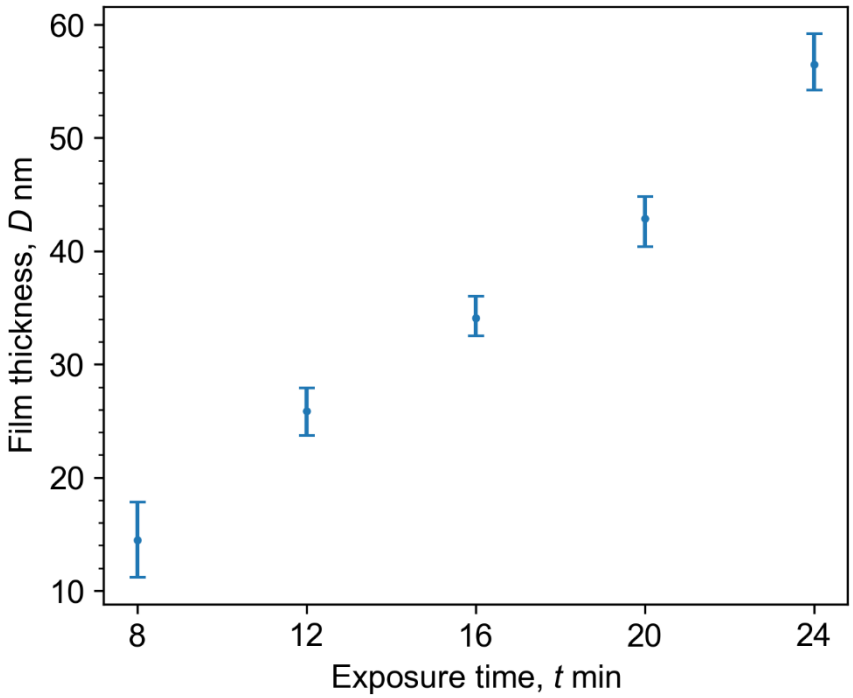

Fig. 3.4 Relationship between exposure time and film thickness.

We tested the graft density of the polymer brush film by neutron reflectivity (NR) measurements. The details of the NR measurements are described in Section 4.2. The thickness of the brush film measured in air (relative humidity of 30%) was approximately 23 nm. Subsequently, the MPC polymer brush films were immersed in deuterated water. The NR measurement results are shown in Fig. 3.5(a). The open symbols and solid lines represent the experimental and fitted results, respectively. We used the MPC polymer brush film's volume fraction ϕ to estimate its density in the D_2O solution. ϕ was calculated according to SLD $= SLD_{MPC}\phi + SLD_{D_2O}(1-\phi)$; the results are shown in Fig. 3.5(b). The volume fraction of MPC polymer brushes near the parylene C film surface,

corresponding to the brush density, was approximately 0.05. Thus, our brush film can be categorized as a semidilute polymer brush film. The result in Fig. 3.5(b) also shows that the film thickness in water was approximately 130 nm, indicating that the film swelled by approximately five times its thickness in air.

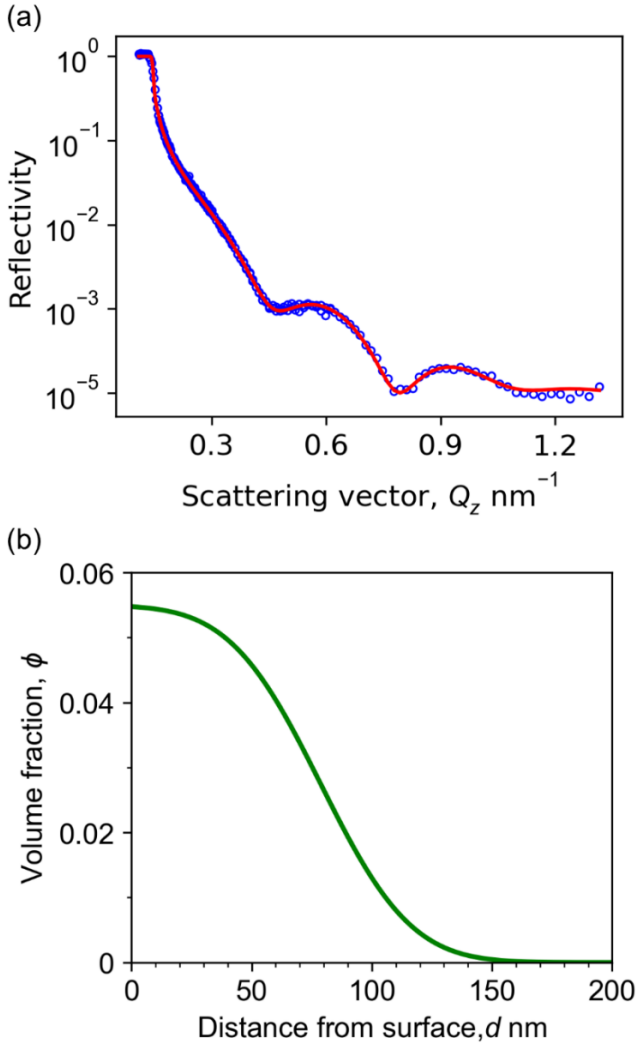

Fig. 3.5 (a) NR measurements of the MPC polymer brush on the parylene C film in D_2O solution. (b) Volume fraction of the MPC polymer brush against distance from the surface of the parylene C film.

Due to the influence of environmental humidity on the measurement results of the MPC polymer brush film's thickness obtained by ellipsometry, to accurately determine the film swelling ratio caused by hydration, it is essential to further verify the influence of humidity on the thickness variation of the film. This was characterized by X-ray reflectivity (XRR) measurements. The XRR measurements were performed at the Aichi Synchrotron Radiation Center using the BL8S1 beamline. A schematic of the setup is shown in Fig. 3.6(a). The sample was placed in a chamber with two windows covered by a polyimide film through which X-rays passed. The relative humidity in the chamber was adjusted by flowing humidity-controlled air using a moisture regulator (AHCU-1, Kitz Micro Filter Corporation). We measured the film thickness in air at different relative humidities at 25°C. The results are shown in Fig. 3.6(b). In air, when the humidity was increased from 5% to 80%, the film thickness increased by approximately 30%. Considering that the humidity during the film thickness measurement does not exceed 50%, the film thickness measured in air is moderately affected, with a deviation not exceeding 10%. This result also verifies the accuracy of the film swelling ratio obtained in the NR measurements. The thicknesses of the brush films used for the shear viscoelasticity measurements were 50 ± 2.5 nm and 70 ± 3.5 nm in air. Hereafter, the former is referred to as the MPC film (50 nm in air), and the latter as the MPC film (70 nm in air). The diameter of both the patterned films was 10 μm.

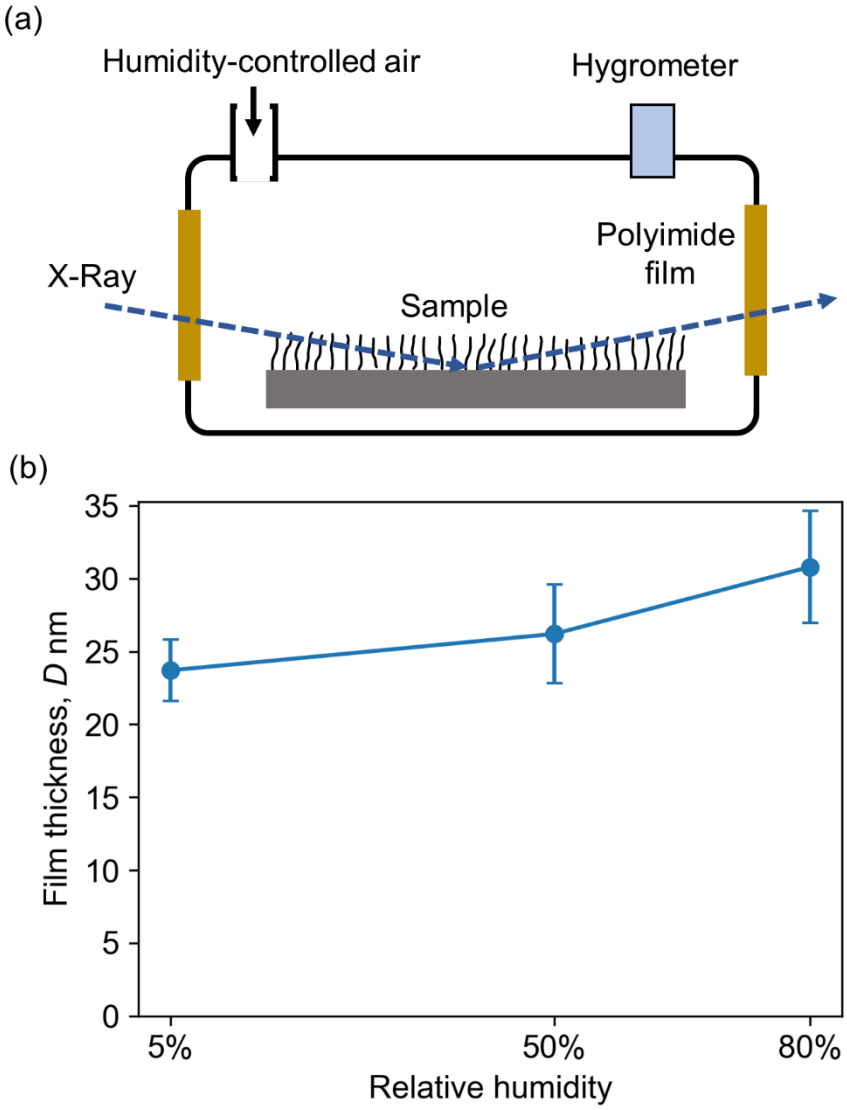

Fig. 3.6 (a) Setup of the XRR measurement. (b) Thickness of MPC polymer brush films at different relative humidities at approximately 25°C.

3.2 Experiment procedure

We immersed the MPC polymer brush films in pure water for at least 3 h to hydrate them before the viscoelasticity measurement. According to Kobayashi's report, salt

concentration had a small effect on the friction properties of the MPC polymer brush film [27]. This is because the swelling of the zwitterionic MPC polymer brush was not affected by the solution's salt concentration [61]. Thus, in our experiments, we only examined samples in pure water. During the viscoelasticity measurement, the spherical tip of the probe and the brush film below it, including the entire substrate, were completely immersed in the water. We oscillated the probe sinusoidally with a frequency of 1000 Hz and amplitude of 50 nm. The initial gap between the probe tip and the substrate was greater than 400 nm, and the probe tip did not make contact with the hydrated polymer brush film. The gap decreased linearly at a speed of 10 nm/s. As the gap decreased, the probe began to contact the polymer brush film. The amplitude and phase shift of the probe and interference fringes were recorded simultaneously. Finally, the probe compressed the polymer brush film, and the gap became constant. For the MPC film (70 nm in air), after the gap reached a constant value, we stopped increasing the voltage on the piezo stage for 10 s. Subsequently, we conducted an additional viscoelasticity measurement during the retraction process (increasing the shear gap) at the same speed as the compression. Since the entire measurement was completed in approximately 1 min, the effect of the water evaporation was negligible.

3.3 Results

3.3.1 Amplitude, phase shift and gap measurement results

Figure 3.7 shows the shear gap width h determined by interference fringe measurement using the hydrated MPC polymer brush film whose thickness in air is approximately 50 nm. Qualitatively similar results were obtained for samples with a 70-nm-thick MPC film (data not shown). The horizontal axis z in Fig. 3.7 represents the displacement of the piezo stage, which brings the sample surface closer to the probe. An increase in z implies a decrease in h. When we denote the relative changes in z and h as Δz and Δh, respectively, the dashed line in the figure represents the relationship $\Delta h = \Delta z$. The relationship $\Delta h = \Delta z$ held in a gap larger than approximately 200 nm, thus implying that the deformation of the optical fiber probe in its axial direction is negligible.

In contrast, $\Delta h < \Delta z$ at gaps of 200 nm or less. This result indicates that the optical fiber probe was compressively deformed in the gap direction owing to the repulsive force caused by the elasticity of the hydrated MPC polymer film. We could not reduce the gap below 50 nm, thus implying that the MPC film remained in the gap between the probe and the substrate, and it was not drained out or further deformed within the vertical force range that this measurement system applied. We could not measure the gaps in the region above 270 nm because the interference fringes overlapped with the central MPC film. However, we can estimate h from z because $\Delta h = \Delta z$ holds in this gap range.

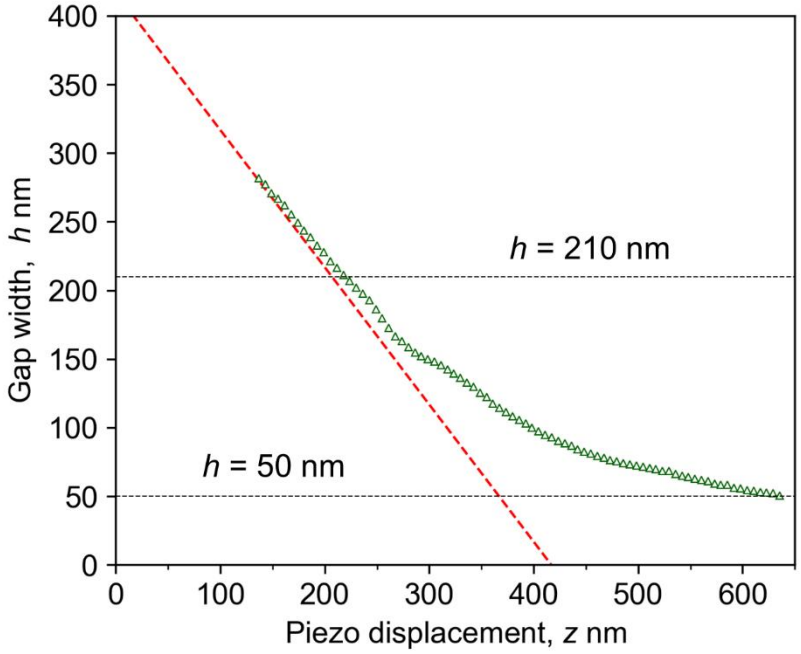

Fig. 3.7 Shear gap width *h* against the displacement of the piezo stage *z* measured with the hydrated MPC film (50 nm in air). The dotted line indicates the case when *Δ*z is equal to *Δh*.

The viscosity and elasticity of the MPC polymer brush film were evaluated using damping coefficient *c* and spring coefficient *k*, respectively. According to the mechanical model and equations described in Section 2.1.1, *c* and *k* were calculated using the measured amplitude *X* and phase shift *δ* of the probe. The measurement results of *X* and *δ* are shown in Fig. 3.8(a) and (b), where the horizontal axis represents the measured gap width *h* shown in Fig. 3.7. For comparison, Fig. 3.8 (a) and (b) show the *X* and *δ* results for the parylene C film without the brush film, measured under the same experimental conditions. Both *X* and *δ* for the MPC polymer brush film began to change when the gap

width was larger than the film thickness in air (50 nm). These changes represent the viscoelastic response due to the brush film. In contrast, in the case without the brush film (parylene C film only), X decreased suddenly at the contact, indicating that the parylene C film was too elastic to be measured by our method. Young's modulus of the parylene C film is 2.8 GPa. Young's modulus of the hydrated brush film estimated herein based on the maximum shear resistance force measured in this study was approximately 5×10^{-4} GPa. As the parylene C film is sufficiently stiff compared with the hydrated brush film, we can consider it as a rigid body in the viscoelasticity measurements of the brush film. Therefore, the influence of the mechanical properties of parylene C on the results of the brush film's viscoelasticity can be considered negligible.

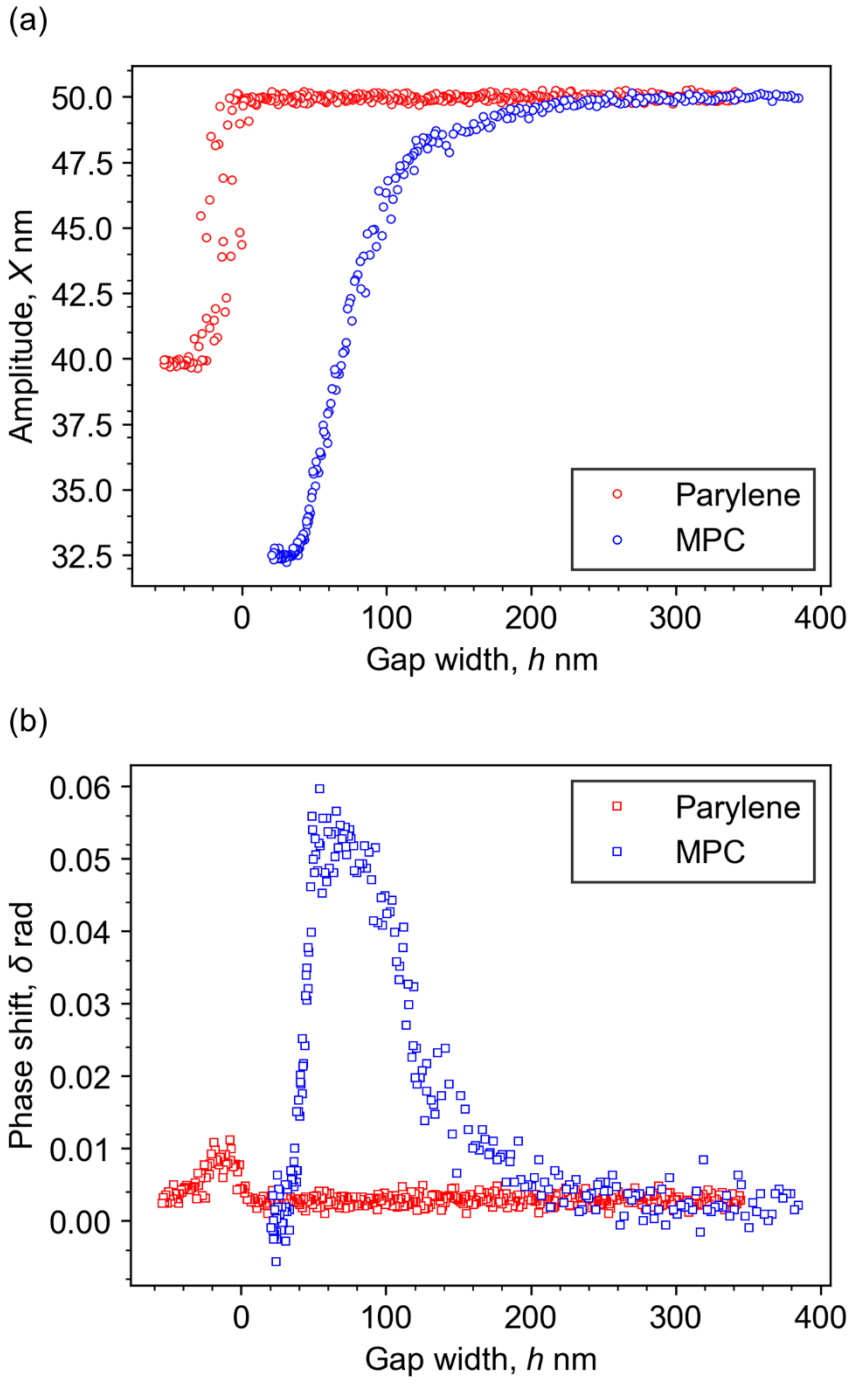

Fig. 3.8 (a) Amplitude X and (b) phase shift δ of the probe tip in the narrowing gap measured with the hydrated MPC film (50 nm in air).

3.3.2 Shear viscoelasticity

Figure 3.9(a) and (b) show plots of c and k/ω calculated from the amplitude and phase shift measurements versus the gap width for MPC films (50 and 70 nm in air), respectively. Note that k is shown as k/ω (where ω is the oscillation frequency) for quantitative comparison with c. As the gap decreased, c and k/ω of the MPC film (50 nm in air) gradually increased from 300 nm. For the MPC film (70 nm in air), the same phenomenon occurred at gaps of 380 nm or less. These increases were caused by the contact between the probe tip and swollen polymer brush. As the thickness of the parylene film underlying the MPC was 30 nm, the net thickness of the MPC film in the hydrated state was approximately 270 and 350 nm, respectively, indicating that both polymer brushes swelled approximately five times owing to hydration. This swell ratio agrees with the NR measurement results in Section 3.1.3 and with the result reported by Tairy [24]. Furthermore, c and k/ω increased monotonically with the narrowing gap and reached their maximum at gap widths of approximately 80 nm and 100 nm with the MPC films (50 and 70 nm in air), respectively. Considering the thickness of the parylene C film, these gaps corresponded to the thickness of the MPC brush film in air. As the gap further narrowed, c decreased rapidly, whereas k/ω remained high.

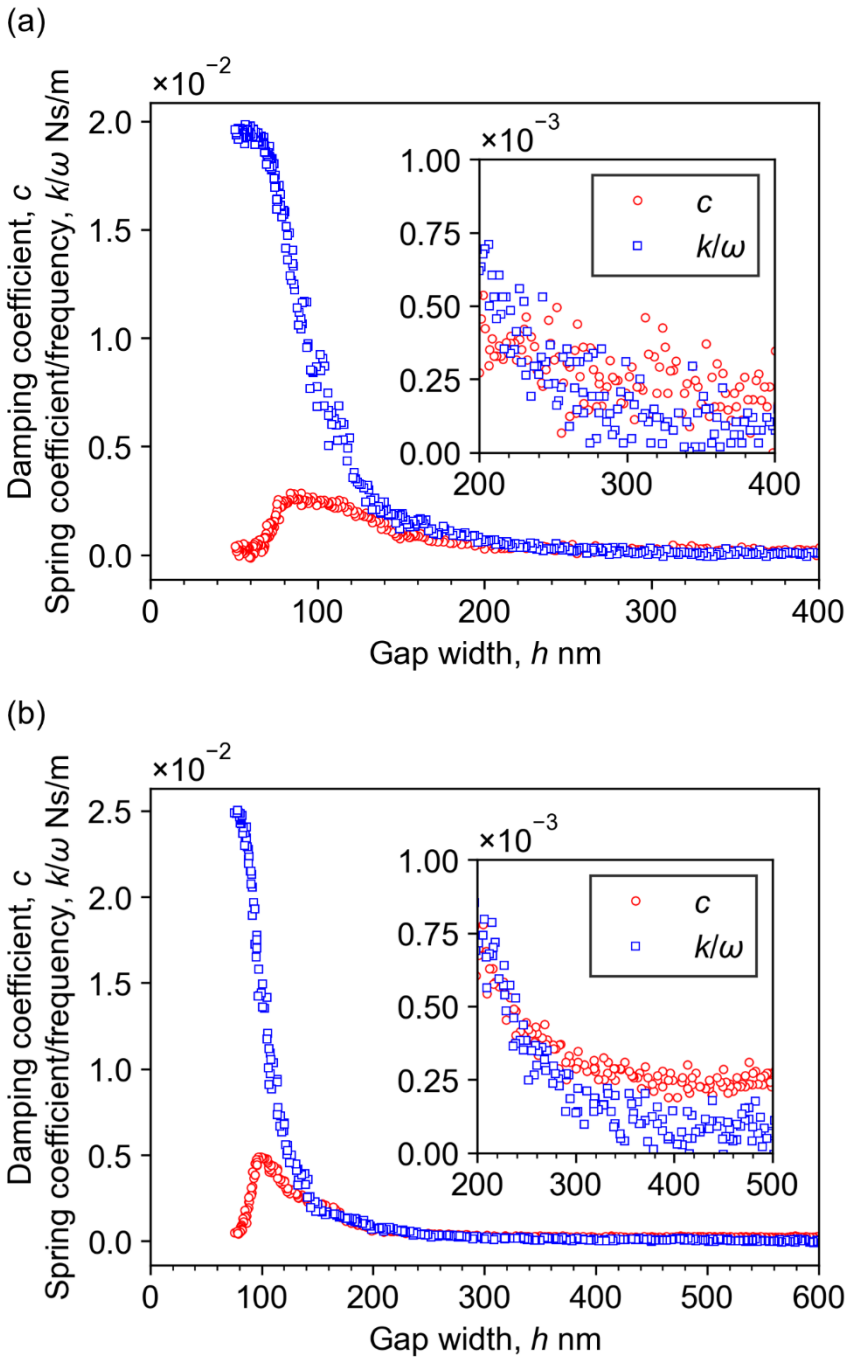

Fig. 3.9 Damping coefficient and spring coefficient over oscillation frequency against gap width of MPC polymer brush film whose film thickness in air is (a) 50 nm and (b) 70 nm.

3.4 Discussion

3.4.1 Loss tangent and hydration status of the film

The damping coefficient c and spring coefficient k depend on the contact area between the probe tip and film. To discuss the gap dependence of viscoelasticity while excluding the effect of the contact area, we calculated the loss tangent ($\tan\Delta$) by dividing c by k/ω, that is, $\tan\Delta = c/(k/\omega)$, at the gap range where the tip makes contact with the MPC film (h < 300 nm). From the definition, $\tan\Delta$ is the ratio of viscosity to elasticity and is a measure of the energy loss of a viscoelastic material independent of the contact area. If $\tan\Delta$ is greater than 1, the film is viscous; if $\tan\Delta$ is less than 1, the film is elastic. Specifically, $\tan\Delta$ calculated in this study should be called the "apparent" loss tangent. This is because the hydrated MPC film is a complex of polymer and water, and the ratio of the two changes as the gap narrows, as described below ($\tan\Delta$ in this study was not material specific). Direct measurement of the water content and frequency dependence of the viscoelasticity of the polymer chains are required to clarify the details of the breakdown of $\tan\Delta$ measured in this study; these are our future tasks. Note that the viscoelasticity discussed below based on the apparent $\tan\Delta$ is strictly the viscoelastic response of a polymer brush film containing water.

As shown in Fig. 3.10(a), the calculated $\tan\Delta$ of the MPC film (50 nm in air) is plotted against the MPC film thickness, which is determined by subtracting the parylene film thickness from the measured gap width (h). Essentially, this figure shows the viscoelastic

change in the MPC film as the film thickness decreases during compression in the gap direction by the probe. Figure 3.10(b) shows tanΔ for the MPC film (70 nm in air) as measured when the probe approached to and retracted from the substrate.

The gap dependence of tanΔ for the MPC film (50 nm in air) is detailed below. During the compression process from 270 nm to 150 nm, tanΔ decreased and exhibited an elastic trend. This elastic trend was attributed to the increasing number density of the polymer brush that interacted with the probe tip. In the film thickness range of 150 nm to 105 nm, tanΔ increased. This increase in tanΔ can be attributed to an increase in the viscous dissipation. In this gap range, the hydrated polymer brush film can deform flexibly in the in-plane direction, but the volume involved in viscous dissipation may decrease due to the narrowing of the gap. When this occurs while maintaining the water content, the internal pressure increases, possibly increasing viscous dissipation (damping coefficient). Another possibility is that in this gap region, the polymer brush film contains sufficient water to behave like a fluid so that the viscosity does not depend on the gap as it does in liquids. In this case, the damping coefficient increases proportionally to the inverse of the gap. The increasing curve of tanΔ may indicate this inversely proportional relationship. The exact cause of this phenomenon is unknown, and we would like to address this issue in future research.

The most rapid decrease in tanΔ was observed when the film thickness was below 50 nm. As described in Section 3.1.3, at this gap, the volume of the film is close to its dry

state, implying that the film almost no longer contained any free water. Below 40 nm, tanΔ was almost 0, indicating that the film was primarily elastic. Therefore, we considered that water retained by the osmotic pressure was mostly drained out in this contact region, and the density of the polymer inside the film increased rapidly owing to compression that led to the rapid decrease of tanΔ to zero (almost losing its viscosity). Consequently, the decrease in tanΔ for a film thickness of 105 nm to 50 nm can be attributed to an elasticity increase owing to the drainage process of water by compression.

As described above, the gap dependence of tanΔ showed characteristic changes at 150, 105, 50, and 40 nm for the MPC film (50 nm in air). These film thicknesses are respectively named D_1, D_2, D_3, and D_4 and are summarized in Table. 3.1. The ratio to the film thickness in air is also listed in parentheses next to the film thicknesses.

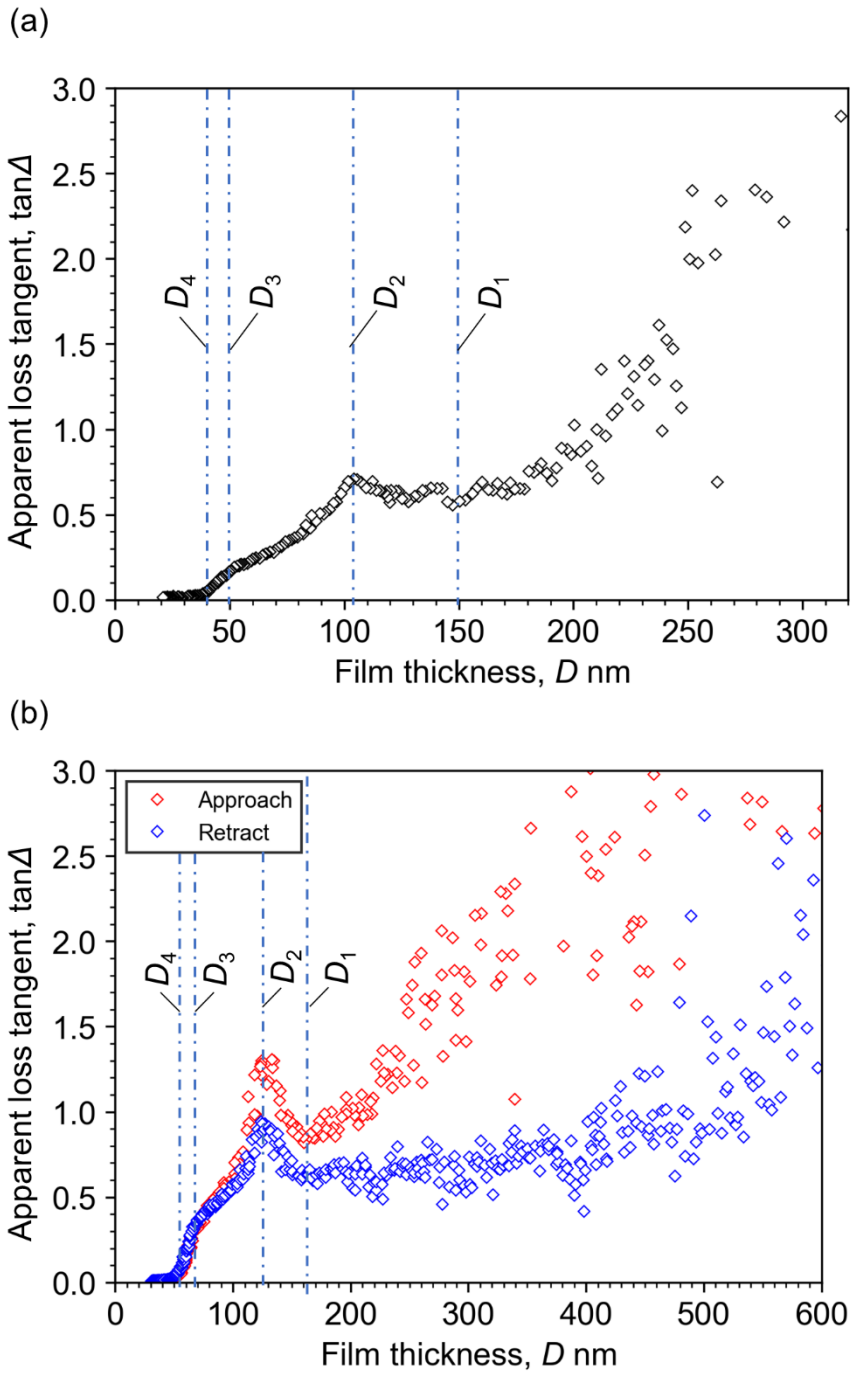

Fig. 3.10 Apparent loss tangent of MPC polymer brush whose film thickness in air is (a) 50 nm and (b) 70 nm.

As shown in Fig. 3.10(b), tanΔ of the MPC film (70 nm in air) exhibited a gap dependence similar to that of the MPC film (50 nm in air) in both the approaching and retracting processes. The characteristic film thicknesses of D_1−D_4 are summarized in Table. 3.1. Note that the film thickness ratios in D_2, D_3, and D_4 to that in air were nearly the same in the three cases, despite the difference in the value of tanΔ. This suggests that the dependence of the apparent tanΔ on the gap shown in Fig. 3.10 resulted from the dominant effect of the change in water content, which was determined by the film thickness in air (polymer chain length).

A comparison of the tanΔ values measured during the approach and retract processes revealed that tanΔ during the latter process was smaller for film thicknesses greater than D_3, thus implying that the elasticity contribution was larger in the retraction process. This may be because the polymer brush adsorbed on the probe's tip, thus bridging the two surfaces, and consequently, the entropic elasticity became more apparent. Another possibility is that water did not return completely during the retraction process, resulting in increased elasticity. Experiments with varying retracting speeds are needed to determine the cause of hysteresis and its effect on frictional properties, which is one of our future targets. If tanΔ's gap dependence depends on the polymer's relaxation, D_2−D_4 would shift in the direction of the film thickness as the value of tanΔ changed. However, D_2−D_4 was nearly identical to that in the approach process. These results also suggest that the gap dependence of tanΔ is dominantly affected by water content.

Table. 3.1 Characteristic film thickness in gap dependence of apparent loss tangent; the ratio to the film thickness in air is also listed in parentheses next to the thicknesses.

	MPC film (50 nm in air) in approach process	MPC film (70 nm in air) in approach process	MPC film (70 nm in air) in retracting process
D_1	150 nm (3.0)	160 nm (2.29)	155 nm (2.21)
D_2	105 nm (2.1)	130 nm (1.86)	130 nm (1.86)
D_3	50 nm (1.0)	70 nm (1.0)	70 nm (1.0)
D_4	40 nm (0.8)	55 nm (0.79)	50 nm (0.71)

3.4.2 Evaluation of coefficient of friction

To estimate the coefficient of friction of the sample, we estimated the normal and shear force acting on the probe tip. As the upper end of the probe was fixed, the displacement of the piezo stage Δz to bring the sample surface closer to the probe caused shear gap deformation Δh and probe deformation in its axial direction Δl. We can estimate $\Delta l = \Delta z - \Delta h$. If we simplify the optical fiber probe as a combination of a cylinder and a sphere having respective axial deformations of Δl_c and Δl_s, we obtain $\Delta l = \Delta l_c + \Delta l_s$. If the axial stiffness of the cylinder and sphere are K_c and K_s, respectively, the normal repulsive force of the film during shearing with the probe, which will balance the load, is expressed as

$$F_n = K_c \Delta l_c = K_s \Delta l_s \tag{3.1}$$

By solving Δl_c and Δl_s, we can obtain F_n. The axial deformation of the probe Δl_c is expressed as

$$\Delta l_c = \frac{F_n l_c}{EA} \tag{3.2}$$

where l_c is the length of the probe (2.2 mm); F_n, the axial force; E, the elastic modulus; and A, the cross-sectional area.

The Hertzian compression deformation of the probe tip Δl_s was considered to occur only on the contact area with the film, and it is expressed as [62]

$$\Delta l_s \times 10^3 = \frac{(9)^{1/3}}{2}\left(F_N/_{9.8\times10^{-3}}\right)^{2/3}\left(\frac{1-\sigma^2}{E/_{9.8\times10^3}}\right)^{2/3}\left(\frac{1}{D\times10^3}\right)^{1/3} \tag{3.3}$$

where F_n is the axial force; σ, Poisson's ratio; E, the elastic modulus of the contact surface material; and D, the probe tip diameter. Thus, Eq. (3.2) can be rewritten as

$$F_n = \left[\frac{\Delta l_s\times10^3}{\frac{(9)^{1/3}}{2}\left(\frac{1-\sigma^2}{E/_{9.8\times10^3}}\right)^{2/3}\left(\frac{1}{D\times10^3}\right)}^{1/3}\right]^{3/2} \times 9.8\times10^{-3} = \frac{\Delta l_c EA}{l_c} \tag{3.4}$$

where only Δl_c and Δl_s are unknown. To determine F_n, we combine Eq. (3.4) and $\Delta l = \Delta l_c + \Delta l_s$ to solve for Δl_c and Δl_s. We need to note that in the FWM experiments, it was the gap that was controlled by a piezo stage, so strictly speaking, the normal force measured when the gap decreases, i.e., when the film is compressed, indicates the maximum load capacity that can be supported under that film thickness condition. In this study, for the purpose of estimating the friction coefficient, the load capacity is considered as the

normal force under specific film thickness conditions.

Because the hydrated MPC film is viscoelastic, the shear force acting on the probe tip consists of the viscous force F_c and elastic force F_k. They are respectively expressed as

$$F_c = c\dot{x} = \frac{cX\omega}{\sqrt{2}} \tag{3.5}$$

$$F_k = kx = \frac{kX}{\sqrt{2}} \tag{3.6}$$

Here, X is the amplitude of the probe tip. Because the phase difference between the viscous force and elastic force was π/2, we estimated the shear force as $F_s = \sqrt{{F_c}^2 + {F_k}^2}$. The results of normal and shear force against the film thickness for the two samples are shown in Fig. 3.11. The contact area between the probe and the film is estimated based on the area of the film pattern (radius 5×10^{-6} m). the load capacity of the hydrated MPC film can be estimated to be in the order of several tens of MPa. Considering that the actual contact area might be smaller and given the limitations of the FWM probe measurement, the film may actually possess an individually higher load capacity.

Considering the possibility of probe buckling under relatively high normal forces, we estimated the buckling load of the probe using Eq. (3.7) [63]:

$$F_c = C\frac{\pi^2 EI}{l_c^2} \tag{3.7}$$

Here, C is the end condition coefficient, I is the moment of inertia of area. For end

conditions of an optical fiber probe, with one end fixed and the other end free, the end coefficient C is 0.25. The estimated F_c is 2×10^{-1} N. The estimated maximum normal force is 2×10^{-2} N which is an order of magnitude smaller than the buckling load. Therefore, buckling due to normal forces is unlikely to occur.

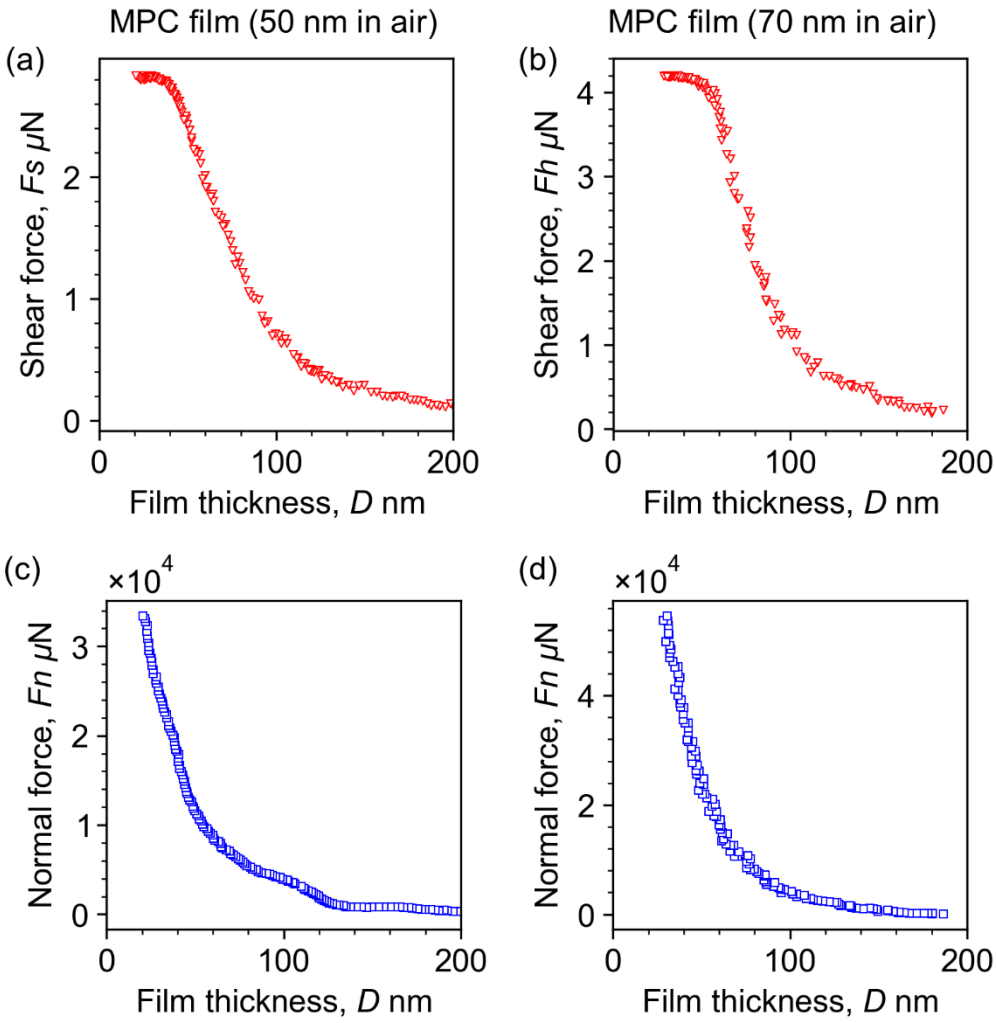

Fig. 3.11 (a), (b) Shear and (c), (d) normal force against film thickness of MPC films (50 and 70 nm in air, respectively).

The relationship between the shear force and normal force of the MPC films (50 and 70 nm in air) is shown in Fig. 3.12(a) and (c), respectively. The normal force is balanced by the load. Therefore, the shear force and normal force most commonly exhibit a linear relationship. A nonlinear relationship, as shown in Fig. 3.12, implies that the viscoelasticity of the brush film contributes dominantly to the frictional properties despite its nanoscale thickness. The coefficient of friction, μ, of the film was derived by determining the inclination of the curve, which can capture the local changes in μ. μ varied with decreasing gap and was generally very low (on the order of 0.0001). This result was consistent with the results of earlier studies using SFA [48]. Considering the error in the measured data, μ is obtained by averaging every ten sets of normal force and shear force data, and then calculating the inclination. The relationship between COF and shear gap is shown in Fig. 3.12(b) and (d). tanΔ and the four characteristic film thicknesses which were classified according to the change in tanΔ, as summarized in Table. 3.1, were shown as comparison. The changing of μ in response to the change in shear gap could be observed despite of the error. The four characteristic film thicknesses are also shown in their corresponding normal force positions in Fig. 3.12(a) and (c), indicating that μ changed in response to the change in tanΔ. However, the normal force was greater for the MPC film (70 nm in air) when compared at the characteristic gaps (D_2, D_3, and D_4) where similar film compressibility was reached. This suggests that the thicker film had better load-bearing capacity. However, since the frictional force increases with film thickness,

COF was similar.

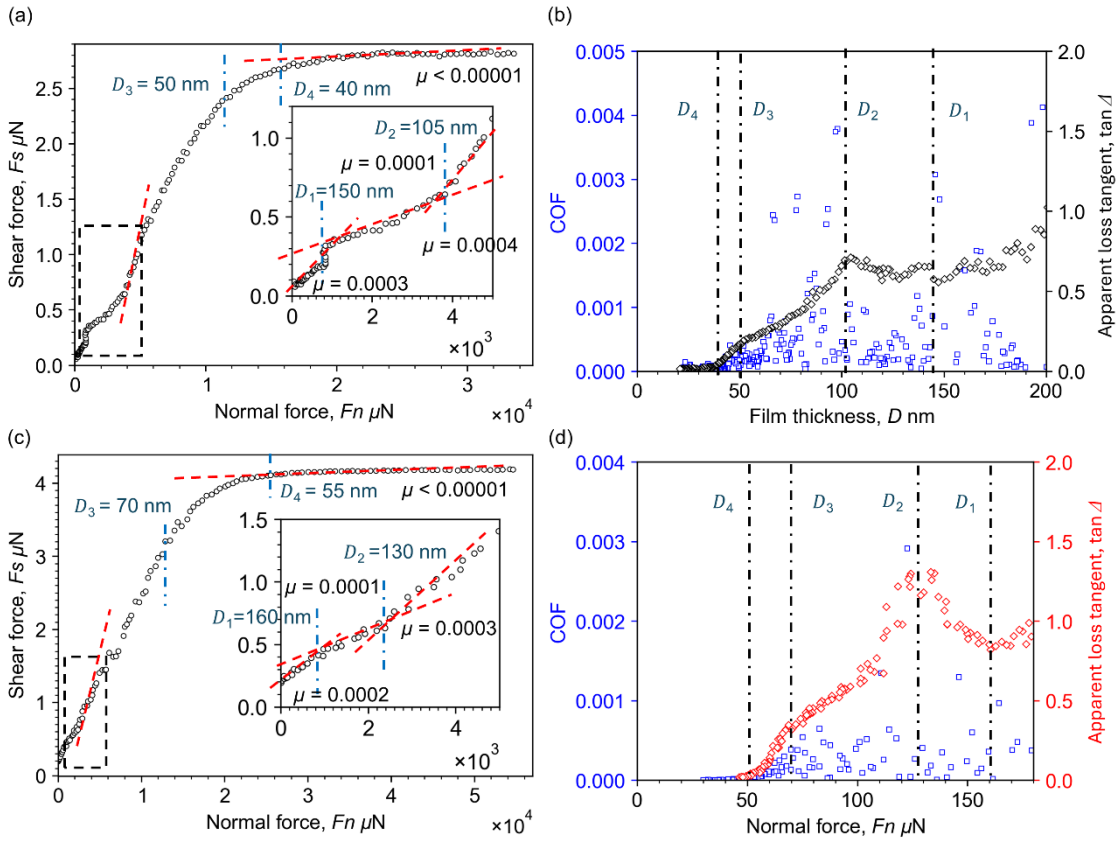

Fig. 3.12 Relationship between shear force and normal force and COF's film thickness dependence of hydrated MPC polymer brush film whose film thickness in air is (a), (b) 50 nm and (c), (d) 70 nm. tanΔ is plotted as comparison.

The gap dependence of μ of the MPC film (50 nm in air) is discussed in detail as follows. Over the gap of D_1 (150 nm), the coefficient of friction was approximately 0.0003. In the gap range from D_1 (150 nm) to D_2 (105 nm), the coefficient of friction reduced to 0.0001; however, tanΔ increased, as shown in Fig. 3.10. This increase in tanΔ can be interpreted as an increase in damping along with narrowing the gap, which led to

an increased shear force. However, as the density of the polymer brush increased, the osmotic pressure of the dense polymer chains generated a larger vertical force (load-bearing capacity), thus resulting in a lower coefficient of friction. Essentially, water was difficult to drain from the film, and the brush could deform flexibly. The flexible deformation of the brush may be responsible for the smaller coefficient of friction with increased polymer density as the gap decreases.

The coefficient of friction increased again at the gap region from D_2 (105 nm) to D_3 (50 nm). This was attributed to the normal force overcoming the osmotic pressure, as in the rapid decrease of tanΔ [64]–[66]. The loss of water not only reduces the load-bearing capacity but also causes the polymer brush to lose its flexibility. Thus, the coefficient of friction increased.

Below D_3 (50 nm), the coefficient of friction decreased rapidly, corresponding to a faster decrease in tanΔ. Below D_4 (40 nm), the film was almost elastic and the coefficient of friction decreased to 0.00001. If the polymer brush film becomes elastic due to compression, it can be interpreted as transitioning to a boundary lubrication state. The friction coefficient generally increases after a transition to a boundary lubrication state, but the opposite occurred in our results. One reason for this is the smoothness of the probe surface roughness (Ra: 0.2nm). The surface roughness of the probe is sufficiently small compared to the thickness of the polymer brush film in the compressed state, that direct contact between solid surfaces does not occur, and friction does not increase after the

transition to the boundary lubrication state.

Even if solid contact does not occur, the coefficient of friction should increase if the elastic force of the film increases due to compression, which potentially acts as frictional resistance. The reason why this does not occur is thought to be that the hydration water intervenes at the friction interface and behaves fluidly, creating a slip interface. Klein et al. showed in their experiments on SFA that the low coefficient of friction is maintained even when free water is drained away, and only hydrated water intervenes at the friction interface [67]. They explained that although the relaxation time of hydration water increased compared to that of free water, the hydration water remained in a liquid state and provided sufficient lubricity. A similar phenomenon can be inferred from the measurement results. Although the polymer brush is elastic due to compression, the presence of fluid hydration water at the interface is thought to cause a slip on the surface of the compressed polymer film, resulting in a low coefficient of friction. In the case of the MPC film (70 nm in air), the correlation between the characteristic film thicknesses D_1−D_4 and the increase or decrease in the COF was consistent.

3.4.3 Correlation of shear viscoelasticity and friction properties

The relationship between the change in the hydration state of the brush film and the coefficient of friction with respect to the gap change, as estimated from the experimental

results of this study, is schematically summarized in Fig. 3.13. For gaps larger than D_1 (Fig. 3.13(a)), hydrated polymer brushes could flow flexibly to the shear, and water molecules were easily squeezed out by the normal force. For the gap between D_1 and D_2 (Fig. 3.13(b)), osmotic pressure kept water inside the film against the normal force. For the gap between D_2 and D_3 (Fig. 3.13(c)), the normal force overcame the osmotic pressure and the water began draining from the film. For a gap under D_4 (Fig. 3.13(d)), the brushes were compressed further and almost lost their viscosity; nonetheless, we assumed a thin film of hydrated water molecules was retained as a lubricant on the surface. In summary, the coefficient of friction of a hydrated polymer brush sheared in a nanogap is very low over a gap range of several hundred nanometers. Two states of low coefficients of friction were observed: one in which the brush film with sufficient water molecules is dominant in the gap (Fig. 3.13(b)), and the other in which most of the free water is drained from the brush film (Fig. 3.13(d)). In the former case, the flexibility of the polymer brush is essential for low friction, whereas in the latter case, as highlighted by Klein et al., as the origin of hydration lubrication [6], the intervention of water at the sliding interface must be essential.

Since this study aimed to clarify the relationship between shear viscoelasticity and friction, which varies with gaps, FWM used a probe with an extremely smooth surface. In a typical friction interface with surface roughness, gaps are distributed. Therefore, for sliding surfaces where COF is significantly dependent on the gap, as revealed in this study,

the averaged COF will act on the entire sliding surface. To apply the results obtained in this study to lubrication design, we can conclude that it is effective to realize two gap regions (between D_2 and D_1, or D_4 or less) in which a lower coefficient of friction is achieved over as wide an area as possible within the sliding surface. This requires the reduction of the gap distribution, which can be achieved by reducing the surface roughness or using soft surfaces. Wang et al. showed that superlubricity occurred on a soft gel surface containing MPC polymer in a macro-scale friction test [68]. When the surface pressure was increased, the soft surface was deformed, and a uniform gap distribution was created, which may be one of the reasons for achieving superlubricity.

The normal force shown in Fig. 3.12 is calculated from the model-based estimates of the vertical stiffness of the probe. Therefore, they may not be quantitatively comparable to the values measured in other studies. However, the fact that the coefficients of friction are similar suggests that our estimates have some validity.

The graft density of the polymer is another critical factor that influences the friction property [69]–[71]. Increasing the polymer density led to a higher osmotic pressure, which in turn improved the load-bearing capacity. Conversely, higher densities result in lower flexibility of the brush film, which may increase shear forces. Such a trade-off relationship was assumed. An increase in density also changes the viscoelasticity of polymer brushes. As the apparent viscoelastic response is closely related to the coefficient of friction, as shown in this study, the relationship between density and viscoelasticity

should be clarified, which is the target of our future study. Understanding the relationship between graft density and friction properties can provide key parameters for the design of hydrated lubrication using polymer brushes.

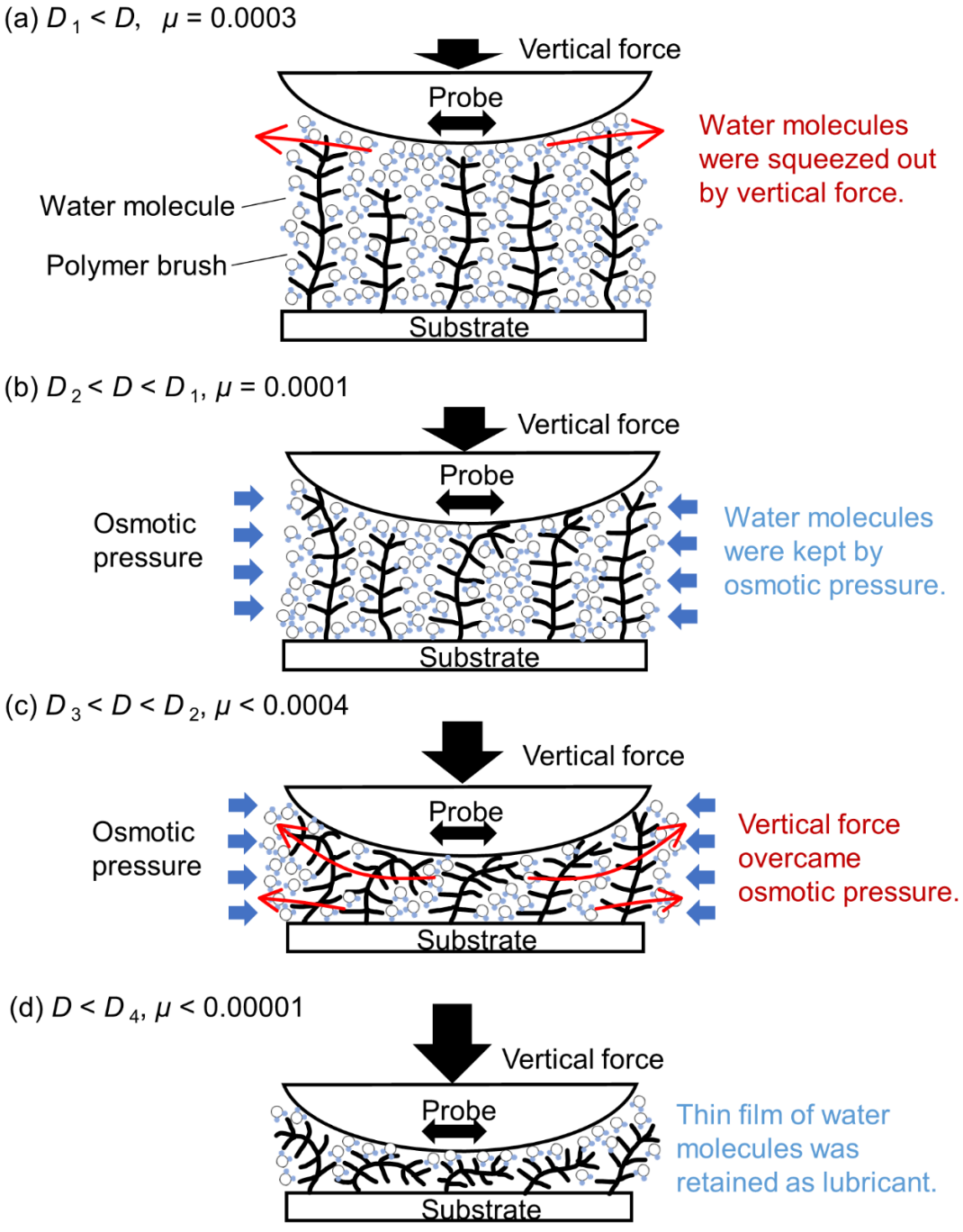

Fig. 3.13 Schematic of hydrated MPC polymer brush film (50-nm thickness in air) in a narrowing gap: (a) gap over 150 nm, (b) gap of 105–150 nm, (c) gap of 50–100 nm, and (d) gap under 50 nm.

3.5 Conclusion of Chapter 3

A hydrated MPC polymer brush exhibits superior lubricity. In earlier studies, the physical origin of this lubricity was attributed to either the low shear resistance offered by the highly flexible hydrated polymer brush or the presence of a thin water film on the hydrophilic brush surface [8], [25], [27]–[29]. We hypothesized that quantifying the gap dependence of the shear viscoelasticity of hydrated polymer brush films would provide a comprehensive understanding of the lubrication mechanism.

We evaluated the viscoelastic response of the film by its apparent loss tangent and found that the gap dependence of viscoelastic response can be classified into five different states divided by four characteristic film thicknesses (D_1 to D_4). We considered that the water content mainly influenced the viscoelastic response of these five states. We estimated COF from the measured data and found that it differed depending on the viscoelastic state. Among the five aforementioned viscoelastic states, those for film thicknesses of D_1−D_2 nm and D_4 or less were found to be more lubricious. In the former case, the brush film is flexible and deforms, and sufficient water is present to hold the load and achieve a low COF. In the latter case, most of the water retained by the osmotic pressure in the brush film is assumed to be discharged, and the film becomes elastic, thereby supporting the normal force; the thin water layer remaining at the sliding interface should contribute to lubrication.

The results of this study provide the first direct evidence of a relationship between

the viscoelastic response and coefficient of friction of the brush film. Our findings show that the two different explanations proposed in previous studies for the physical origin of hydration lubricity can be comprehensively understood through the gap-dependent viscoelastic response of the film under varying loads.

The fact that frictional properties depend on the shear viscoelasticity implies that the shear frequency dependence of the frictional properties must also be verified. This will be addressed in our future research. We believe that hydration lubrication can be developed as an applied technology by optimizing molecular-level parameters such as graft density and chain length of brushes, thus manifesting two lubricious states with lower COF. For example, we must consider that surface roughness exists on the actual sliding surface and that shear gaps are distributed. Therefore, we believe that an appropriate dispersion of brush length that achieves a robust lubrication design must exist, and this is one of the issues to be verified in our future research.

4. Lubrication improvement via synergistic effects of free polymers and polymer brushes

4.1 Friction tests

Friction tests were conducted using a POD tribometer. As shown in Fig. 4.1, the test samples were fixed on a rotating stage using a fixture. Then, an external load was applied by placing weights on the pin. The frictional force acting on the pin was measured, as the force applied to the load cell, using a rotating lever. We used a urethane pin with a radius of 3.96 mm, and the sliding speed was 1.2 mm/s. All the measurements were conducted at room temperature (approximately 25 ℃). The applied load was varied up to 10 N in steps of 2.5 N. The corresponding average pressure estimated using Hertzian contact theory was in the range of 2.3–8 MPa, which was within the typical pressure range observed in human joints [72]. The average frictional force was obtained after the pin was sliding against the sample for 300 s under each load. The COF was determined from the slope of the change in the frictional force against the load.

The MPC polymer brush used in the friction test was 33 nm thick in air. Before testing, the MPC polymer brush film was soaked in a lubricating fluid (pure water or free polymer solution) for more than 24 h to ensure full hydration. For comparison, we prepared a substrate without the MPC brush film, i.e., a silicon wafer covered with a parylene C film.

We conducted friction tests on these two types of substrates with and without brushes and water with and without free polymers, i.e., under four different conditions. The combinations of the four conditions and sample names are listed in Table. 4.1.

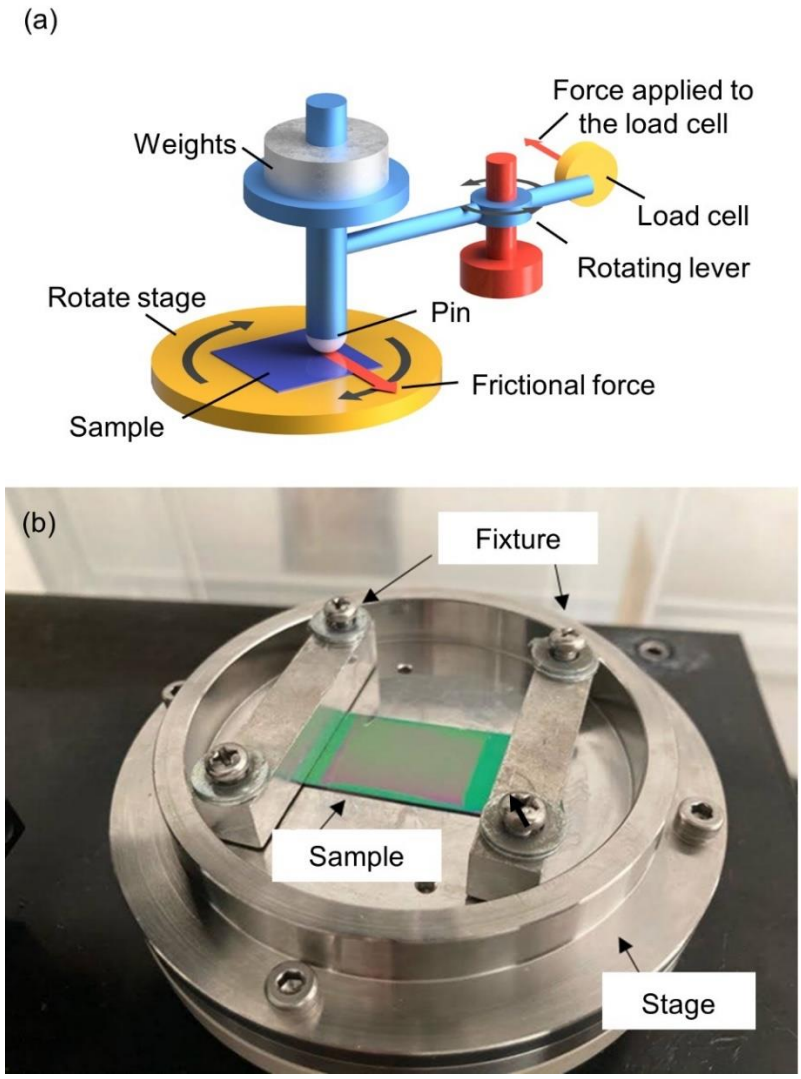

Fig. 4.1 (a) Schematic representation of POD tribometer. (b) Photograph of the substrate with the MPC brush sample fixed on the rotating stage.

Pure water and water containing a free polymer were used as lubrication fluids. The

free polymer was a commercially available MPC polymer with an average molecular weight of approximately 343,000 (LIPIDURE-BL203, Nippon Oil & Fats Co., Ltd.). The concentration of the free polymer solution was adjusted to 0.5 wt.%. We also prepared free polymer solutions with concentrations of 2.5 and 0.1 wt.% for the friction tests to investigate the effect of the solution concentration.

Table. 4.1 Sample conditions for friction tests.

Sample name	**Substrate**	**Lubricating fluid**
Water w/o brush	Without MPC polymer brush film	Pure water
Free polymer solution w/o brush	Without MPC polymer brush film	MPC polymer solution
Water with brush	With MPC polymer brush film	Pure water
Free polymer solution with brush	With MPC polymer brush film	MPC polymer solution

Based on Hamrock and Dowson's equations, in our experimental conditions, the minimum gap (h_{min}) in the isoviscous–elastic regime was estimated to be of the order of 0.1 nm [73]. The surface roughness of the slider used in this experiment was 16 nm, which exceeded the value of h_{min}, suggesting that the lubrication condition of our friction test was boundary lubrication. Therefore, the difference between the viscosities of lubricants with and without the free polymer did not affect the friction characteristics.

4.2 Neutron reflectivity measurements

4.2.1 Samples

For the NR measurements, we prepared three samples with polymer brush films of different thicknesses: 17, 23, and 35 nm. These thicknesses were measured in air (room temperature of 25 °C and approximately 30% relative humidity). Hereafter, we denote this thickness as h_{air}. A parylene-covered silicon substrate without a polymer brush was also prepared for comparison. We used heavy water (D_2O) in the NR measurements to enhance the neutron contrast between the polymer and the solvent; in detail, heavy water was used to hydrate the polymer brush film before the NR measurement, fill the chamber during the NR measurement, and prepare the free polymer solution. Table. 4.2 summarizes the combinations of substrate types and liquids used in NR measurements.

Table. 4.2 Sample conditions in the adsorption test.

Sample name	Substrate	Flowing liquid
Free polymer solution w/o brush	Without MPC polymer brush film	MPC polymer solution
Water with brush	With MPC polymer brush film	Pure water
Free polymer solution with brush	With MPC polymer brush film	MPC polymer solution

4.2.2 Experiment procedure

As described in the next section, the friction test results showed that the COF

decreased when a free polymer solution was used as the lubricant fluid under boundary lubrication conditions. This result suggested that the free polymer was adsorbed and formed a layer on the surface of the brush film. NR measurements were performed to observe the formation of this adsorbed layer. Because neutron beams can penetrate silicon substrates, we measured the angular dependence of the reflectance at the interface by detecting neutrons incident from the substrate side. These measurements revealed the interfacial structure formed by the polymer brush film and adsorbed free polymer in water. The NR measurements were conducted using a horizontal neutron reflectometer (Soft Interface Analyzer: SOFIA) at the Materials and Life Science Experimental Facility in the Japan Proton Accelerator Research Complex [74], [75].

In addition, we developed a unique sample chamber for the NR measurements conducted under liquid flow. These measurements under liquid flow were conducted to verify the degree of adsorption of the free polymers in the lubricant fluid at a constant concentration and to verify the adsorption strength of the free polymer adsorbed on the brush film. When the amount of solution in the sample chamber was fixed, the concentration of the solution decreased as adsorption proceeded, and only the equilibrium state was measured. Conversely, in actual lubrication, a sufficient external supply of the lubricant fluid with a constant concentration is assumed. Therefore, we measured the adsorption under constant flow of a free polymer solution with a constant concentration. Further, after observing adsorption under a free polymer solution flow, the flowing liquid

was switched to water, and the NR measurements were repeated to quantify the amount of adsorbed free polymer remaining on the surface under water flow.

A schematic of the sample chamber is shown in Fig. 4.2. Using the method described in Section 2.1, a polymer brush film was formed on the surface of a 10-mm-thick silicon plate, which was 50 mm square and exhibited a polished surface with a roughness (R_a) of 0.2 nm. The sample chamber consisted of a U-shaped top cover and a bottom plate with a channel to introduce the liquid. The silicon plate was inserted into the recess of the top cover such that its surface with the polymer brush film faced the bottom plate. The silicon plate was fixed to the bottom plate by silicon rubber packing, with a gap of ~0.5 mm between the silicon and bottom plate surfaces. The lubricating fluid was pumped into the gap through a channel in the bottom plate, and a neutron beam was irradiated onto the interface from the side face of the silicon plate.

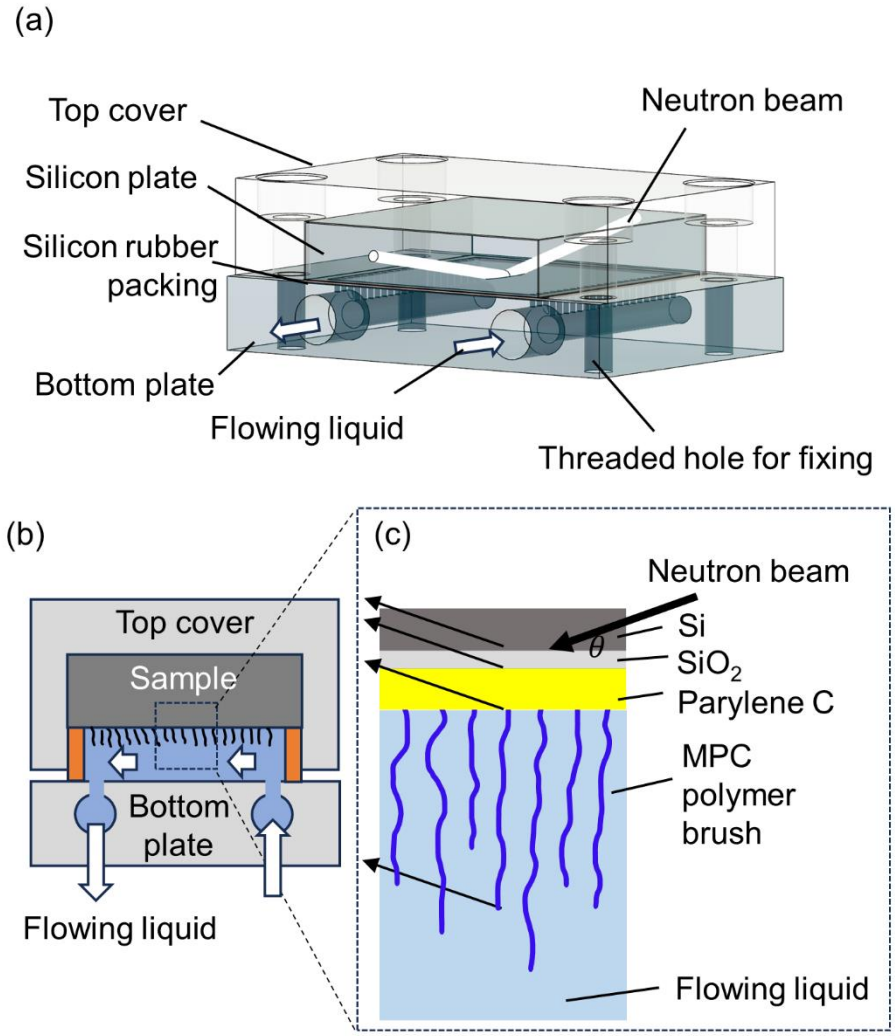

Fig. 4.2 Schematic of the sample chamber: (a) Three-dimensional structure, (b) cross-sectional view, and (c) sample's interface.

The NR measurement process is illustrated in Fig. 4.3. Prior to the measurement, the polymer brush film was immersed in water for 30 min for complete hydration. Initially, water was flowed at a rate of 5 mL/min, and the initial state of the polymer brush film was measured. Subsequently, the measurements were performed when the flow stopped. The results obtained under these two conditions were then compared to determine the

effect of flow on the molecular conformation of the brush film. Furthermore, we identified the initial state of the brush film before the free polymer adsorption. The free polymer solution was then pumped at a rate of 5 mL/min, and the amount of free polymer adsorbed on the brush film surface was measured. Finally, water was pumped again to assess the desorption of the free polymer adsorbed onto the brush film surface. These three steps are referred to as the initial condition test, adsorption condition test, and rinsing test. In the rinsing test, the NR measurements were performed under three different flow rates (1, 3, and 5 mL/min). The free polymer solution was flowed at 5 mL/min for 2 min before starting the adsorption state test to replace the water in the chamber. Further, water was flowed at 1 mL/min for 10 min before starting the rinsing test to drain the free polymer solution from the chamber completely. All the measurements were performed on a temperature-controlled stage at 25 ℃.

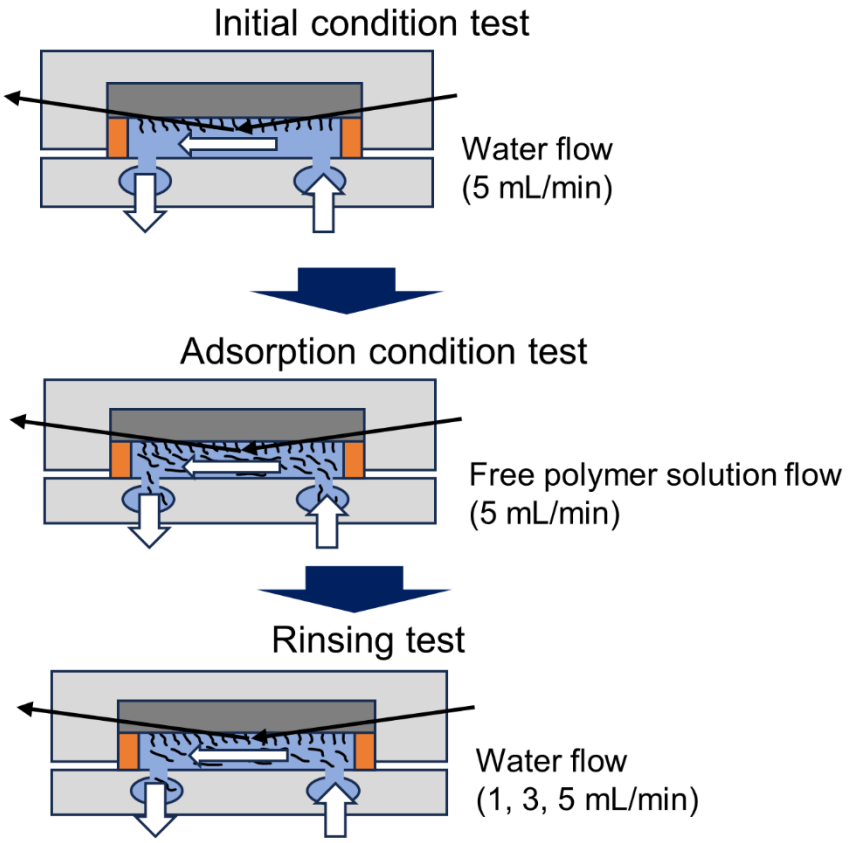

Fig. 4.3 Schematic of the NR measurement process: (a) Initial condition test, (b) adsorption condition test, and (c) rinsing test.

The incident angles θ of the neutron beam were set at 0.3°, 0.6°, and 1.2° to acquire the reflectivity profiles against the scattering vector Q_z (0.1–1.2 nm^{-1}), which was calculated as $Q_z = 4\pi\sin(\theta/\lambda)$, where λ represents the wavelength of the incident neutrons. These reflectivity profiles were then analyzed and fitted using GenX 3.6 [76], and the χ^2 figure of merit (FOM), including error bars, were used to assess the agreement between the model-based calculation results and measured data. The fitting process was terminated after 500 iterations, when the FOM ceased to change, to ensure an optimized comparison

of the results.

4.2.3 Models and analysis method

Fig. 4.4 shows the calculation model of the interface, which contains four main layers: SiO_2, a parylene C film, an MPC polymer layer (comprising brush, adsorbed free polymer, or their combination), and a flowing liquid (D_2O or free polymer solution). To determine the density distribution of the swollen polymer film along its thickness in water with a high accuracy, the MPC was subdivided into ten layers. The scattering length densities (SLDs) at different distances from the surface of the parylene C film were extracted from the fitted reflectivity profiles. The measured SLD of a mixture of the MPC polymer and D_2O is expressed as

$$SLD = SLD_{MPC}\phi + SLD_{D_2O}(1 - \phi) \quad (4.1)$$

where $SLD_{MPC} = 0.983 \times 10^{-6}/Å^2$, and $SLD_{D2O} = 6.393 \times 10^{-6}/Å^2$. This equation was used to compute the volume fraction (ϕ) of the MPC polymer film, which was then utilized to estimate the density of the MPC polymer at each distance from the parylene film surface as well as to estimate the grafting or absorption rate. If we assume that the density of a 0.5 wt.% D_2O solution of the free MPC polymer (with a bulk density of 1.3 g/cm^3) is similar to that of D_2O (1.1 g/cm^3), then the volume fraction of the free polymer in the D_2O solution is approximately 0.0042. Using this value in Eq. (4.1), the SLD of the free

polymer solution can be estimated as $6.368 \times 10^{-6}/Å^2$.

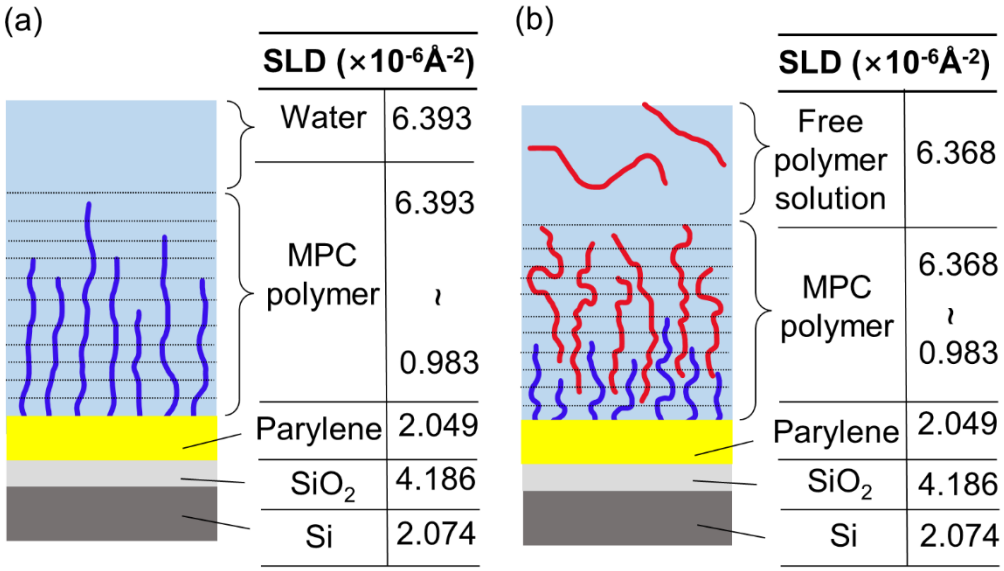

Fig. 4.4 Models of the interface and SLD for each layer under different sample conditions: (a) water with brush and (b) free polymer solution with brush. The polymer brush and free polymer are depicted in blue and red, respectively.

4.3 Indentation experiment by FWM

4.3.1 Samples

The h_{air} value of the MPC polymer brush used in the FWM measurements was 34 nm, which was consistent with the thickness used in the friction test. A substrate with no brush film formed (only a parylene film) was also used for comparison. We used two different lubricating fluids: water and a free polymer solution. The conditions for the three samples are listed in Table. 4.3.

Table. 4.3 Sample conditions for FWM measurements.

Sample name	Substrate	Lubricating fluid
Free polymer solution w/o brush	Without MPC polymer brush film	MPC polymer solution
Water with brush	With MPC polymer brush film	Pure water
Free polymer solution with brush	With MPC polymer brush film	MPC polymer solution

4.3.2 Experiment procedure

We used FWM to examine the effect of the presence (or absence) of free polymers in water on the mechanical properties (shear viscoelasticity) of MPC polymer brush films. Diverging from the techniques utilized in Chapter 3, as shown in Fig. 4.5(a), we used a probe with a spherical tip of which curvature radius was 5 μm to penetrate the thin film vertically.

The polymer brush film was immersed in water or the free polymer solution to allow sufficient swelling before the measurement. An appropriate amount of the lubricant fluid (water or free polymer solution) drop was used to ensure that only the probe tip was immersed. The probe-excitation amplitude and frequency were 50 nm and 1 kHz, respectively. The initial gap between the probe and the substrate surface was set to 1 μm. The sample surface was brought into contact with the probe tip using a piezo stage at a constant speed of 10 nm/s while the probe was continuously vibrated. The shear viscoelastic response of the probe tip was measured during this process. Initially, there

was no contact between the brush film and the probe tip; therefore, the shear viscoelasticity of the lubricating fluid dominated the overall response. As the probe approached the surface, the contribution of the brush film in the resultant response was detected. Using this procedure, we measured the gap dependence of the shear viscoelastic response, and verified the effect of the free polymer on the mechanical properties of the brush film.

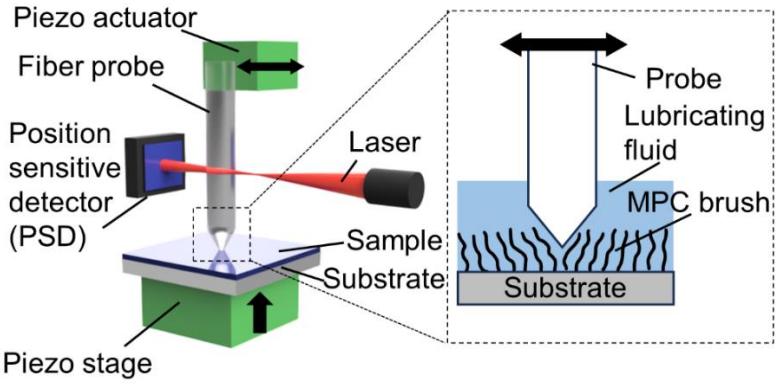

Fig. 4.5 Schematic representation of indentation experiment using FWM.

4.4 Results and Discussion

4.4.1 Friction test

Figure 4.6 shows the time-varying frictional force measured at each load under the four sample conditions listed in Table. 4.1. The friction force became almost constant approximately 150 s after the start of the measurement. Therefore, we used the average friction force from 200 to 300 s to calculate the COF. For the substrate with the polymer brush film, the frictional force shows periodic fluctuations with increasing load, and this

periodicity corresponds to the rotational periodicity of the POD test. This result implies that these periodic fluctuations can be attributed to the position-dependent variation in the frictional force on the substrate plane. Empirically, our experimental results indicate that the uniformity of brush film thickness affects the amplitude of these fluctuations. The difference in the frictional force owing to the difference in the film thickness becomes apparent at high loads, which causes periodic fluctuations. After sliding for longer than 300 s, the friction force gradually increased with continued sliding owing to the wear of the brush film. Because this study focused on clarifying the contribution of free polymers to lubrication, the relationship between the wear of the brush film and the COF was not analyzed in detail and will be investigated in the future.

Figure 4.7(a) shows the correlation between the friction force and the load. The error bars indicate the maximum and minimum frictional forces. Similarly, Fig. 4.7(b) shows the correlation between the friction force and load measured on the polymer brush surface using free polymer solutions with different concentrations as the lubricant fluid. The COF was determined from these measurements by assuming a linear relationship between the load and the frictional force. The corresponding results are presented in Fig. 4.8, where the error bars indicate the maximum and minimum COF values. The COF (μ) values measured for the free polymer solution with no brush film, water with brush film, and free polymer solution with brush film were μ = 0.074, 0.048, and 0.021–0.026, respectively, which were lower than those measured in the case of water without brush

film.

These results indicate that the smallest COF was achieved when both the free polymer solution and the brush film were used. Although the average value of the COF decreases slightly with increasing concentration of the free polymer solution, this difference is smaller than the measurement error. Therefore, we can conclude that the COF measured in this study was almost independent of the concentration of the free polymer solution. Further, the viscosity of the free polymer solutions with a concentration of 2.5 wt.% is approximately 1.3 times that of the solution with a concentration of 0.1 wt.%. Nevertheless, the COFs were almost the same, verifying that this friction test was conducted under boundary lubrication conditions, as described in Section 4.1. The observed low friction under the boundary lubrication conditions can be attributed to the free polymer layer adsorbed on the surface of the polymer brush. Therefore, NR measurements were conducted to observe the adsorption states, as described in the following section.

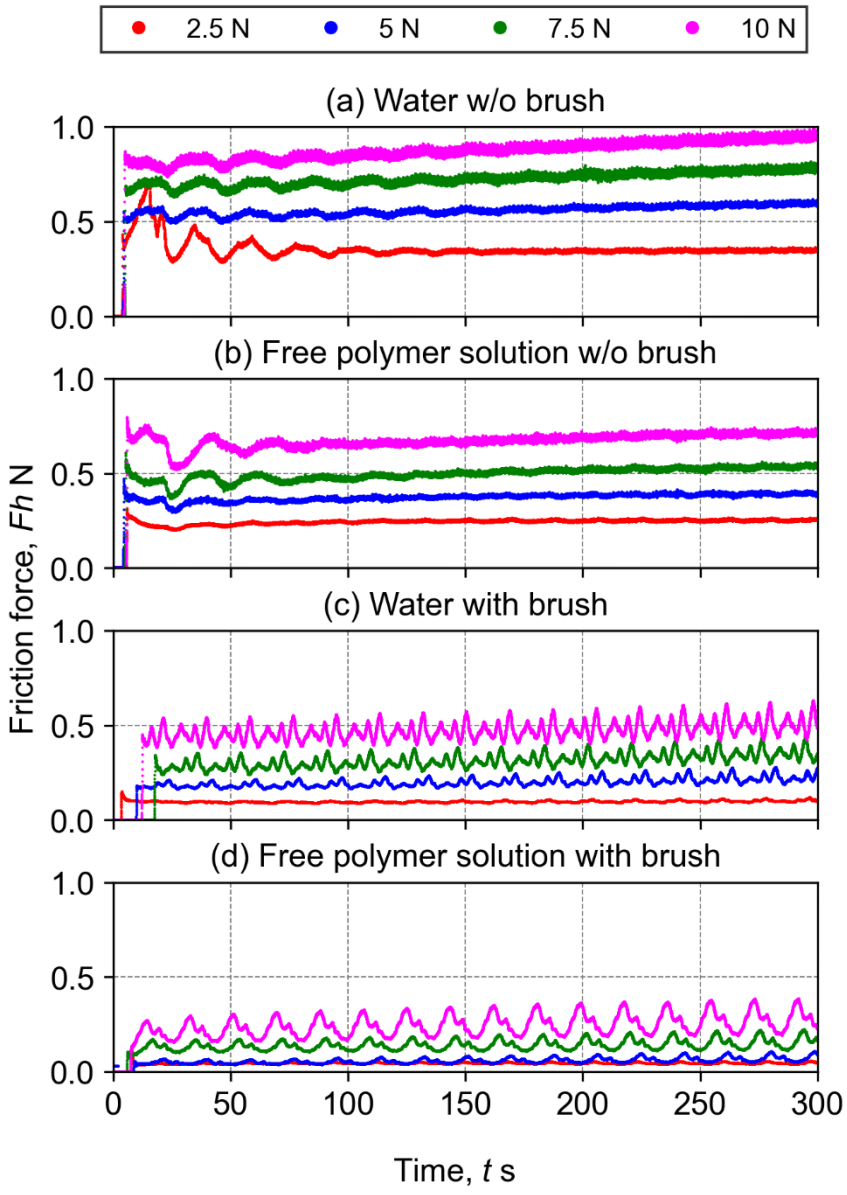

Fig. 4.6 Time variation of the frictional force measured under different sample conditions: (a) water without brush, (b) free polymer solution without brush, (c) water with brush, and (d) free polymer solution with brush under different loads from 2.5 to 10 N.

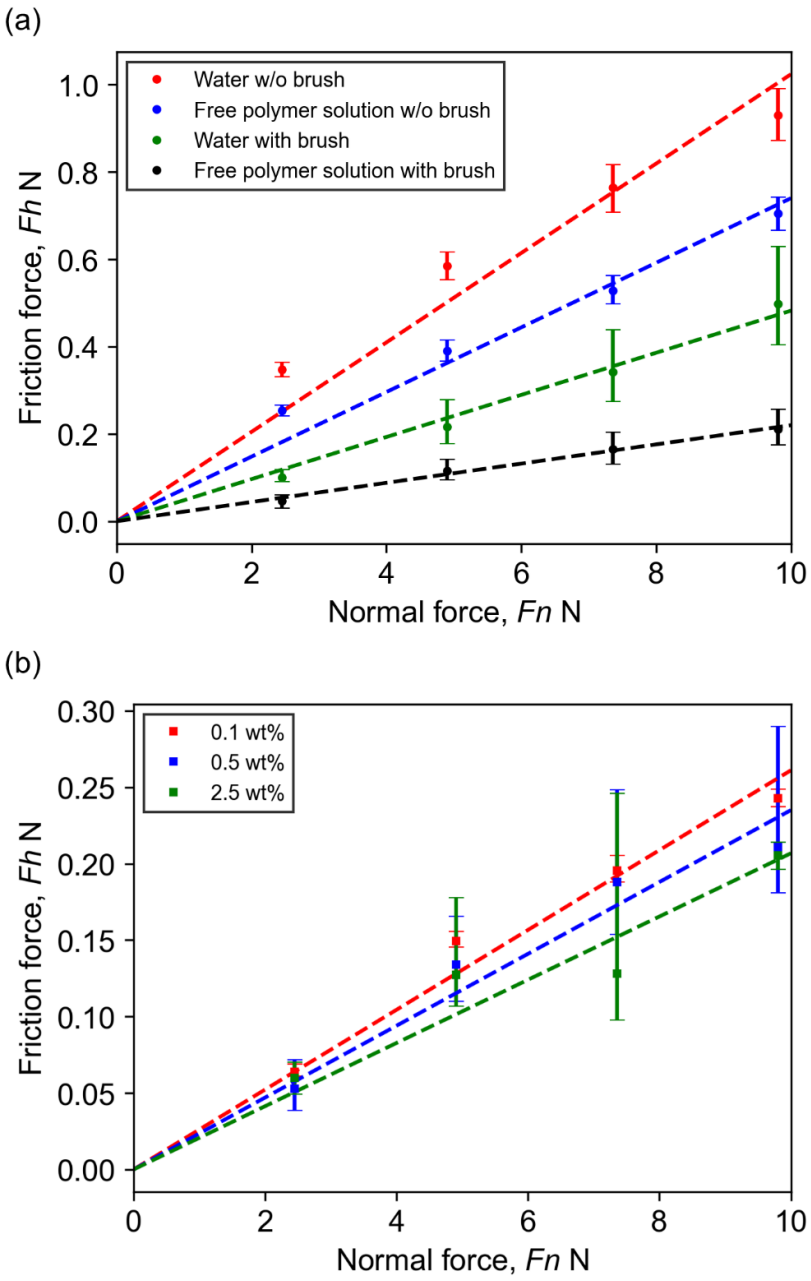

Fig. 4.7 Correlation between the friction force and load for (a) the four sample conditions (water without brush, free polymer solution without brush, water with brush, and free polymer solution with brush) and (b) for the polymer brush surface with the free polymer solution (with different concentrations) as the lubricant fluid.

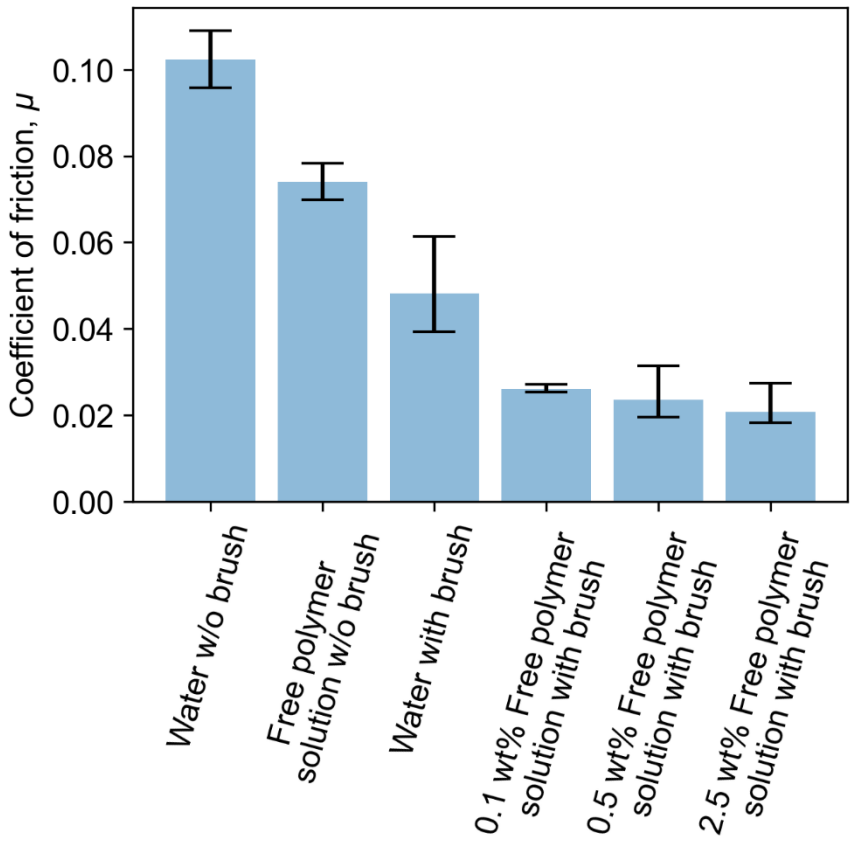

Fig. 4.8 Comparison of the COFs measured for the combinations of water with and without free polymer and substrate with and without polymer brush film. Free polymer solution of three different concentrations.

4.4.2 NR measurement

4.4.2.1 Initial condition test

Because the NR measurements were performed under lubricant fluid flow, we examined the effect of fluid flow on the molecular morphology of the polymer brush film in the hydrated state in the initial condition test. Fig. 4.9(a) shows the measured reflectance versus Q_z for a polymer brush film (h_{air} = 17 nm) with and without water flow

at a rate of 5 mL/min. In this figure, the open symbols represent the measured values; the "gentle shoulder" of the reflectance curve in the 0.2 $nm^{-1} < Q_z < 0.4$ nm^{-1} region indicates that the polymer brush is swollen in water; the fringes observed in the 0.4 $nm^{-1} < Q_z$ region indicate the presence of high-density thin parylene (density: 1.289 g/cm^3, thickness ~18 nm) and SiO_2 (density: 2.65 g/cm^3, thickness ~1 nm) films under the polymer brush film [61]. The dashed lines in the figure indicate the results of model fitting described in Section 4.2.3. The fitting results are in good agreement with those obtained experimentally.

We calculated the polymer volume fraction distribution from the model-fitting results, and the determined fractions varied as the distance from the parylene film surface increased; the corresponding results are presented in Fig. 4.9(b). The volume fraction of the polymer brushes near the surface is approximately 0.055, which corresponds to the graft density. Additionally, the volume fraction decreased as the distance from the substrate increased. According to the self-consistent field theory, for a uniform chain length in a good solvent, the dependence of the volume fraction on the distance from the substrate can be expressed by the following parabolic function [61]:

$$\phi(z) = \phi_0[1 - (z/h^*)^2] \tag{4.2}$$

where ϕ_0 is the volume fraction at z = 0, and h^* is the swelling thickness of the brush film. The solid line in Fig. 4.9(b) represents the results obtained by fitting this function to

the experimental data. Evidently, the experimental results can be fitted well by the parabolic function expressed in Eq. (4.2). The observed discrepancy between the experimental and fitted results in the $z > 100$ nm region may be attributed to variations in the length of the brush chain. The resulting h^* values are 114 and 115 nm for the without and with flow conditions, respectively, indicating good agreement between the two cases. This result implies that the volume fraction distributions are identical in both cases, and the morphology of the polymer brush film in water changes only negligibly because of liquid flow. Therefore, we did not consider the effect of liquid flow on the change in the distribution of the brush film during the measurement of the free polymer adsorption characteristics. The thickness of the hydrated sample was approximately five times larger than its pre-hydration thickness, which is consistent with the findings of previous studies [48].

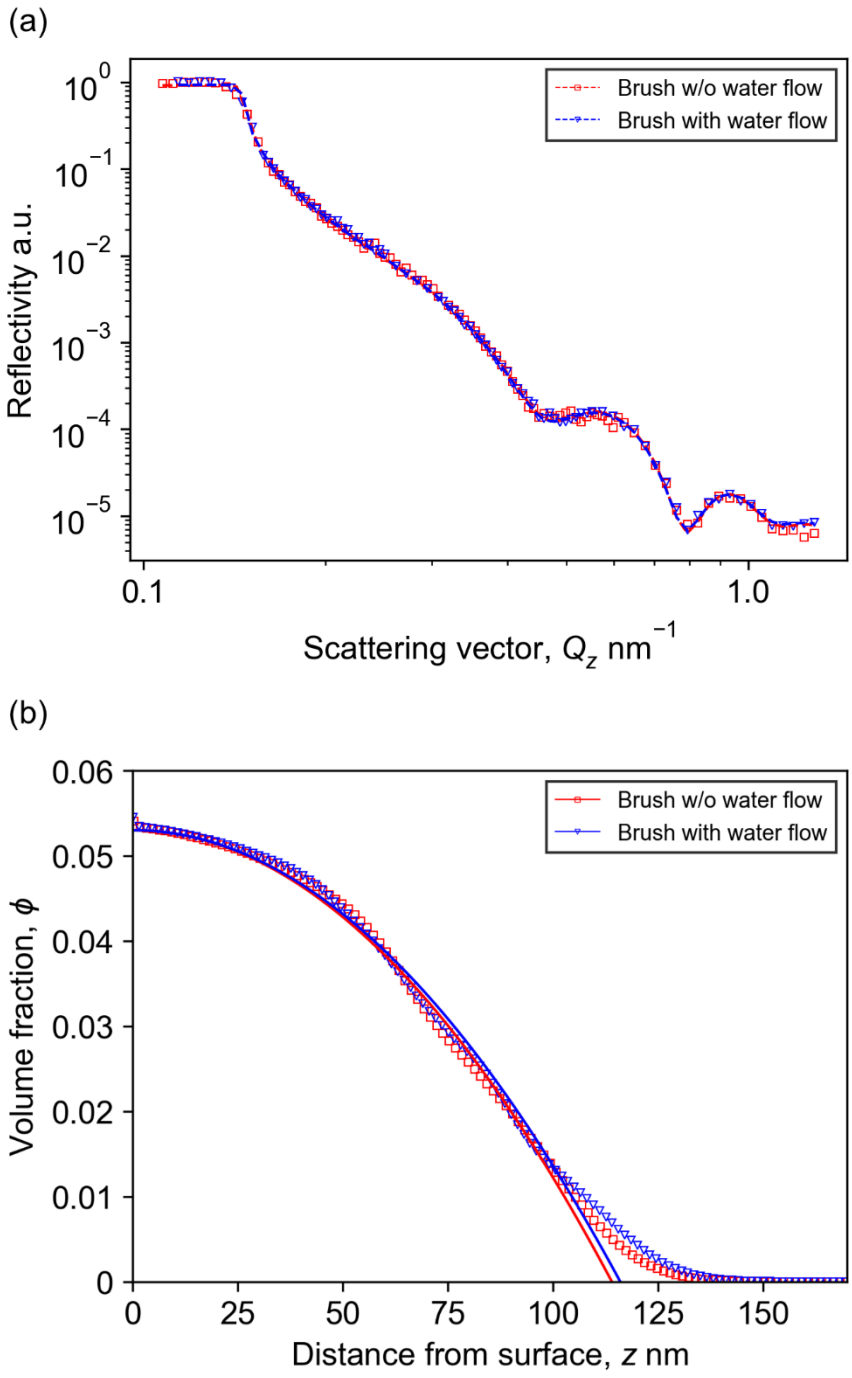

Fig. 4.9 (a) Reflectance versus Q_z and (b) polymer volume fraction distribution versus distance from the parylene film surface measured for the polymer brush film (h_{air} = 17 nm) with and without water flow.

4.4.2.2 Adsorption condition test

Next, we conducted initial and adsorption condition tests using the polymer brush films with h_{air} = 17, 23, and 35 nm. Figure 4.10(a) and (b) show the results of the initial condition test with water flow and those of the adsorption condition test. For comparison, Fig. 4.10(b) also shows the results of the measurements performed on the parylene film surface without the polymer brush film. The initial volume fractions shown in Fig. 4.10(a) are indicated by dotted lines in Fig. 4.10(b).

Based on these measurements, five characteristic quantities for each sample, viz. film thickness in the hydrated state (h*), volume fraction at the substrate surface (ϕ_0), maximum volume fraction (ϕ_{max}), position of the maximum volume fraction (h_{peak}), and average volume fraction (ϕ_{ave}), were calculated, and the corresponding values are summarized in Table. 4.4. ϕ_0 for a polymer brush film with no free polymer adsorption corresponds to the graft density. For the free polymer solutions, h* is the distance from the substrate, in which the volume fraction is higher than that in the solution by 0.001. The average volume fraction was obtained by integrating the volume fraction from z = 0 to $z = h$* and dividing it by h*. Figure 4.11 shows a schematic of the interfacial structure of the brush film and adsorbed free polymer revealed by the adsorption condition test results discussed below.

Initially, all polymer brush films exhibited a volume fraction distribution represented by a parabolic function, as well as a swelling ratio of approximately 5. Evidently, a large

h_{air} indicates a high ϕ_0, and the resulting thickness (h^*) of the swollen film is also large. The measured results of free polymer adsorption on the surface without the polymer brush film, shown in Fig. 4.10(b), indicate that h_{peak} is observed at a distance of 17 nm away from the substrate surface, and the volume fraction at the surface ϕ_0 is slightly lower than the maximum value ϕ_{max}. This result may be ascribed to the molecular structure of the commercially available MPC polymer (Lipidure-BL203), which was used as the free polymer in this study. Lipidure-BL203 is a copolymer of hydrophilic phosphorylcholine and hydrophobic groups (chemical structure not disclosed). Since the entire free polymer exhibits hydrophilicity, it can be inferred that the hydrophobic side chains are fewer than the hydrophilic ones. Consequently, the portion of the main chain that adsorbs onto the parylene surface is less than the portion extending into the water above. The parts of the main chain that are more abundant detach from the hydrophobic parylene surface and exist in the water above. Therefore, the ϕ_{max} appeared away from the parylene surface. The low ϕ_0 value may be attributed to the small proportion of the hydrophobic groups in the total volume of the polymer.

As shown in Fig. 4.10(b), when the free polymer solution was introduced (adsorption condition test), the volume fraction distribution of the polymer brush films changed drastically. First, the average volume fraction ϕ_{ave} almost doubled for all the film thicknesses, indicating the adsorption of the free polymer on the polymer brush film. The ϕ_{ave} values are also higher than that for the free polymer adsorption on the surface

without the polymer brush film, indicating that the polymer brush film effectively promotes adsorption of the free polymers. A thick polymer brush film results in a large h^* value and thus a large ϕ_{max}. Thus, we can conclude that the thicker the polymer brush film, the larger the amount of free polymer adsorbed, even if ϕ_{ave} is similar. The increase in the volume fraction owing to the adsorption of the free polymer implies that the osmotic pressure required to support the load during sliding increases, which may play a role in reducing the COF.

When the free polymer was adsorbed on the polymer brush film, ϕ_0 increased, indicating that a small fraction of the free polymer reached the substrate. However, all these ϕ_0 values are smaller than those for the free polymer adsorbed on the parylene surface without the polymer brush film. This discrepancy may be attributed to the exclusion-volume effect of the polymer brush film. Even if the area for adsorption on the substrate surface remains, the polymer brush occupies a certain amount of space near the interface, thereby preventing the free polymer from approaching the substrate surface and accordingly suppressing the adsorption on the surface. However, as mentioned before, the average volume fraction was high in the presence of the polymer brush film, indicating that the free polymer was adsorbed on the parylene surface as well as on the polymer brush. This interpretation is supported by the observed increase in the amount of adsorbed free polymer with increasing thickness of the polymer brush film; that is, a thick polymer brush film enables the adsorption of a large amount of free polymer. Van der Waals

interactions or physical entanglement are assumed between the polymer brush and the free polymer, and the corresponding details will be analyzed in future studies.

The above discussion indicates that in the case of a polymer brush film with an adsorbed free polymer, h_{peak} is determined by the balance between the free polymer adsorption-induced increase in the volume fraction and the polymer brush's exclusion-volume effect. Evidently, for a thick polymer brush film, a large h_{peak} value supports the exclusion-volume effect. In other words, the thicker the polymer brush film, the thicker the layer containing more water on the surface, and accordingly, the higher the water content (i.e., the lower the volume fraction of the polymer), the lower the shear resistance. These results demonstrated that the formation of such a layer on the surface contributed to the low friction of the polymer brush film used in combination with the free polymer solution.

When the free polymer was adsorbed on the surface of the polymer brush film, the value of h^* was lower than that measured before adsorption. In other words, the swelling rate of the polymer brush films decreased because the osmotic pressure of the free polymer solution was higher than that of pure water; therefore, water was expelled from the brush film. This phenomenon was also observed in the experiments performed using SFA by Eiser et al. [50]. Notably, this effect slightly increased ϕ_{max}.

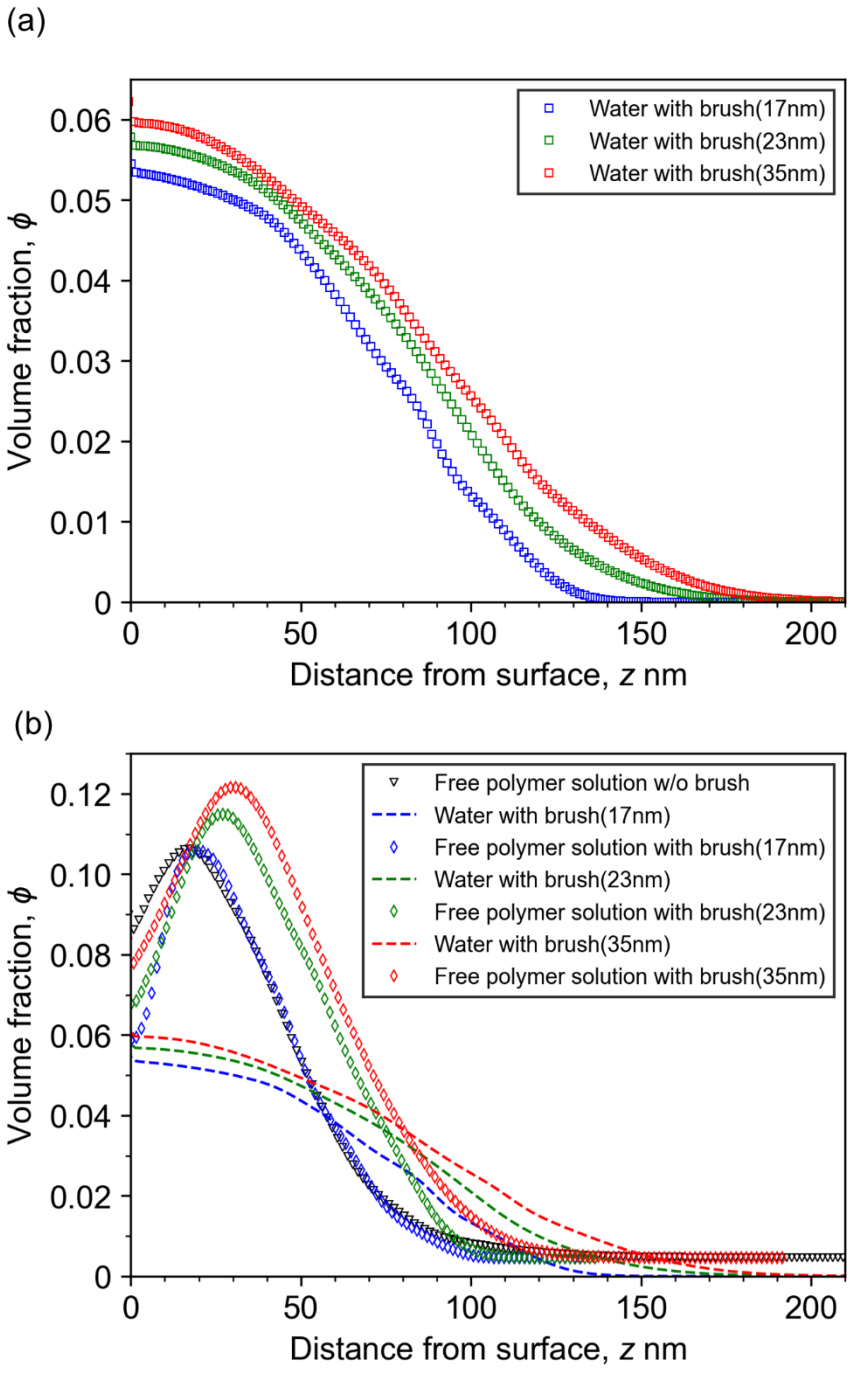

Fig. 4.10 Polymer volume fractions determined by the (a) initial condition test and (b) adsorption condition test (dotted lines show the results of the initial condition test).

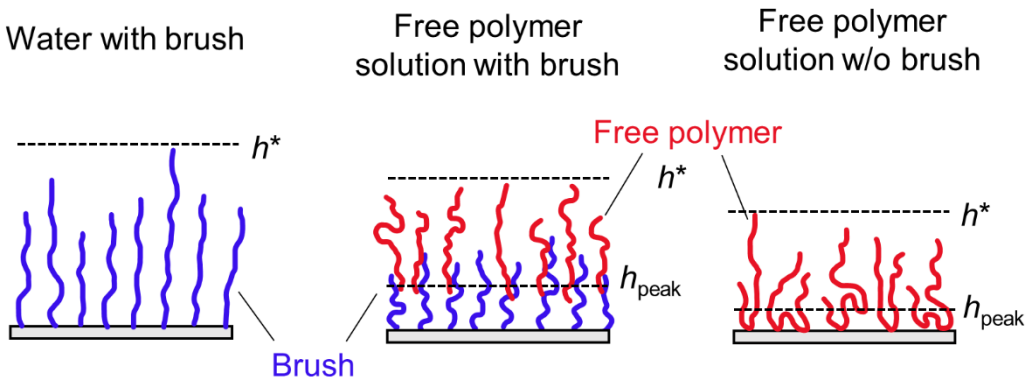

Fig. 4.11 Schematic of the interfacial structure of the brush film and adsorbed free polymer.

Table. 4.4 Five characteristic quantities determined for each sample.

Sample name	h_{air} **(nm)**	h^* **(nm)**	ϕ_0	ϕ_{max}	h_{peak} **(nm)**	ϕ_{ave}
Free polymer solution w/o brush	N.A.	124.3	0.086	0.106	17.0	0.046
Water with brush	17	132.2	0.055	N.A.	N.A.	0.031
	23	163.2	0.057	N.A.	N.A.	0.030
	35	179.3	0.060	N.A.	N.A.	0.031
Free polymer solution with brush	17	98.2	0.059	0.106	19.5	0.054
	23	104.0	0.068	0.115	27.1	0.065
	35	125.2	0.077	0.122	30.2	0.063

4.4.2.3 Rinsing test

Figure 4.12(a) shows the rinsing test results of the free polymer layer adsorbed on the parylene surface without a polymer brush film. For comparison, the volume fraction distribution of the adsorbed layer before rinsing, as shown in Fig. 4.10(b), is indicated by a dotted line. The maximum volume fraction of the adsorbed layer before rinsing exceeds 0.1 and decreases to <0.01 after the rinsing process. The volume fraction slightly decreased as the flow rate of the rinsing water increased from 1 to 3 mL/min and then to 5 mL/min; however, overall, it remained almost unchanged. These results indicated that the adsorbed free polymer film remained on the parylene surface under the flow conditions used in this study. Parylene is hydrophobic and tends to minimize its contact area with water, thus making the hydrophobic side chains of the free polymer approach the surface. This process of approach leads to molecular aggregation. Furthermore, the van der Waals forces between molecules maintain this aggregated state and enhance the stability of the aggregates. As a result, they develop resistance to the flow of water.

Figure 4.12(b) shows the rinsing test results for the free polymer layer adsorbed on the polymer brush film (h_{air} = 17 nm). For comparison, the volume fraction distribution of the initial condition shown in Fig. 4.10(a) and that of the adsorbed layer before rinsing, shown in Fig. 4.10(b), are indicated by dotted lines. These results demonstrate that the distribution of the volume fractions after rinsing was consistent with that in the initial state, irrespective of the water flow rate. Therefore, free polymer was completely removed

at a water flow rate of 1 mL/min.

The results of the rinsing test indicate that the adsorbed layer was easily desorbed when the polymer brush film was placed on the surface. This desorption phenomenon may be attributed to the excluded-volume effect of the polymer brush film as well as to the relatively weak interactions between the free polymer and polymer brush. The hydrophilic groups of the polymer brush and the free polymer are surrounded by water molecules due to hydration, forming a hydration layer. This hydration layer reduces direct contact between hydrophilic groups, thereby weakening their interaction [4]. Although the adsorbed layer was easily desorbed, the polymer brush film enhanced free polymer adsorption, as discussed in the previous section. This observation suggests that the enhanced adsorption on the polymer brush film is due to the increased probability of trapping free polymer molecules; not stronger interactions between the free polymer and the brush.

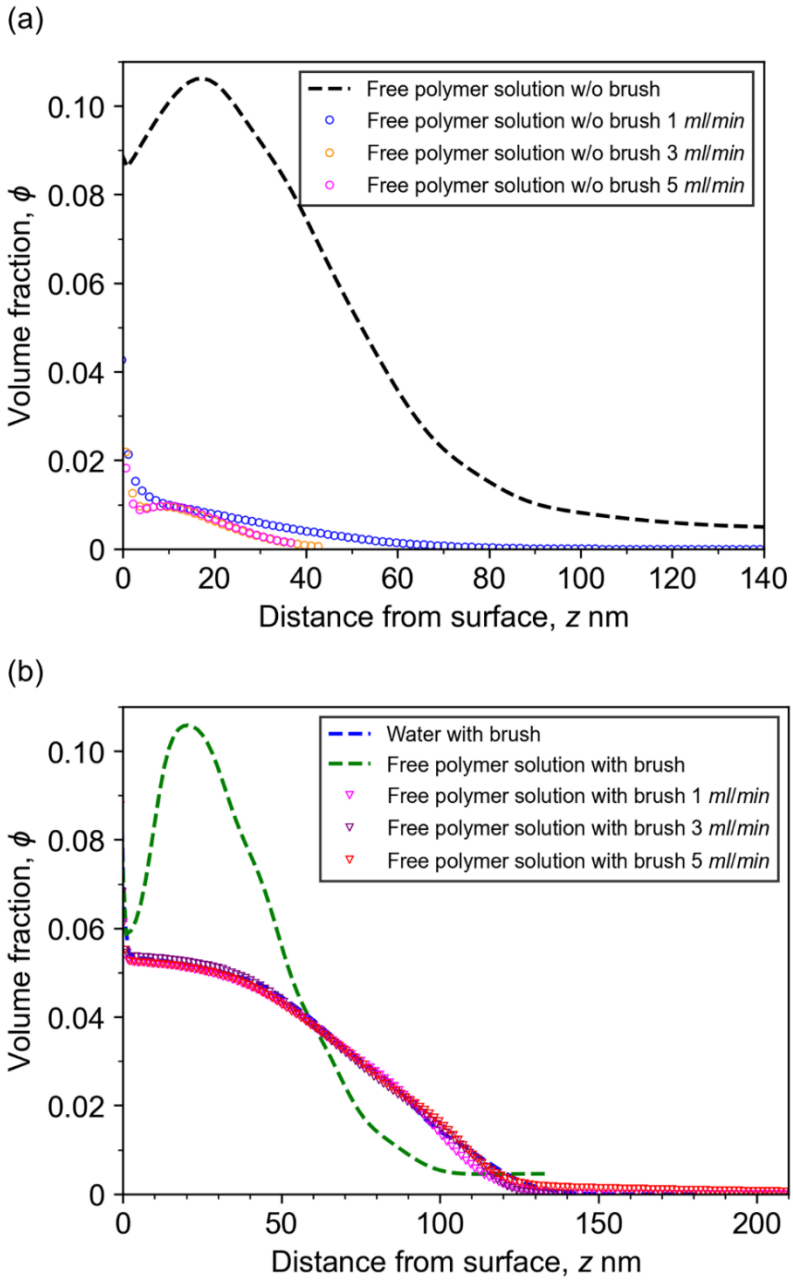

Fig. 4.12 Polymer volume fraction determined by rinsing test of the free polymer solution (a) without brush (the dotted line shows the result before rinsing) and (b) with brush (the dotted line shows the result before adsorption and rinsing).

4.4.3 FWM measurement

Figure 4.13 shows the results of the FWM measurements. For all samples, the measured damping coefficients at wider shear gaps (above approximately 150 nm) may reflect the viscosity of the lubricant fluid because the damping coefficients for the water and free polymer solutions are identical in each case, irrespective of the presence or absence of the brush film.

The spring constant is almost zero for all the samples with gaps > ~150 nm, indicating that the water and free polymer solutions are non-elastic liquids. For all three samples, the damping coefficient and spring constant increased monotonically with decreasing gap width for shear gaps < ~150 nm. In this experiment, we used polymer brush films with an average thickness of 34 nm. Compared to the NR measurements of approximately the same film thickness (35 nm; shown in Fig. 4.10), we observe that the thickness of 150 nm is nearly consistent with the swollen film thickness. Therefore, the increase in the damping coefficient and spring constant can be attributed to the contact between the probe tip and film. Thus, FWM can be used to measure the thickness of the swollen film, although the results are less accurate than those of the NR measurements.

The damping coefficients below 150 nm are the largest for the free polymer solution without the brush film, followed by those of the free polymer solution with the brush film and water with the brush film. Generally, a high damping coefficient is due to the high polymer concentration (volume fraction) in the gaps. The observed lowest damping

coefficient for water with the brush film is reasonable because it exhibits the lowest volume fraction, which is evidenced by the NR measurement results. Interestingly, the damping coefficient of the free polymer solution with the brush film, which contained a large amount of adsorbed free polymer, was lower than that of the solution without the brush film. This damping coefficient trend may be ascribed to the suppression of the physical adsorption of the free polymer onto the substrate by the excluded-volume effect of the brush film, as previously described. Because of the lower volume fraction near the surface, the free polymer was more easily desorbed from the brush surface upon shearing and penetration of the probe, resulting in lower damping. This interpretation is qualitatively consistent with the results of the NR-measurement-based rinsing test, in which the free polymer was removed more easily when a brush film was present.

The differences between the spring constants of the samples can be interpretated similarly to the differences in their damping coefficients. The spring constants of the samples exhibited the following sequence: water with the brush film < free polymer solutions with the brush film < free polymer solutions without the brush film. The brush film tends to eject the free polymer from the shear gap, resulting in a spring constant that is smaller than that for the without the brush film case. At gaps of ≦ 30 nm, the damping coefficients and spring constants were almost identical with and without the free polymer when the brush film was present on the surface. This result suggests that the free polymer was almost completely expelled from the shear gap.

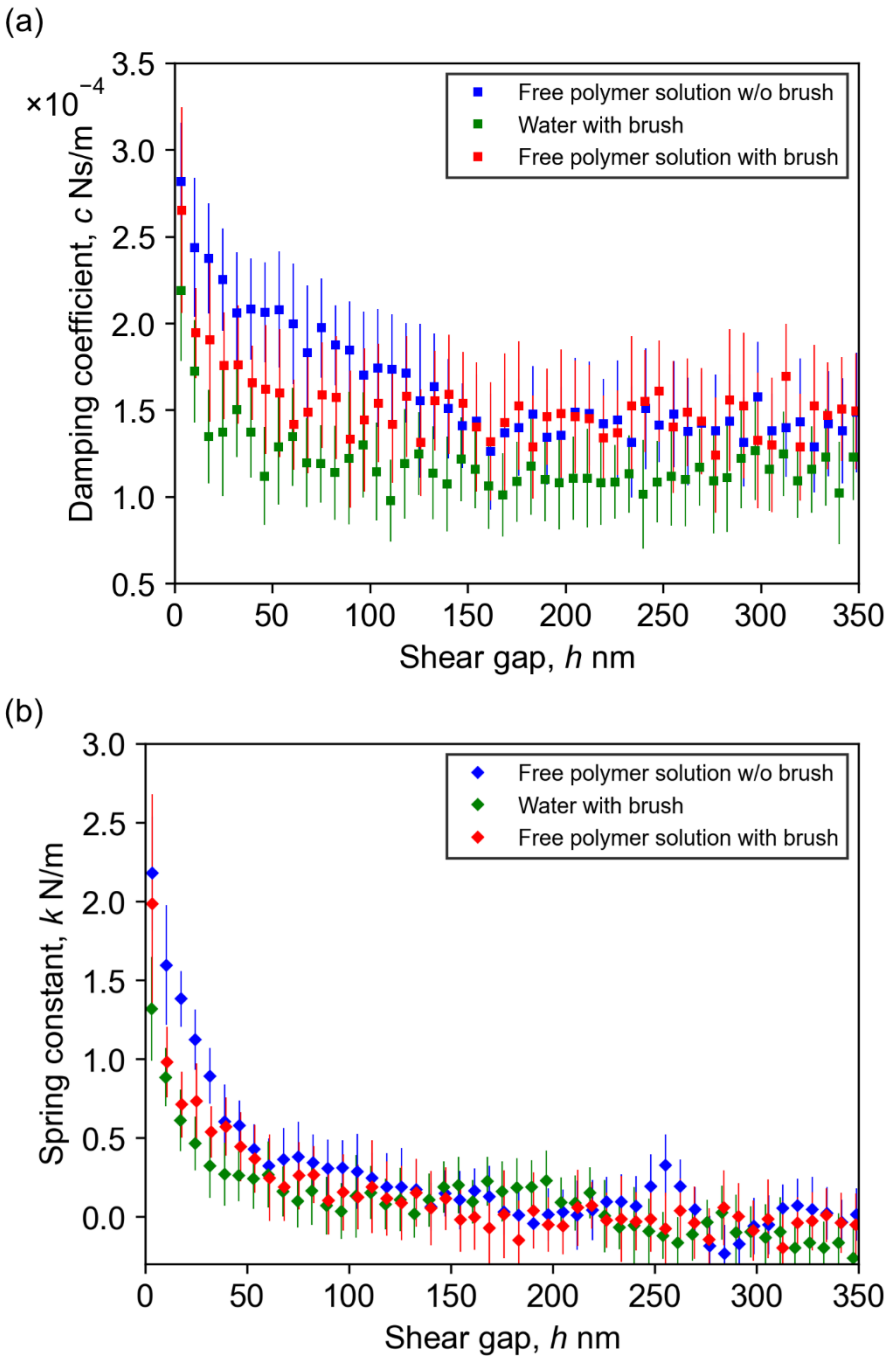

Fig. 4.13 (a) Damping coefficient and (b) spring constant measured at different shear gap widths. Error bars show the standard deviations.

4.5 Effect of free polymers on enhancing lubricity

NR measurements indicated that the adsorbed free polymer formed a layer on the surface of the brush film. The lowest COF observed for the brush film with the free polymer solution can be attributed to the adsorption of free polymers at the friction interface. The COF is defined as the frictional force divided by the load. Therefore, to decrease the COF, the load-bearing capacity of the film should be increased, the resistance of the film to shear deformation should be decreased, or both the conditions should be fulfilled. In addition, NR measurements suggest that when the adsorbed free polymer forms a layer on the surface of the brush film, the average volume fraction is almost double that of the brush film alone. This result indicates that the osmotic pressure of the film increased, and the load-bearing capacity was improved.

Furthermore, even when a free polymer was adsorbed on the brush film, a water-rich layer existed near the surface, which allowed easy detachment of the adsorbed free polymer from the surface and decreased its shear resistance, as revealed by the rinsing test during the NR and FWM measurements. Two mechanisms may be responsible for the low shear resistance, as shown in Fig. 4.14 First, the intermolecular interactions between the brush film and free polymer are weak, and therefore, the shear strain on the polymer is low. Second, the water-rich layer near the interface exhibits low viscosity and is responsible for the apparent slip flow of the adsorbed free polymer layer.

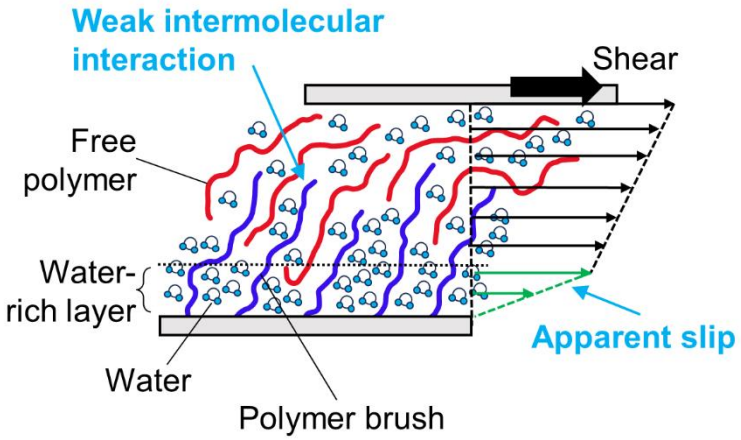

Fig. 4.14 Schematic of the desorbed free polymer layer on the surfaces with brush film under shear.

The slip plane may be located in the adsorbed free polymer region because of the difference in viscosity caused by the difference between the volume fractions of the adsorption film and the polymer solution. However, as shown in Fig. 4.12(b), the free polymer adsorbed on the brush surface is completely desorbed by rinsing. Based on this result, we can hypothesize that a slip plane exists near the surface of the water-rich polymer brush, and if a slip plane exists in the free polymer layer, the free polymer remains on the brush film surface after rinsing. In the case without the brush film, the free polymer remained after rinsing (Fig. 4.12(a)). In other words, slip may occur in the free polymer-adsorbed layer depending on the surface conditions.

For hydrated films, such as those investigated in this study, distinctly defining the slip plane may be inherently challenging because of the unclear interface boundaries

caused by the continuously varying density. Based on a comparison of the results obtained with and without the brush film, we can speculate that the water-rich layer formed on the surface contributed to the slip. To clarify our hypothesis, in the future, we will investigate the dependence of film desorption on the shear stress applied to the adsorbed layer of the free polymer by systematically varying the water flow rate during rinsing.

Although the conditions of the friction tests conducted in this study corresponded to the boundary lubrication regime, the strategy of combining free polymers with polymer brushes could be effective in the hydrodynamic lubrication or EHL (elastohydrodynamic lubrication) regime. The NR experimental results indicated that the volume fraction of the free polymer adsorbed on the brush exceeded that in the solution, and the adsorbed free polymer exhibited low shear resistance. Consequently, we believe that when transitioning to hydrodynamic lubrication or EHL regimes, the adsorbed free polymer is released into the lubricant, thus increasing its concentration as well as the dynamic pressure, which are expected to enhance the load-carrying capacity. If the water-rich layer at the interface promotes interfacial slip, friction can be reduced. However, excessive slip reduces the load capacity. Therefore, it is necessary to strike an appropriate balance between the slip and load capacity in the design of fluid lubricants and EHL.

Estimating the Weissenberg number (W_i) allows for a more generalized evaluation of the viscoelastic properties of films and may allow for further discussion of the influence of viscoelasticity on the lubrication performance. The Weissenberg number is

defined as: $W_i = \dot{\gamma}\lambda$, where $\dot{\gamma}$ is the shear rate, and λ is the relaxation time. To estimate the relaxation time, we calculated the loss tangent ($\tan\Delta$) using the formula $\tan\Delta = c/(k/\omega)$ with the results of the FWM measurements (Fig. 4.13). A low $\tan\Delta$ indicates more elastic behavior, i.e., the material stores more energy during deformation. In contrast, a high $\tan\Delta$ implies a predominant viscous behavior with increased energy dissipation, such as in the form of heat, and poor elastic recovery. The inverse of the shear frequency at which $\tan\Delta = 1$ corresponds to the relaxation time. The experimental results obtained using the FWM indicate that $\tan\Delta$ = 1 when the shear gap is approximately 10 nm for all the samples. Thus, as the shear frequency is 1 kHz, the relaxation time for a film sheared at a gap of 10 nm is estimated to be approximately 1 ms. A shorter relaxation time was expected for a gap ≥10 nm. We should note that, in this study, FWM-based shear viscoelasticity measurements were primarily performed to demonstrate the low shear resistance of the combined free polymer–brush film system, and viscoelastic tests over a wider frequency band are required for the accurate determination of the relaxation time, which will be investigated in detail in the future. The sliding speed in the POD friction test was 1.2 mm/s. Precise determination of the shear gap during the friction test was challenging; however, because the maximum thickness of the adsorption film was approximately 100 nm, the gap during friction was estimated to be 10–100 nm, and consequently, the estimated shear rate was 10^4–10^5 s^{-1}. If the relaxation time is assumed to be of the order of 1 ms, then W_i is estimated to be in the range of 10–100, which aligns

with the findings reported by Gamaniel et al., who suggests that large W_i correlate with small COF [56]. The observed viscoelastic thin-film-mediated lubricity improvement is a new framework for lubrication technology and differs from the principles of fluid and boundary lubrication.

4.6 Conclusion of Chapter 4

In this study, we examined the synergistic effects of free MPC polymers present in a lubricant fluid and MPC polymer brushes formed on a substrate on the hydration lubrication properties. POD friction tests revealed that the addition of the free polymer to the lubricant fluid effectively decreased the COF under the boundary lubrication condition, and this COF was lower than that observed when only a brush film was used. To elucidate the mechanism of the improved lubricity, we performed NR measurements and employed FWM. The NR measurement results revealed the structure of the hydration interface, which was composed of a polymer brush and an adsorbed free polymer. The FWM results revealed the shear viscoelasticity of the adsorbed and brush films. The following conclusions were drawn from the findings of this study:

1. The adsorbed free polymer forms a layer on the surface of the polymer brush film; a long brush allows the adsorption of a large amount of free polymer. Furthermore, the volume fraction of the polymer increased with adsorption. These results suggest that

osmotic pressure increases, resulting in improved load-bearing performance.

2. When a polymer brush film is present on the surface, a water-rich layer remains in the vicinity of the surface after the free polymer adsorption because of the exclusion-volume effect of the polymer brush film. In this case, the adsorbed free polymer layer can be easily removed from the surface, and the shear resistance is low.

In summary, the lubricity improved because the adsorbed free polymers improved the load-carrying capacity, and the water-rich layer formed on the surface reduced the shear resistance. Increasing the load-carrying capacity by increasing the volume fraction of the polymer film near the interface and decreasing the shear resistance of the polymer film are generally contradictory (it is clear that increasing the volume fraction increases the shear resistance). We believe that a lubrication system that combines a polymer brush film with a lubricant containing free polymers, as verified in this study, can be a breakthrough technology to overcome this contradiction. In this lubrication system, the excluded-volume effect of the polymer brush film is used to maintain a water-rich (low volume fraction of polymer) layer near the interface, while a layer of adsorbed polymer with a high volume fraction forms on top of it. The former layer resulted in low shear resistance, whereas the latter enhanced the load-bearing performance. An optimal design of such a layered structure can be developed by controlling the molecular structure and adsorption configuration of the polymer brush film and free polymers, and this feature

will aid in further improving hydration lubricity.

5. Conclusion

This thesis embarked on a comprehensive journey to explore the complex domain of hydration lubrication by phospholipid polymer brushes, critical for reducing the coefficient of friction (COF) in mechanical systems such as artificial joints. With two primary research objectives, the study was meticulously designed to unravel the intricate dynamics of MPC polymer brush films and their interaction with free MPC polymers in a lubrication environment. The first objective aimed to reveal the mechanisms of hydration lubrication by measuring the shear viscoelasticity of hydrated MPC polymer brush films and its correlation with frictional properties, emphasizing the influence of gap width on lubrication properties. This is crucial in bridging the theoretical understanding and practical application of hydration lubrication, where surface roughness leads to a distribution of gaps. The second objective was to elucidate the role of free polymers in the lubricant fluid and investigate how their interaction with polymer brush films could enhance overall lubrication performance. This research is anticipated to contribute to extending the lifespan of artificial joints with polymer brush coatings.

Chapter 2 presents the implementation of the fiber wobbling method (FWM), a novel approach developed to measure shear viscoelasticity. This method proved essential for understanding the behavior of hydrated MPC polymer brush films under various shear gaps. To achieve precise measurements of both shear gap and viscoelasticity, the study

integrated the original FWM with an inverted microscope and introduced a patterned film measurement approach. The newly constructed FWM apparatus achieved a shear force measurement accuracy of 0.2 nN and a shear gap measurement precision of 5 nm, thereby facilitating simultaneous measurements of shear viscoelasticity and gap.

Chapter 3 describes the preparation of MPC polymer brush films, including photo-induced polymerization, patterning, and characterization processes. Two film thicknesses of 50 nm and 70 nm were prepared, and film patterns with a diameter of approximately 10 μm were successfully created via photolithography. The NR measurements confirmed the graft density of the prepared MPC polymer brush at around 5%, and their swelling in water was verified. Subsequently, the shear viscoelasticity's gap dependence was measured, and the normal force was estimated from the probe's axial deformation, from which the COF's gap dependence was calculated. The MPC polymer brush films achieved ultra-high lubrication with a COF lower than 0.0001. By comparing the changes in shear viscoelasticity and COF with gap variation, we established a direct correlation between the film's viscoelastic response and its friction coefficient. It was found that the MPC polymer brush films were in an effective lubrication state under two conditions: when the film was compressed to a certain extent but osmotic pressure maintained free water within the film, and when the film was compressed to a gap less than its thickness in air, where hydrated water played a significant role in lubrication. Therefore, these two different hydration lubrication mechanisms can be comprehensively explained through the

viscoelastic properties of the film.

Chapter 4 examines the synergistic effects of free MPC polymers and MPC polymer brushes. POD tribometry friction tests indicated that the COF of MPC polymer could be as low as 0.01 order, demonstrating the effectiveness of free polymers in improving the lubrication of hydrated polymer brush films from a macroscopic perspective. Through NR measurements and FWM, we explored the mechanism behind this phenomenon at a microscopic level. NR measurements confirmed the adsorption of free polymers on the polymer brush, and the increased osmotic pressure due to increased film density was considered to enhance load capacity. Additionally, the results from NR measurements and FWM demonstrated different adsorption characteristics of free polymers on surfaces with and without polymer brushes. On surfaces with polymer brushes, adsorbed free polymers formed a low-viscosity, water-rich layer near the substrate, and free polymers were more easily desorbed from the brush. These findings suggest that the presence of a polymer brush can reduce the shear resistance of free polymers, thereby lowering friction. This chapter highlights the potential of combining polymer brush films with free polymers in a lubricant to create surfaces with superior lubricating qualities, thus, to improve the use life of artificial joints.

In conclusion, this thesis makes a significant contribution to the field of tribology, focusing on hydration lubrication. It addresses two critical research areas: an in-depth analysis of the shear viscoelastic properties of hydrated MPC polymer brush films and

their gap dependence, and an investigation into the role of free polymers in enhancing lubrication properties. The research elucidates how variations in gap width significantly affect the lubrication characteristics of these films and how the interaction between free polymers and MPC polymer brush films can improve lubrication efficiency.

Looking forward, the potential for future research is vast. Building on the foundation laid by this thesis, subsequent studies could explore the optimization of molecular-level parameters in these systems, considering aspects such as graft density and chain length. Moreover, understanding the role of surface roughness and the distribution of shear gaps could lead to the development of more robust and efficient lubrication designs. This thesis contributes significantly to our scientific understanding of hydration lubrication and holds great promise for practical applications where reducing friction is crucial, such as in the design of artificial joints. Estimates of the contact pressure that the hydrated MPC polymer brush can withstand revealed that it is higher than the typical pressure in human hip joints. Therefore, when applying MPC films in artificial joints, it is believed that the film will not be fully compressed, maintaining a certain thickness. This highlights the importance of controlling the optimal gap. However, there are still unresolved issues regarding how changes in gaps caused by relative motion between surfaces with roughness affect lubrication properties. Research on the normal viscoelastic properties of the polymer layer is considered to have significant implications, especially for the dehydration-rehydration characteristics of the film and the impact of surface roughness.

In the context of artificial joint design, the study highlights the importance of material hardness and surface roughness. The materials used in actual artificial joint surfaces are resin and metal alloys, with surface roughness comparable to the urethane slider used in POD tests. Thus, the COF measured in POD tests is considered close to the actual conditions of artificial joints. The results of the first research objective suggest that the gap dependence of the COF of polymer brush films measured by FWM indicates possibilities for maintaining optimal gaps by improving surface uniformity or using soft materials. This implies that while the current COF of artificial joints is close to the results obtained in POD tests, advancements in lubrication design could potentially achieve the ultra-low friction phenomenon observed in FWM tests. As for the second research objective, prior studies have shown that injecting free MPC polymers can reduce cartilage friction and alleviate symptoms of arthritis [77]. Our results suggest that introducing free polymers might also play a role in improving the lubrication and extending the lifespan of artificial joints with MPC polymer brush coatings.

Therefore, the findings of this study not only enhance the theoretical framework of lubrication mechanisms but also provide a solid foundation for the development of more efficient and effective lubrication systems, marrying rigorous scientific research with practical technological innovation.

Reference

[1] K. Holmberg, P. Andersson, and A. Erdemir, “Tribology International Global energy consumption due to friction in passenger cars,” *Tribiology Int.*, vol. 47, pp. 221–234, 2012, doi: 10.1016/j.triboint.2011.11.022.

[2] K. Holmberg and A. Erdemir, “Global Impact of Friction on Energy Consumption , Economy and Environment,” pp. 181–185, 2015, doi: 10.5937/fmet1503181H.

[3] J. Luo and X. Zhou, “Superlubricitive engineering — Future industry nearly getting rid of wear and frictional energy consumption,” vol. 8, no. 4, pp. 643–665, 2020.

[4] J. Klein, “Hydration lubrication,” *Friction*, vol. 1, no. 1, pp. 1–23, 2013, doi: 10.1007/s40544-013-0001-7.

[5] W. Lin and J. Klein, “Recent Progress in Cartilage Lubrication,” vol. 2005513, pp. 1–23, 2021, doi: 10.1002/adma.202005513.

[6] J. M. Coles, D. P. Chang, and S. Zauscher, “Current Opinion in Colloid & Interface Science Molecular mechanisms of aqueous boundary lubrication by mucinous glycoproteins,” *Curr. Opin. Colloid Interface Sci.*, vol. 15, no. 6, pp. 406–416, 2010, doi: 10.1016/j.cocis.2010.07.002.

[7] T. Han, S. Zhang, and C. Zhang, “Unlocking the secrets behind liquid superlubricity : A state-of- the-art review on phenomena and mechanisms,” vol. 10, no. 8, pp. 1137–1165, 2022.

[8] L. Ma, A. Gaisinskaya-Kipnis, N. Kampf, and J. Klein, “Origins of hydration lubrication,” *Nat. Commun.*, vol. 6, pp. 8–13, 2015, doi: 10.1038/ncomms7060.

[9] W. Lin and J. Klein, “Hydration Lubrication in Biomedical Applications : From Cartilage to Hydrogels,” 2022, doi: 10.1021/accountsmr.1c00219.

[10] D. L. Burris and A. C. Moore, “Biotribology Cartilage and Joint Lubrication : New Insights Into the Role of Hydrodynamics,” *Biotribology*, vol. 12, no. May, pp. 8–14, 2017, doi: 10.1016/j.biotri.2017.09.001.

[11] T. Murakami, K. Nakashima, Y. Sawae, N. Sakai, and N. Hosoda, “Roles of adsorbed film and gel layer in hydration lubrication for articular cartilage,” vol. 223, 2009, doi: 10.1243/13506501JET536.

[12] W. Lin, Z. Liu, N. Kampf, J. Klein, “The Role of Hyaluronic Acid in Cartilage Boundary Lubrication,” 2020.

[13] Z. Li, S. Ma, G. Zhang, D. Wang, and F. Zhou, “Soft / Hard-Coupled Amphiphilic Polymer Nanospheres for Water Lubrication,” 2018, doi: 10.1021/acsami.8b00405.

[14] S. Jahn and J. Klein, “Hydration Lubrication : The Macromolecular Domain,” 2015, doi: 10.1021/acs.macromol.5b00327.

[15] U. Raviv, S. Giasson, and N. Kampf, “Lubrication by charged polymers,” pp. 163–165, 2003.

[16] M. Chen, W. H. Briscoe, S. P. Armes, H. Cohen, and J. Klein, “Polyzwitterionic brushes : Extreme lubrication by design,” *Eur. Polym. J.*, vol. 47, no. 4, pp. 511–523, 2011, doi: 10.1016/j.eurpolymj.2010.10.007.

[17] K. Ishihara, “Highly lubricated polymer interfaces for advanced artificial hip joints through biomimetic design,” *Polym. J.*, vol. 47, no. 9, pp. 585–597, 2015, doi: 10.1038/pj.2015.45.

[18] W. Yang and F. Zhou, “Polymer brushes for antibiofouling and lubrication,” *Biosurface and Biotribology*, vol. 3, no. 3, pp. 97–114, 2017, doi: 10.1016/j.bsbt.2017.10.001.

[19] K. Ishihara, Y. Iwasaki, S. Ebihara, Y. Shindo, and N. Nakabayashi, “Photoinduced graft polymerization of 2-methacryloyloxyethyl phosphorylcholine on polyethylene membrane surface for obtaining blood cell adhesion resistance,” *Colloids Surfaces B Biointerfaces*, vol. 18, no. 3–4, pp. 325–335, Oct. 2000, doi: 10.1016/S0927-7765(99)00158-7.

[20] T. Moro, Y. Takatori, K. Ishihara, K. Nakamura, and H. Kawaguchi, “2006 Frank Stinchfield award: Grafting of biocompatible polymer for longevity of artificial hip joints,” in *Clinical Orthopaedics and Related Research*, 2006, no. 453. doi: 10.1097/01.blo.0000246553.33434.5f.

[21] T. Moro *et al.*, “Surface grafting of artificial joints with a biocompatible polymer

for preventing periprosthetic osteolysis," *Nat. Mater.*, vol. 3, no. 11, pp. 829–836, 2004, doi: 10.1038/nmat1233.

[22] M. Z. Baykara, M. R. Vazirisereshk, and A. Martini, "Emerging superlubricity: A review of the state of the art and perspectives on future research," *Appl. Phys. Rev.*, vol. 5, no. 4, 2018, doi: 10.1063/1.5051445.

[23] S. Feng, Y. Liu, J. Li, and S. Wen, "Superlubricity Achieved with Zwitterionic Brushes in Diverse Conditions Induced by Shear Actions," *Macromolecules*, vol. 54, no. 12, pp. 5719–5727, 2021, doi: 10.1021/acs.macromol.1c00430.

[24] O. Tairy, N. Kampf, M. J. Driver, S. P. Armes, and J. Klein, "Dense, highly hydrated polymer brushes via modified atom-transfer-radical-polymerization: Structure, surface interactions, and frictional dissipation," *Macromolecules*, vol. 48, no. 1, pp. 140–151, 2015, doi: 10.1021/ma5019439.

[25] W. Lin and J. Klein, "Control of surface forces through hydrated boundary layers," *Curr. Opin. Colloid Interface Sci.*, vol. 44, pp. 94–106, 2019, doi: 10.1016/j.cocis.2019.10.001.

[26] M. Kobayashi *et al.*, "Friction behavior of high-density poly(2-methacryloyloxyethyl phosphorylcholine) brush in aqueous media," *Soft Matter*, vol. 3, no. 6, pp. 740–746, 2007, doi: 10.1039/b615780g.

[27] M. Kobayashi and A. Takahara, "Tribological properties of hydrophilic polymer

brushes under wet conditions," *Chem. Rec.*, vol. 10, no. 4, pp. 208–216, 2010, doi: 10.1002/tcr.201000001.

[28] R. Zhang *et al.*, "The Weak Interaction of Surfactants with Polymer Brushes and Its Impact on Lubricating Behavior," *Macromolecules*, vol. 48, no. 17, pp. 6186–6196, 2015, doi: 10.1021/acs.macromol.5b01267.

[29] T. Røn, I. Javakhishvili, S. Hvilsted, K. Jankova, and S. Lee, "Ultralow Friction with Hydrophilic Polymer Brushes in Water as Segregated from Silicone Matrix," *Adv. Mater. Interfaces*, vol. 3, no. 2, pp. 1–11, 2016, doi: 10.1002/admi.201500472.

[30] S. T. Milner, T. A. Witten, and M. E. Cates, "Theory of the Grafted Polymer Brush," *Macromolecules*, vol. 21, no. 8, pp. 2610–2619, 1988, doi: 10.1021/ma00186a051.

[31] D. Shim, M. Cates, "Finite extensibility and density saturation effects in the polymer brush," *Journal de Physique* vol. 50, no. 1989, pp. 3535–3551, 1989.

[32] P. Lai, "Structure of a bidisperse polymer brush: Monte Carlo simulation and self-consistent field results," pp. 5201–5207, 1992.

[33] S. Ji and J. Ding, "Rheology of polymer brush under oscillatory shear flow studied by nonequilibrium Monte Carlo simulation," *J. Chem. Phys.*, vol. 123, no. 14, 2005, doi: 10.1063/1.2018630.

[34] W. M. de Vos and F. A. M. Leermakers, "Modeling the structure of a polydisperse polymer brush," *Polymer (Guildf).*, vol. 50, no. 1, pp. 305–316, 2009, doi:

10.1016/j.polymer.2008.10.025.

[35] S. Z. He, H. Merlitz, L. Chen, J. U. Sommer, and C. X. Wu, "Polyelectrolyte brushes: Md simulation and SCF theory," *Macromolecules*, vol. 43, no. 18, pp. 7845–7851, 2010, doi: 10.1021/ma101230v.

[36] W. A. Hamilton, G. S. Smith, N. A. Alcantar, J. Majewski, R. G. Toomey, and T. L. Kuhl, "Determining the density profile of confined polymer brushes with neutron reflectivity," *J. Polym. Sci. Part B Polym. Phys.*, vol. 42, no. 17, pp. 3290–3301, 2004, doi: 10.1002/polb.20170.

[37] D. J. Mulder and T. L. Kuhl, "Polymer brushes in restricted geometries," *Soft Matter*, vol. 6, no. 21, pp. 5401–5407, 2010, doi: 10.1039/c0sm00444h.

[38] M. Moglianetti, J. R. P. Webster, S. Edmondson, S. P. Armes, and S. Titmuss, "A neutron reflectivity study of surfactant self-assembly in weak polyelectrolyte brushes at the sapphire-water interface," *Langmuir*, vol. 27, no. 8, pp. 4489–4496, 2011, doi: 10.1021/la200211x.

[39] A. Korolkovas *et al.*, "Polymer Brush Collapse under Shear Flow," *Macromolecules*, vol. 50, no. 3, pp. 1215–1224, 2017, doi: 10.1021/acs.macromol.6b02525.

[40] H. Nakano, Y. Noguchi, S. Kakinoki, M. Yamakawa, I. Osaka, and Y. Iwasaki, "Highly Durable Lubricity of Photo-Cross-Linked Zwitterionic Polymer Brushes

Supported by Poly(ether ether ketone) Substrate," *ACS Appl. Bio Mater.*, vol. 3, no. 2, pp. 1071–1078, 2020, doi: 10.1021/acsabm.9b01040.

[41] L. Tsarkova, X. Zhang, N. Hadjichristidis, and J. Klein, "Friction and relaxation dynamics of highly extended polymer brush melts under compression and shear," *Macromolecules*, vol. 40, no. 7, pp. 2539–2547, 2007, doi: 10.1021/ma062503g.

[42] M. L. Oyen, "Nanoindentation of hydrated materials and tissues," *Curr. Opin. Solid State Mater. Sci.*, vol. 19, no. 6, pp. 317–323, 2015, doi: 10.1016/j.cossms.2015.03.001.

[43] K. Binder, T. Kreer, and A. Milchev, "Polymer brushes under flow and in other out-of-equilibrium conditions," *Soft Matter*, vol. 7, no. 16, pp. 7159–7172, 2011, doi: 10.1039/c1sm05212h.

[44] J. Seror, L. Zhu, R. Goldberg, A. J. Day, and J. Klein, "Supramolecular synergy in the boundary lubrication of synovial joints," *Nat. Commun.*, vol. 6, 2015, doi: 10.1038/ncomms7497.

[45] S. Jahn, J. Seror, and J. Klein, "Lubrication of Articular Cartilage," *Annu. Rev. Biomed. Eng.*, vol. 18, pp. 235–258, 2016, doi: 10.1146/annurev-bioeng-081514-123305.

[46] W. Lin and J. Klein, "Recent Progress in Cartilage Lubrication," *Adv. Mater.*, vol. 33, no. 18, pp. 1–23, 2021, doi: 10.1002/adma.202005513.

[47] D. Xiong, Y. Deng, N. Wang, and Y. Yang, “Influence of surface PMPC brushes on tribological and biocompatibility properties of UHMWPE,” *Appl. Surf. Sci.*, vol. 298, pp. 56–61, 2014, doi: 10.1016/j.apsusc.2014.01.088.

[48] M. Chen, W. H. Briscoe, S. P. Armes, and J. Klein, “Lubrication at physiological pressures by polyzwitterionic brushes,” *Science (80-.).*, vol. 323, no. 5922, pp. 1698–1701, 2009, doi: 10.1126/science.1169399.

[49] W. Yan, S. N. Ramakrishna, M. Romio, and E. M. Benetti, “Bioinert and Lubricious Surfaces by Macromolecular Design,” 2019, doi: 10.1021/acs.langmuir.9b02316.

[50] E. Eiser and J. Klein, “The effect of mobile polymers on the normal and shear forces between polymer brushes,” *Macromolecules*, vol. 40, no. 23, pp. 8455–8463, 2007, doi: 10.1021/ma071000n.

[51] F. Goujon, P. Malfreyt, and D. J. Tildesley, “Interactions between polymer brushes and a polymer solution: Mesoscale modelling of the structural and frictional properties,” *Soft Matter*, vol. 6, no. 15, pp. 3472–3481, 2010, doi: 10.1039/c002204g.

[52] A. Gama Goicochea, R. López-Esparza, M. A. Balderas Altamirano, E. Rivera-Paz, M. A. Waldo-Mendoza, and E. Pérez, “Friction coefficient and viscosity of polymer brushes with and without free polymers as slip agents,” *J. Mol. Liq.*, vol. 219, pp. 368–376, 2016, doi: 10.1016/j.molliq.2016.03.039.

[53] S. Itoh, K. Ishii, K. Fukuzawa, and H. Zhang, “Shear thinning of nanometer-thick liquid lubricant films measured at high shear rates,” *Tribol. Lett.*, vol. 53, no. 3, pp. 555–567, 2014, doi: 10.1007/s11249-014-0294-3.

[54] H. Ahmed and L. Biancofiore, “Modeling polymeric lubricants with non-linear stress constitutive relations,” *J. Nonnewton. Fluid Mech.*, vol. 321, no. July, p. 105123, 2023, doi: 10.1016/j.jnnfm.2023.105123.

[55] H. Ahmed and L. Biancofiore, “A new approach for modeling viscoelastic thin film lubrication,” *J. Nonnewton. Fluid Mech.*, vol. 292, no. November 2020, p. 104524, 2021, doi: 10.1016/j.jnnfm.2021.104524.

[56] S. S. Gamaniel, D. Dini, and L. Biancofiore, “The effect of fluid viscoelasticity in lubricated contacts in the presence of cavitation,” *Tribol. Int.*, vol. 160, no. December 2020, p. 107011, 2021, doi: 10.1016/j.triboint.2021.107011.

[57] Z. Tang and X. Zhang, “Efficient algorithm for detecting concentric circles in binary images,” *ICIC Express Lett.*, vol. 4, no. 6 B, pp. 2495–2500, 2010.

[58] S. Itoh, Y. Ohta, K. Fukuzawa, and H. Zhang, “Enhanced viscoelasticity of polyalphaolefins confined and sheared in submicron-to-nanometer-sized gap range and its dependence on shear rate and temperature,” *Tribol. Int.*, vol. 120, no. December 2017, pp. 210–217, 2018, doi: 10.1016/j.triboint.2017.12.022.

[59] G. Gazzola, I. Filipucci, A. Rossa, K. Matyjaszewski, F. Lorandi, and E. M. Benetti,

"Oxygen Tolerance during Surface-Initiated Photo-ATRP: Tips and Tricks for Making Brushes under Environmental Conditions," pp. 1–7, 2023, doi: 10.1021/acsmacrolett.3c00359.

[60] M. Fromel, E. M. Benetti, and C. W. Pester, "Radical Polymerizations : Are Polymer Brushes Turning into," 2022, doi: 10.1021/acsmacrolett.2c00114.

[61] M. Kobayashi, K. Ishihara, and A. Takahara, "Neutron reflectivity study of the swollen structure of polyzwitterion and polyeletrolyte brushes in aqueous solution," *J. Biomater. Sci. Polym. Ed.*, vol. 25, no. 14–15, pp. 1673–1686, 2014, doi: 10.1080/09205063.2014.952992.

[62] M. J. Puttock and E. G. Thwaite, "Elastic Compression of Spheres and Cylinders at Point and Line Contact," *Natl. Stand. Lab. Tech. Pap.*, vol. 25, no. 25, p. 64, 1969.

[63] Alastair Cameron, *The principles of lubrication*. London: Longmans, 1966.

[64] Y. Shi, D. Xiong, Y. Liu, N. Wang, and X. Zhao, "Swelling, mechanical and friction properties of PVA/PVP hydrogels after swelling in osmotic pressure solution," *Mater. Sci. Eng. C*, vol. 65, pp. 172–180, 2016, doi: 10.1016/j.msec.2016.04.042.

[65] K. D. Schulze *et al.*, "Polymer Osmotic Pressure in Hydrogel Contact Mechanics," *Biotribology*, vol. 11, no. November 2016, pp. 3–7, 2017, doi: 10.1016/j.biotri.2017.03.004.

[66] A. Bhattacharyya, C. O'Bryan, Y. Ni, C. D. Morley, C. R. Taylor, and T. E. Angelini,

"Hydrogel compression and polymer osmotic pressure," *Biotribology*, vol. 22, no. March, p. 100125, 2020, doi: 10.1016/j.biotri.2020.100125.

[67] A. Gaisinskaya *et al.*, "Hydration lubrication: Exploring a new paradigm," *Faraday Discuss.*, vol. 156, pp. 217–233, 2012, doi: 10.1039/c2fd00127f.

[68] Z. Wang, J. Li, Y. Liu, and J. Luo, "Macroscale superlubricity achieved between zwitterionic copolymer hydrogel and sapphire in water," *Mater. Des.*, vol. 188, p. 108441, 2020, doi: 10.1016/j.matdes.2019.108441.

[69] G. Liu, Z. Liu, N. Li, X. Wang, F. Zhou, and W. Liu, "Hairy polyelectrolyte brushes-grafted thermosensitive microgels as artificial synovial fluid for simultaneous biomimetic lubrication and arthritis treatment," *ACS Appl. Mater. Interfaces*, vol. 6, no. 22, pp. 20452–20463, 2014, doi: 10.1021/am506026e.

[70] C. M. Beddoes, M. R. Whitehouse, W. H. Briscoe, and B. Su, "Hydrogels as a replacement material for damaged articular hyaline cartilage," *Materials (Basel).*, vol. 9, no. 6, 2016, doi: 10.3390/ma9060443.

[71] G. Morgese *et al.*, "Chemical Design of Non-Ionic Polymer Brushes as Biointerfaces: Poly(2-oxazine)s Outperform Both Poly(2-oxazoline)s and PEG," *Angew. Chemie - Int. Ed.*, vol. 57, no. 36, pp. 11667–11672, 2018, doi: 10.1002/anie.201805620.

[72] A. Wang, A. Essner, and R. Klein, "Effect of contact stress on friction and wear of

ultra-high molecular weight polyethylene in total hip replacement," *Proc. Inst. Mech. Eng. Part H J. Eng. Med.*, vol. 215, no. 2, pp. 133–139, 2001, doi: 10.1243/0954411011533698.

[73] B.J. Hamrock D. Dowson, *Ball bearing lubrication*. 1981.

[74] N. L. Yamada *et al.*, "Design and performance of horizontal-type neutron reflectometer SOFIA at J-PARC/MLF," *Eur. Phys. J. Plus*, vol. 126, no. 11, pp. 1–13, 2011, doi: 10.1140/epjp/i2011-11108-7.

[75] K. Mitamura *et al.*, "Novel neutron reflectometer SOFIA at J-PARC/MLF for in-situ soft-interface characterization," *Polym. J.*, vol. 45, no. 1, pp. 100–108, 2013, doi: 10.1038/pj.2012.156.

[76] A. Glavic and M. Björck, "{\it GenX 3}: the latest generation of an established tool," *J. Appl. Crystallogr.*, vol. 55, no. 4, pp. 1063–1071, 2022, doi: 10.1107/S1600576722006653.

[77] Q. Yue *et al.*, "Bioinspired Polysaccharide-Derived Zwitterionic Brush-like Copolymer as an Injectable Biolubricant for Arthritis Treatment," *Adv. Healthc. Mater.*, vol. 11, no. 13, pp. 1–12, 2022, doi: 10.1002/adhm.202200090.

Acknowledgement

I would like to express my deepest gratitude to my advisor, Professor Shintaro ITOH, for his invaluable guidance, patience, and support throughout this research. His expertise and insightful feedback were instrumental in shaping the direction and success of this thesis.

My sincere thanks also go to the members of my thesis committee, Kenji FUKUZAWA, Noritsugu UMEHARA, and Satoru MAEGAWA, for their constructive comments and suggestions, which have contributed significantly to the improvement of this work.

I am grateful to my colleagues and friends in the Fukuzawa laboratory for their stimulating discussions, encouragement, and camaraderie. The time spent with them was both enriched and enjoyable.

I would also like to thank Hedong ZHANG, Naoki AZUMA, and Tomoko HIRAYAMA for their expert advice and valuable perspectives on my research.

My heartfelt appreciation goes to my family, for their unwavering love, understanding, and support. They have been a constant source of strength and motivation throughout my academic journey.

Finally, I acknowledge the DII collaborative graduate program and the THERS

Interdisciplinary Frontier Next Generation Researcher Project for their financial support and the opportunities provided to me during my studies.

This thesis would not have been possible without the collective guidance, support, and encouragement of those mentioned above.